# *Primary Somatosensory Cortical Outputs Bidirectionally Modulate Nociceptive Perception, Cortical Excitability, and Thalamic Firing Mode*

Presented by

M.Sc. Ross Folkard

Inaugural dissertation

for

obtaining the doctoral degree

of the

Combined Faculty of Mathematics, Engineering and Natural Sciences

of the

Ruprecht - Karls - University

Heidelberg

Presented by

M.Sc. Ross Folkard

born in: London, United Kingdom

Oral examination: 17.12.2024

*Primary Somatosensory Cortical Outputs*

*Bidirectionally Modulate Nociceptive Perception,*

*Cortical Excitability, and Thalamic Firing Mode*

Referees: PD. Dr. Georg Köhr

Prof. Dr. Alexander Groh

# Table of Contents

# Abbreviations

A1: Primary Auditory Cortex

ACC: Anterior Cingulate Cortex

AP: Action potential

CCI: Chronic Constriction Injury

CFA: Complete Freund's Adjuvant

CPA: Conditioned Place Aversion

CPG: Central Pattern Generator

CPP: Conditioned Place Preference

DCML: Dorsal Column-Medial Lemniscal pathway

DLF: Dorsolateral Funiculus

dSTT: Dorsal Spinothalamic Tract

FO: First-Order

FS: Fast-Spiking

GPCR: G-Protein Coupled Receptor

HO: Higher-Order

I/O: Input-Output

I.p.: Intraperitoneal

ISI: Inter-spike Interval

L2/3: Cortical layer 2 and 3

L4: Cortical Layer 4

L5: Cortical Layer 5

L6CT: Corticothalamic L6

LTS: Low-Threshold $Ca^{2+}$ Spikes

MD: Medio-dorsal thalamic nucleus

mRNA: Messenger Ribonucleic Acid

NK1: Neurokinin 1

NS: Nociceptive-Specific

PAG: Periaqueductal Grey

PFC: Prefrontal Cortex

PKCγ+: Protein Kinase C gamma isoform positive

POm: Posterior Medial Nucleus

PSTH: Peri-Stimulus Time Histogram

RMP: Resting Membrane Potential

RNA: Ribonucleic Acid

S1: Primary Somatosensory Cortex

S1-HL: S1 Hindlimb Cortex

S2: Secondary Somatosensory Cortex

SCI: Spinal Cord Injury

SOM+: Somatostatin-positive

SRT: Spino-reticulo-thalamic pathway

STT: Spinothalamic tract

TC: Thalamocortical

TRN: Thalamic Reticular Nucleus

TRP: Transient Receptor Potential

V1: Primary Visual Cortex

VB: Ventrobasal thalamus

VLF: Ventrolateral Funiculus

VP: Ventral Posterior thalamic nuclei

VPL: Ventral Posterolateral thalamic nucleus

VPm: Ventral Posteromedial thalamic nucleus

vSTT: Ventral Spinothalamic Tract

WDR: Wide Dynamic Range

ZI: Zona Incerta

# List of Figures and Tables

# 1. Abstract

Pain is a perceptually salient association of a distressing, unpleasant emotional experience with actual or potential tissue damage. The combination of sensory perception with an emotional valence that gives rise to a singular painful experience is thought to rely on cortical communication with thalamic contributions. As a modulator of both thalamocortical signalling and signalling in cortical layer 5 (L5), the numerous corticothalamic cells in cortical layer 6 (L6CT) can potentially influence both what and how sensory information reaches and leaves the cortex. Alteration in sensory L6CT activity has been implicated in altering sensory perception but has not been directly investigated in the context of pain perception in a targeted, cell-specific manner. Here, I used *in vivo* cell-type specific optogenetic manipulation of L6CT and L5 during extracellular electrophysiological recordings in primary somatosensory cortex (S1) to show that L6CT excitation inhibits cortical output in L5 whilst increasing thalamocortical throughput. In collaboration with colleagues, we demonstrate that this L6CT inhibition of L5 can account for the increased mechanical sensitivity and aversive effect of L6CT excitation through its stifling of anti-nociceptive signalling from L5. My research subsequently reveals that L6CT can in fact bidirectionally modulate cortical activity as a function of its own activity levels, causing facilitation in cortical subpopulations and entraining these subpopulations to its firing patterns. The firing patterns of L6CT also bidirectionally influence the degree of thalamic burst-firing in a manner that is somewhat dissociable from total L6CT activity. This research further demonstrates that S1 L6CT can be a flexible and potent modulator of signalling to and from the cortex, providing a partial mechanistic basis for its dramatic modulation of multiple qualia underlying pain perception. My observations that S1 L6CT can bidirectionally modulate cortical firing and thalamic firing mode reveal a more complex role for L6CT than previously recognised.

Schmerz ist eine saliente, wahrnehmbare Assoziation zwischen einer beunruhigenden, unangenehmen emotionalen Erfahrung und einer tatsächlichen oder potenziellen Gewebeschädigung. Es wird angenommen, dass die Kombination von Sinneswahrnehmung mit emotionaler Valenz, welche zu einer einzigartigen schmerzhaften Erfahrung führt, auf kortikaler Signalübertragung mit thalamischen Beiträgen beruht. Als potenzieller Modulator sowohl der thalamokortikalen Signalübertragung als auch der Signalübertragung in der kortikalen Lamina 5 (L5) können die zahlreichen kortiko-thalamischen Zellen der kortikalen Lamina 6 (L6CT) potenziell beeinflussen, welche und wie sensorische Informationen den Kortex erreichen und verlassen. Eine Veränderung der somatosensorischen L6CT-Aktivität wird mit einer veränderten sensorischen Wahrnehmung in Verbindung gebracht, wurde aber in Zusammenhang mit der Wahrnehmung von Schmerzen noch nicht gezielt untersucht. In meiner Doktorarbeit verwendete ich *in-vivo* zelltyp-spezifische optogenetische Manipulation von L6CT und L5 während extrazellulärer elektrophysiologischer Aufzeichnungen im primären somatosensorischen Kortex (S1), um zu zeigen, dass die Anregung von L6CT den kortikalen Output von L5 hemmt und gleichzeitig die thalamokortikale Signalübertragung erhöht. In Zusammenarbeit mit Kolleginnen und Kollegen konnten wir zeigen, dass L6CT L5 hemmt und in Folge zu erhöhter mechanischer Sensibilität und Aversion führt, indem es die anti-nozizeptiven Signale von L5 unterdrückt. Des Weiteren zeigt meine Forschung, dass L6CT

in der Lage ist, die kortikale Aktivität in Abhängigkeit von seinem Aktivitätsniveau bidirektional zu modulieren, indem es eine Fazilitierung in kortikalen Subpopulationen hervorruft und diese Subpopulationen an seine Feuermuster anpasst. Die Feuerungsmuster von L6CT haben auch einen bidirektionalen Einfluss auf das Ausmaß des thalamischen Burst-Feuerns in einer Weise, die etwas von der Gesamtaktivität von L6CT entkoppelt ist. Diese Forschung zeigt weiter, dass S1 L6CT ein flexibler und komplexer Modulator der thalamischen und kortikalen Outputs sein kann, was eine teilweise mechanistische Grundlage für die dramatische Modulation mehrerer Wahrnehmungsqualitäten bietet, die der Schmerzwahrnehmung zugrunde liegen. S1 L6CT kann das kortikale Feuern und den thalamischen Feuermodus bidirektional modulieren, was auf eine komplexere Rolle von L6CT hinweist als bisher angenommen.

# 2. General Introduction

The International Association for the Study of Pain (IASP) defines pain as “An unpleasant sensory and emotional experience associated with, or resembling that associated with, actual or potential tissue damage” (Raja et al. 2020). Biological tissue can be damaged in numerous ways at numerous rates to numerous extents, and organisms that respond optimally to these noxious stimuli may stand a better chance at survival and reproduction (Maren 2001; Fanselow 1994). A consequence of this is that organisms have evolved many specialised receptors and pathways to differentiate between noxious agents and non-noxious agents (Bennett et al. 2019; Willis 2007; Basbaum et al. 2009; Dubin & Patapoutian 2010; Abraira & Ginty 2013). However, exactly how a unified painful experience is rendered from this configuration, one that under certain circumstances may not require any external agent, remains poorly understood, though is thought to rely on cortical signalling with thalamic contributions (Kuner & Kuner 2021). It is estimated that at any given time approximately one in five people are suffering from ongoing pain worldwide (Treede et al. 2015; Zimmer et al. 2022). Current treatment strategies are limited, underscoring the need for better causal understanding of central circuit mechanisms contributing to pain perception (Basbaum et al. 2023).

## 2.1. Following nociception from the origin

Nociception, the signalling that underlies pain perception, is thought to have evolved as a mechanism to protect from injury and enforce avoidance behaviours of external stimuli that have the potential to damage organismal tissue, with acute pain representing a failure to avoid said stimuli (Baliki & Apkarian 2015). To understand what neuronal signalling causes pain versus what neuronal signalling pain causes, if such a distinction can cleanly be made, remains one of the critical questions in pain research (Kuner & Kuner 2021). This is particularly important as signals duplicate, diverge, and converge as information travels through the nervous system, adding complexity and complicating the investigation of the causal contributions behind many percepts (Barack et al. 2022). Additionally, top-down influences can shape bottom-up signalling, altering perception of sensory events, with one example being descending corticofugal pathways from S1 L5 and L6CT altering bottom-up signalling at the level of the spinal cord and thalamus (Liu et al. 2018; Mease et al. 2014). It is important to have an impression of what bottom-up information a brain region receives to make appropriate inferences about how it influences pain perception. As a simplistic example, one might expect S1 activity to influence pain more than activity in the primary auditory (A1) or visual (V1) cortices, given the supposed nature of the bottom-up sensory inputs to both regions. Despite this, the degree of cross-talk throughout the brain means that contextual auditory and visual information could potentially influence pain perception through modulation in somatosensory regions, as has recently been reported (Zhou et al. 2022; Cao et al. 2023). Both studies imply that these respective effects nevertheless arise from modulation of a more proximal mediator of pain perception. To contextualise the contributions of S1 activity to pain perception it is useful to start at the periphery with a nociceptive stimulus to see what neuronal activity is

required for pain perception, and how much of this nociceptive information reaches or can be influenced by changes in S1 activity.

## 2.2. Mechanically-transductive peripheral sensors

For the nervous system to sense physical contact with an external stimulus, it must transduce mechanical pressures into electrical signals. It does so through a variety of specialised mechanically-transductive sensory receptors. These specialised cells change conformation under physical pressure, either directly, or indirectly through e.g. extracellular proteins, which alter the ion permeability of these cells and cause depolarisation. This depolarisation, if sufficiently large, can induce voltage-gated $Na^+$ channel activation and action potential (AP) propagation along the axon (e.g. Pacinian Corpuscle), or in other cell-types can induce transmitter release to another cell that reaches action potential threshold (e.g. Merkel cell). Sensory receptors vary in their receptive field sizes and excitability, depending on their size, shape, and structural properties. For example, connective tissue that surrounds the Pacinian corpuscle filters its responses to low frequencies of stimulation, and as such its depolarisations are largest during the onsets and offsets of stimuli. In contrast, Merkel cells are small, have smaller receptive fields, and do not show as much adaptation to continuous stimulation (Vallbo & Johansson 1984). Slowly-adapting and rapidly-adapting mechanoreceptors can also be further subdivided based on spiking regularity, receptive field sizes and tuning properties (Abraira & Ginty 2013).

These low threshold mechanoreceptors of the skin transmit the receptor potentials via Aβ fibres; large diameter (6-12 μm), myelinated axons that conduct up to 75 m/s (Horch et al. 1977). The larger the diameter of the axon, the lower the axial resistance, and the greater the current along the axon for a given potential difference. This thereby facilitates current flow down the axon rather than across the membrane (Suminaite et al. 2019). Voltage-gated sodium channels are also more concentrated in the nodes of Ranvier allowing for quicker depolarisation. As such, both a large diameter axon and a high degree of myelination gives Aβ a relatively fast action potential (AP) transmission.

## 2.3. Nociceptors transduce damaging stimuli.

In contrast to mechanical touch, mechanical nociception is thought to be transduced by free nerve endings that are small in diameter and either lightly myelinated or unmyelinated. The unmyelinated fibres, known as C fibres, are narrow afferent nerves that conduct at ~1 m/s. Aδ fibres conduct at ~3 m/s due to a wider diameter than C fibres and slight myelination (Horch et al. 1977). As such, Aδ fibres are implicated in the short, sharp experience of pain, whereas C fibres mediate the prolonged dull pain associated with peripheral tissue damage (Julius & Basbaum 2001). These two classes of nociceptor, receptors activated by stimuli actually or potentially damaging to tissue, tend to be polymodal, but can be further subdivided into subclasses depending on characteristics such as thresholds to different modalities and stimulus adaptation (Dubin & Patapoutian 2010). Temperature is transduced through a family

of transient receptor potential (TRP)-related ion channels that are thought to mediate both non-noxious and noxious temperatures ranging from hot to cold, with TRPV1+ neurons necessary for heat pain and TRPV8+ neurons necessary for cold pain sensation (Caterina et al. 1997; Tominaga et al. 1998; McKemy et al. 2002; Peier et al. 2002; Moqrich et al. 2005; Lee & Caterina 2005; Mishra et al. 2011).

Aδ fibres consist of Type 1 mechanoreceptors with a low mechanical threshold, but a high heat threshold. Type 2 Aδ fibres have low heat thresholds and high mechanical thresholds (Basbaum et al. 2009). C fibre responsiveness also varies between populations; most are polymodal, but there exist subpopulations that are more selective and for example respond only to thermal stimulation under normal physiological conditions, whereas others are non-nociceptive and respond only to innocuous touch (Olausson et al., 2008; Schmidt et al., 1995). C fibres can also be subdivided neurochemically, with peptidergic and non-peptidergic C fibres hypothesised to play roles in inflammatory and neuropathic pain states respectively (Molliver et al. 1997; Snider & McMahon 1998). C fibres are estimated to account for ~80 % of cutaneous primary afferents, with approximately a 50/50 ratio between peptidergic and non-peptidergic C fibres (Todd 2010).

## 2.4. Acute nociceptive processing in the spinal cord

Sensory afferents synapse predominantly in the dorsal horn of the spinal cord, which is divided into six laminae (Rexed 1952). Aβ fibres tend to synapse from the inner section of lamina 2 to lamina 5 (Todd 2010; Neumann et al. 2008; Li et al. 2011; Hughes et al. 2003) with Aδ fibres terminating mainly in lamina 1 though also to a lesser extent in lamina 5 (Light & Perl 1979). The majority of C fibres synapse in the dorsal horn in laminae 1 and 2, with peptidergic C fibres synapsing in laminae 1 and the outer part of lamina 2, and non-peptidergic in the central part of lamina 2 respectively (Sugiura et al. 1986; Sugiura et al. 1993; Sugiura et al. 1989; Snider & McMahon 1998; Hunt et al. 1997; Lawson et al. 1997; Todd et al. 2000; Molliver et al. 1997). Prior to synapsing in the dorsal horn, both Aδ and C fibres branch along the rostrocaudal axis and extend along the zone of Lissauer, synapsing in the substantia gelatinosa (Sugiura et al. 1986; Lidierth 2007; Traub et al. 1986).

Substance P expressing neurons respond to noxious stimulation, are predominantly C and Aδ fibres synapsing in lamina 1, and make synapses with projection neurons in lamina 1 (Lawson et al. 1997; Mantyh et al. 1997; Todd et al. 2002). Neurokinin-1 (NK1) receptors are the receptors that substance P binds to and are expressed in ~80 % lamina 1 neurons, and to a lesser extent in laminae 3 and 4 (Marshall et al. 1996; Todd et al. 2000). Substance P-expressing C fibre ablation attenuates responses to highly noxious stimuli and thermal and mechanical hyperalgesia, although mild noxious stimuli are unchanged, implicating substance P signalling in nociceptive transmission (Mantyh et al. 1997).

In contrast, the non-peptidergic class of C fibres in lamina 2 are the predominant location of NaV1.8 expression, which appears necessary for appropriate mechanical and cold perception (Abrahamsen et al. 2008; Braz et al. 2005). *Cavanaugh et al.* observed that genetic ablation of non-peptidergic C fibres expressing the G-protein coupled receptor (GPCR) Mrgprd, which constitutes >90 % of all non-peptidergic C fibres, selectively suppresses behavioural

responses to noxious mechanical stimulation, but not hot or cold stimulation (Cavanaugh et al. 2009; Zylka et al. 2005). They also observed that ablation of TRPV1+ fibres selectively impaired noxious heat sensitivity, with ablation of both fibres resulting in a summation of the deficits but no multiplicative effects or further deficits, suggesting relative separation between the two C fibre populations (Cavanaugh et al. 2009). These selective ablations were also reflected in these non-peptidergic neurons in lamina 2 very rarely terminating on NK1-positive neurons in dorsal horn, unlike the peptidergic population, indicating relatively segregated dorsal horn recipient populations (Braz et al. 2005; Todd et al. 2002).

Whilst non-peptidergic C fibres seem to mediate mechanical nociception under normal circumstances, highly noxious mechanical stimulation is suppressed by ablation of NK1 neurons, suggesting a contribution to mechanical sensitivity from peptidergic C fibres (Mantyh et al. 1997). The degrees of overlap and separation between peptidergic and non-peptidergic C fibres still lacks complete elucidation, but it appears that peptidergic C fibres are the predominant first-order mediator of heat sensitivity, and non-peptidergic C fibres mechanical sensitivity, though both C fibre classes respond to capsaicin and may mediate thermal and mechanical hyperalgesia (Snider & McMahon 1998; Akopian et al. 1999; Abrahamsen et al. 2008; Wiley et al. 2007; Nichols et al. 1999). Taken together, there is reasonable evidence to suggest that different types of acute pain perception rely significantly on specific and distinct C fibre projections.

Early studies observed that lamina 1 dorsal horn neurons responded preferentially to intense mechanical stimulation and less to non-nociceptive mechanical stimulation (Christensen & Perl 1970). Indeed, the majority of lamina 1 dorsal horn projection neurons are nociceptive-specific (Zhang et al. 2013). Whilst projection neurons are more concentrated in lamina 1 than any other lamina, they still represent approximately only 5 % of neurons in lamina 1 (Spike et al. 2003). Interneurons comprise the vast majority of neurons in the dorsal horn (Spike et al. 2003; Abraira et al. 2017; Bice & Beal 1997; Todd 2017). There is remarkable interneuron diversity in the dorsal horn that can specifically modify information destined for distinct projection neurons (Polgár et al. 1999; Peirs et al. 2020). The complex interneuronal circuitry in the dorsal horn has been implicated in the gating of nociceptive signals to the brain. Excitatory somatostatin-positive (SOM+) interneurons in laminae 2 receive from Aδ, Aβ, and C fibres and project to lamina 1 projection neurons (Duan et al. 2014). When these neurons are ablated, mechanical nociceptive responses are reduced, suggesting that all of these respective afferent fibres can contribute to nociceptive signalling through these SOM+ interneurons. GABAergic inhibition enabled Aβ-driven AP firing in 85 % of lamina 1/2 neurons, compared with 7 % under control conditions, or 4 % in mice lacking these SOM+ interneurons. Conversely, Dynorphin-expressing inhibitory interneurons in laminae 1 and 2 are strongly excited by Aβ inputs, and inhibit firing in the SOM+ population, preventing their activation by low threshold stimuli as well as the reduction in mechanical pain thresholds (Duan et al. 2014). This adds to observations that lamina 2 PKCɣ+ interneuron excitation of pro-nociceptive spinal pathways contribute to neuropathic mechanical allodynia, and are dampened by glycinergic interneurons that can be engaged through Aβ-mediated feedforward inhibition (Lu et al. 2013; Neumann et al. 2008; Malmberg et al. 1997; Torsney & MacDermott 2006; Miraucourt et al. 2007). This more recent research further corroborates previous reports that inhibitory interneurons gate nociceptive thresholds, but elucidates specific circuits in tuning Aβ-mediated nociceptive signalling, and provide some mechanistic support for the long-hypothesised gate-control theory (Yaksh 1989; Melzack & Wall 1965). Other studies further report that excitatory

interneurons in superficial dorsal horn contribute to nociceptive mechanical thresholds and are necessary for full behavioural expression of pain behaviours (Wang et al. 2013). However, it largely seems that the cross-talk in the dorsal horn constitutes highly complex modulation of pain signalling, where previously segregated information streams from specialised first-order neurons may now influence each other. Despite this, the aforementioned studies delineate pathways where disinhibition-associated mechanisms that increase mechanical pain sensitivity so far seemingly converge on projection neurons in lamina 1, implicating lamina 1 projection neurons in causally mediating pain perception (Torsney & MacDermott 2006; Miraucourt et al. 2007; Duan et al. 2014; Peirs et al. 2015; Lu et al. 2013; Cheng et al. 2017). Whilst there is communication from lamina 2 to lamina 1, and at least one mechanism of possible C fibre lateral inhibition, signals from non-peptidergic Nav1.8-expressing C fibres that target inner lamina 2 predominantly ascend the spinal cord from projection cells in lamina 5 via lamina 2, suggesting a degree of parallel circuitry in pain perception (Lu & Perl 2005; Price et al. 1979; Braz et al. 2014; Bennett et al. 1980; Duan et al. 2014; Fernandes et al. 2020; Braz et al. 2005).

The majority of the lamina 5 2$^{nd}$ order neurons that respond to nociceptive stimuli are wide dynamic range neurons (WDRs), in contrast to lamina 1 2$^{nd}$ order neurons that are primarily nociceptive-specific (NS) (Price et al. 2003; Zhang et al. 2013). This is a reflection of convergence of nociceptive and non-nociceptive inputs originating from C fibres and Aβ fibres respectively (Braz et al. 2005; Price & Dubner 1977; Price et al. 1978). Although WDR neurons are thought to be capable of differentiating nociceptive from non-nociceptive stimuli, and display more sensitivity in activity to small shifts in stimuli, little research has explored the causality of spinal WDR neurons in normal pain perception. One study noted that glycinergic inhibition of PKCɣ interneurons prevents NS dorsal horn neuron responses to non-noxious mechanical stimulation and mechanical allodynia, and antagonism of this process in superficial dorsal horn causes NS dorsal horn neurons to respond to non-noxious mechanical stimuli and increased mean arterial blood pressure, an effect not seen when this antagonism occurs in the WDR-rich subnucleus oralis, despite an increase in WDR firing rates (Miraucourt et al. 2007). This suggests that NS spinal cord neurons in lamina 1 may cause pain, WDR neurons may be correlated with mechanical pain, and therefore pain as a displeasurable percept may be more dependent on signalling in NS projection neurons. However, the evidence appears limited to draw these distinctions conclusively.

## 2.5. Ascension of pain through the spinal cord

Whilst there seems to be considerable mixing between nociceptive and non-nociceptive information within the spinal cord, the nature of information ascending the spinal cord has been revealed to be comparably structured into distinct pathways (Willis & Westlund 1997; Jones et al. 1987; Apkarian & Hodge 1989). This first became apparent upon observations that injuries that affect only one half of the spinal cord can give rise to impairments in proprioception and fine sensory discrimination ipsilateral to the injury site, and loss of pain contralateral to the site of spinal injury, known as Brown-Séquard syndrome (Brown-Séquard 1869). This is due to different decussation points in the dorsal column-medial lemniscal pathway (DCML), which decussates in the medial lemniscus in the brain stem, and the spinothalamic tract (STT) that decussates close to its entry into the dorsal horn and ascends

through the lateral funiculus (Apkarian & Hodge 1989; Willis et al. 1979). Cases like these placed much greater emphasis on STT projections in pain perception than DCML projections. Indeed, ablating STT projections leads to deficits in pain perception on the contralateral side (Greenspan et al. 1986; Vierck & Luck 1979) and anterolateral cordotomy, which severs the STT (Price & Mayer 1975; Willis & Westlund 1997) has been used, although with variable success, as a treatment for persistent pain (Spiller 1912). Indeed, stimulating the anterolateral quadrant of the spinal cord evokes pain in humans, suggesting that STT activity can sufficiently cause pain perception (Mayer et al. 1975). STT is thought to be arranged somatotopically, and individual STT cells have receptive restricted fields to a contralateral region of the skin (Willis et al. 1974; Willis & Westlund 1997).

Observations that STT is comprised disproportionately of lamina 1 projection neurons, and that these neurons are almost exclusively NS corroborated STT as a major ascending nociceptive pathway (Trevino et al. 1973; Giesler et al. 1981; Willis et al. 1979; Willis et al. 2001; Apkarian & Hodge 1989; Jones et al. 1987; Martin et al. 1990; Price et al. 1978; Craig et al. 1989). C fibre stimulation causes STT excitation and temporal summation can be observed at C fibre stimulation frequencies as low as 0.33 Hz, a process known as wind-up (Chung et al. 1979; Mendell 1966). Repetitive C fibre activation (1Hz for 20s) has been observed to increase receptive field area of 2$^{nd}$ order neurons in lamina 1 by ~4 times and increase WDR firing by ~3-4x for up to 30 minutes (Cook et al. 1987). Spatial summation of pain can occur even across dermatomes (Douglass et al. 1992). Substance P application in dorsal horn causes sensitisation in STT cells that is dependent on intact NK1 receptors (Dougherty et al. 1993). Most STT projection neurons from lamina 1 respond to mechanical, or a combination of mechanical plus thermal stimulation, with few responding to heat alone (Han et al. 1998; Willis et al. 1974). However, other studies suggest that STT may comprise of less than 15 % lamina 1 projection neurons (Klop et al. 2004), and more recent research is revealing the roles of other spinal pathways in different types of pain perception, such as visceral pain (Willis & Westlund 1997). Nociceptive neurons with ascending projections have been identified in lamina 5 and 6 as well as NK1-positive projections in laminae 1, 3 and 4 (Price et al. 1978; Todd et al. 2000; Zemlan et al. 1978). Indeed further reports indicate that cells that originate in lamina 1 ascend through the dorsolateral STT (dSTT) in the dorsolateral funiculus (DLF), whereas those that originate in deeper laminae (4-10) ascend through the ventrolateral funiculus (VLF) in the ventral quadrant (Jones et al. 1987; Apkarian & Hodge 1989). Whilst the exact nature of the signals ascending through the ventral STT (vSTT) remain relatively unresolved due to the lower representation from lamina 1, stimulation of the ventral quadrant induces pain in humans, suggesting direct causal nociceptive properties of this pathway, and by extension deeper dorsal laminae, possibly due to nociceptive signalling originating from the non-peptidergic C fibres that relay nociception from lamina 2 to deeper laminae (Mayer et al. 1975; Braz et al. 2005; Willis et al. 2001).

The predominant targets for layer 1 projection neurons in STT are thought to be thalamic structures (Willis et al. 2001; Willis et al. 1979; le Gros Clark 1936), though the majority also send collaterals to other regions such as the parabrachial nucleus, which itself targets the amygdala and hypothalamus amongst other limbic structures (Jasmin et al. 1997; Braz et al. 2014; Klop et al. 2005). Lamina 1 projection neurons also target the caudal medulla and the periaqueductal grey (PAG), a region known to be involved in pain modulation, and critical in the placebo effect (Fields 2004; Spike et al. 2003; Todd et al. 2000). It is not uncommon for a single STT fibre to branch and innervate multiple targets, including different thalamic nuclei

(Giesler et al. 1981). Anterograde and retrograde tracing techniques indicate STT heavily projects to the ventral posterolateral thalamic nucleus (VPL) (Gauriau & Bernard 2004; Willis et al. 2001; Yen et al. 1991; Martin et al. 1990). Similarly, anterograde labelling in superficial laminae of medullary dorsal horn reveals major innervation in the ventral posteromedial thalamic nucleus (VPm) and posterior thalamic nucleus (POm) amongst others, whereas deeper projections innervate these to a lesser extent, but project more to zona incerta (ZI) (Iwata et al. 1992).

Across and within species there is debate about the extent of lamina 1 projections to the VPL and the nociceptive processing in the VPL (Klop et al. 2005; Mouton & Holstege 1998; Craig et al. 1994; Willis et al. 2001; Apkarian & Hodge 1989). A possible cause of conflicting data could be from reports that the STT can be subdivided with respect to dorsal horn origin, with the dorsal STT originating in lamina 1 and the ventral STT originating in deeper layers (Apkarian & Hodge 1989; Jones et al. 1987), though an alternative explanation may be be due to species differences in location and distribution of NS neurons in VPL (Martin et al. 1990; Guilbaud et al. 1980; Peschanski et al. 1980; Yokota et al. 1985; Yokota et al. 1988; Honda et al. 1983; Kniffki & Mizumura 1983). Whilst VPL does contain NS neurons, other more medial thalamic regions that receive from STT contain a much higher proportion (Giesler et al. 1981).

## 2.6. The gateway to the cortex

In order for sensory information to reach the cortex from the periphery (with the exception of olfaction) it first has to synapse in the thalamus (Jones 2007). The thalamus, historically labelled the relay centre of the brain, can be divided into thalamic nuclei based on cytoarchitecture (Sherman 2007). Subsequent functional distinctions were made on the basis of differential innervation to thalamic nuclei, with ‘First-Order’ (FO) nuclei receiving their primary afferents from ascending sensory pathways, whereas ‘Higher-Order’ (HO) nuclei receive their primary afferents from cortical L5 neurons (Guillery 1995). Thalamic nuclei, unlike the spinal cord, contain a minority of interneurons, and therefore a long-range projection to the thalamus generally synapses onto long-range thalamic projection neurons (Jones 2007). Recurrent activity is likely to come from corticothalamic feedback and/or lateral inhibition via the thalamic reticular nucleus (TRN) (Pinault & Deschênes 1998; Guillery 1995). Within these nuclei, thalamic cells were further categorised by their projections, with so-called ‘Core’ thalamocortical (TC) projections densely innervating middle layers in the cortex, particularly L4, in a topographic fashion, constituting the major cell-type in FO nuclei (Jones 1998). ‘Matrix’ TC projections sparsely innervate upper layers, particularly L1, and also basal ganglia, unlike core TC cells whose projections are restricted to the cortex (Jones 2001). Additionally, neurons could be categorised based on the types of synapses they form: ‘Driver’ inputs generally possess thick axons with large terminals whose synapses onto proximal dendrites produce large depolarisations that decrease in magnitude with high-frequency stimulation (synaptic depression). ‘Modulator’ inputs are much more numerous than drivers and possess thin axons with small terminals whose synapses onto distal dendrites produce small depolarisations that increase in magnitude with high-frequency stimulation (synaptic facilitation), and also activate metabotropic receptors (Sherman 2017; Reichova & Sherman 2004). However, recent advances in tracing techniques reveal further diversity with respect to

the thalamic output pathways, with at least 4 subclassifications of thalamic cell-type dependent on the number of targets, the targets themselves, and the cortical layer terminations (Clascá et al. 2012). Despite this revised classification scheme, it appears that the majority of FO nuclei contain predominantly unifocal thalamocortical neurons that project mainly to layers 4 and 3 in a single area of isocortex, and collateralise only in the TRN *en route* to the cortex: a pattern consistent with prior classifications of core TC projections from FO nuclei (Familtsev et al. 2016; Rodriguez-Moreno et al. 2020; Jones 2007). FO thalamic nuclei, a group to which VPL belongs, provide the cortex with information from sensory organs (Jones 2007). However, descending L6CT modulatory projections vastly outnumber driving projections from peripheral sense organs to the thalamus (Sherman & Koch 1986; Liu et al. 1995; Van Horn et al. 2000; Sherman 2001a). Therefore, prior to sensory-evoked information reaching the cortex, it potentially undergoes major modulation at the level of the thalamus from L6CT feedback (Sherman 2017).

How might L6CT activity shape incoming sensory data? L6CT modulatory input can induce net depolarisation or hyperpolarisation of TC cells through monosynaptic 'modulatory' glutamatergic input to distal dendrites on TC neurons, and disynaptic inhibition via their modulatory excitation of the TRN, which in turn inhibits thalamic nuclei (Liu & Jones 1999; Lozsádi et al. 1996; Guillery 1995; Bourassa et al. 1995; Ahrens et al. 2015; Pinault & Deschênes 1998). The inhibitory influence of L6CT feedback seemingly wanes as L6CT activity increases, with high L6CT activity exerting net excitation of their recipient TC neurons, resulting in an activity-dependent, corticothalamic switch that modulates the throughput of information from the thalamus to the cortex (Murphy & Sillito 1987; Andolina et al. 2007; Andolina et al. 2013; Wang et al. 2018; Cruikshank et al. 2010; Crandall et al. 2015; Jurgens et al. 2012). Importantly, L6CT cells receive excitatory fibres from outside their cortical modality, and physiological evidence indicates that L6CT neuronal firing may reflect a combination of multimodal information rather than a single modality alone, suggesting that L6CT may impart intra-modality but also inter-modality contextual information on the firing of the unimodal FO nucleus (Whilden et al. 2021; Clayton et al. 2021; Vélez-Fort et al. 2014; Zhou et al. 2022). In the context of pain, L6CT could relay contextual information S1 receives from more associative brain regions or other modalities to the thalamus, which may influence thalamic responsiveness to incoming nociceptive stimuli.

TC neurons operate in two firing modes, 'burst-firing' mode and 'tonic-firing' mode based on the activity/inactivity of T-Type $Ca^{2+}$ channels respectively, which dictates the amplitude of a depolarising, long-duration low-threshold spike (LTS) (Sherman 2001b; Llinás & Jahnsen 1982; Jahnsen & Llinás 1984a; Jahnsen & Llinás 1984b). The availability of T-Type $Ca^{2+}$ channels in practice lies on a spectrum that is heavily influenced by L6CT activity and contributes to tonic spiking even at depolarised membrane potentials (Wolfart et al. 2005; Deleuze et al. 2012). The state of the firing mode prior to peripheral input has great influence on whether subsequent peripheral input will elicit non-adapting but sparse tonic spikes, or a burst of spikes in succession, the latter potentially recruiting cortical circuits more potently and possibly doubling postsynaptic cortical responses (Hu & Agmon 2016; Swadlow & Gusev 2001). As a depressing synapse, it is proposed that the thalamic synapse with L4 under tonic spiking is perpetually in a semi-depressed state, and that the increased potency of thalamic bursts arises as a result of both temporal summation and a pre-burst silence that relieves the synapse of its depressed state (Swadlow & Gusev 2001; Swadlow et al. 2002; Chung et al. 2002; Castro-Alamancos & Oldford 2002). Indeed, burst-firing has been hypothesised to be

the better operating mode when detecting potential features from background, yet inferior to tonic-firing when discriminating between features due to the TC spiking output of tonic-firing more accurately reflecting excitatory peripheral input (Whitmire et al. 2016; Guido et al. 1995). A neuron's firing mode is mediated by the recent history of the its membrane potential; prior depolarisation shifts the firing mode towards tonic-firing, hyperpolarisation towards burst-firing (Sherman 2017; Lesica et al. 2006; Zhan et al. 1999). Through bidirectional modulation of the resting membrane potential (RMP), L6CT cells influence not only the excitability of TC cells, but also their firing mode (Mease et al. 2014; Andolina et al. 2013). Continuous L6CT feedback can depolarise TC cells and induce tonic-firing mode, relaying sustained peripheral input more reliably, which may enable increased feature sampling and precision in the estimation of stimulus features (Mease et al. 2014; Whitmire et al. 2016). Lower L6CT feedback may hyperpolarise TC cells, switching them to burst-firing mode, providing a much more binary threshold such that peripheral input now either does not elicit any response or it causes TC cells to burst, potentially improving detectability by increasing the likelihood that small peripheral inputs trigger the LTS and are relayed as potent bursts (Whitmire et al. 2016; Crandall et al. 2015). As a result, L6CT may modulate how TC cells transfer information from the same environmental peripheral input by emphasising either feature discrimination or stimulus detection though tonic-firing and burst-firing modes respectively.

## 2.7. VPL as a mediator of pain?

VPL receives input from the ascending DCML pathway as well as the vSTT and dSTT, with many cells receiving convergent inputs from DCML and STT fibres (Perl & Whitlock 1961; Ralston & Ralston 1994; Chung et al. 1986; Yen et al. 1991; Martin et al. 1990). Within the STT however, the dorsal (dSTT) and the ventral (vSTT) STT cells may synapse in a relatively non-overlapping manner (Martin et al. 1990). Therefore there seems to be a not inconsiderable number of VPL cells where STT-mediated responses are the result of signalling originating almost exclusively from either lamina 1 or deeper laminae, conserving some parallel information signalling at least until the level of the thalamus (Chung et al. 1986).

Convergence of noxious and non-noxious inputs from NS and WDR neurons increases in the dorsal horn and again in the thalamus (Owens et al. 1992; Kenshalo et al. 1980; Apkarian & Shi 1994). This gives rise to a number of both noxious-encoding and non-noxious-encoding thalamic neurons that receive from a variety of sources. Due to the high degree of convergence it is perhaps unsurprising that NS neurons are consistently the least common response-type in VPL, which could be explained by large innervation of VPL by the DCML pathway that unlike STT projects predominantly to VPL (Chung et al. 1986; Kenshalo et al. 1980; Apkarian & Shi 1994; Casey & Morrow 1983; Guilbaud et al. 1980; Boivie 1971; Berkley 1983). Due to the sparse innervation of VPL by STT, high STT activity may be required to reliably activate VPL neurons (Yen et al. 1991). VPL cells are somatotopically organised, and single VPL cells also respond to multiple modalities, particularly heat signals conveyed from the STT (Kenshalo et al. 1980; Chung et al. 1986; Peschanski et al. 1980). Even with an additional synapse, signals from DCML can activate VPL with shorter latencies than those from STT (Yen et al. 1991). Although VPL innervates multiple cortical regions (Liao & Yen 2008), research suggests that most VPL cells that show nociceptive responses project to S1 (Kenshalo et al. 1980). However, a higher proportion of NS neurons in more medial thalamic

nuclei has placed doubts on the lateral thalamocortical system for conveying affective properties of pain perception, with the displeasure associated with pain hypothesised to be mediated more through the medial thalamocortical pathway via considerable STT projections as well as input from spino-reticulo-thalamic (SRT) pathway, and the lateral thalamocortical pathway more suited to sensory-discriminative aspects of pain perception (Melzack & Casey 1968; Craig et al. 1989; Rainville et al. 1997; Kenshalo et al. 1982; Willis & Westlund 1997; Giesler et al. 1981; Guilbaud et al. 1986; Groh et al. 2018; Willis et al. 1979; Apkarian et al. 2000; Yen et al. 1991; Kuner & Kuner 2021; Bushnell & Duncan 1989).

## 2.8. Acute vs chronic pain in the VPL

It seems very clear that the structures and mechanisms that give rise to acute pain perception are considerably different than those in chronic pain conditions (Kuner & Flor 2016; Kuner & Kuner 2021; Tan et al. 2021; Kuner 2015). Whilst a full account of the all the mechanistic differences is beyond the scope of this introduction, 1$^{st}$ and 2$^{nd}$ order neurons as well as interneurons that synapse locally in the spinal cord are reported to undergo alterations that contribute to allodynic and hyperalgesic states (Miraucourt et al. 2007; Abrahamsen et al. 2008; Akopian et al. 1999; Duan et al. 2014; Peirs et al. 2015; Lu et al. 2013; Torsney & MacDermott 2006; Cheng et al. 2017). Although the degree to which acute pain affect is mediated through VPL is arguably not substantial, changes in VPL activity are implicated in both causing and alleviating pain associated with chronic neuropathic or inflammatory pain (Hains et al. 2005; Huh & Cho 2013a; LeBlanc et al. 2017; Kim et al. 2003; Iwata et al. 2011; LeBlanc et al. 2016; LaBuda et al. 2000). Indeed the thalamus was first hypothesised to play a role in neuropathic pain over one hundred years ago as a candidate central pattern generator (CPG) or *"essential thalamic structure"* that can sustain neuropathic pain (Head & Holmes 1911). Neuropathic pain, defined by IASP as "*pain caused by a lesion or disease of the somatosensory nervous system*", has a fundamentally different aetiology from inflammatory pain, nociceptive pain that signals "*actual or threatened damage to non-neural tissue*" (Merskey & Bogduk 2011).

Early evidence for a central contribution to chronic neuropathic pain reported that complete sympathetic block of sensory signalling at a level above injury proved insufficient to permanently alleviate pain symptoms in patients with chronic neuropathic pain following spinal cord injury (SCI), suggesting maintenance of chronic pain may not depend so much on ascending nociceptive signals from the affected region (Melzack & Loeser 1977). Indeed patients who experience thalamic strokes often experience chronic pain contralateral to the stroke site, suggesting that ischaemic thalamic cell injury and possibly cell death can paradoxically increase pain perception, and therefore that pain perception can be heavily influenced by diencephalic mechanisms (Vartiainen et al. 2016; Klit et al. 2009). Direct electrical stimulation of the ventral thalamus can evoke pain, and somatosensory thalamic neuronal firing rates are higher in the thalamus of SCI patients with chronic pain compared to those without (Lenz et al. 1993; Davis et al. 1996; Lenz et al. 1989).

Neuropathic and inflammatory pain is associated with increased burst firing in the VPL (Lenz et al. 1989; Hains et al. 2005; Hains et al. 2006; LeBlanc et al. 2017; LeBlanc et al. 2016). This increase in burst firing in SCI neuropathic pain is at least partially dependent on increased

excitability dependent on NaV1.3 upregulation in VPL neurons after nerve injury, which lumbar intrathecal administration of antisense oligonucleotides generated against NaV1.3 reverses, and also partially reverses SCI-induced mechanical and thermal allodynia (Hains et al. 2005; Hains et al. 2006).

Increased VPL burst firing is also associated with shifts in cortical oscillatory power towards theta frequencies, a neural correlate of chronic neuropathic pain (Alshelh et al. 2016; Llinás et al. 1999). Moreover, high-frequency stimulation of the VPL reverses burst firing properties and attenuates thermal hyperalgesia associated with peripheral neuropathic pain, as does pharmacologically blocking T-Type $Ca^{2+}$ channels in the VPL, suggesting that multiple types of cation channel may contribute to nociceptive bursting after injury (Iwata et al. 2011; LeBlanc et al. 2016). Conversely, increased thalamic burst firing has also been described to produce anti-nociceptive effects, (Huh & Cho 2013a; Huh et al. 2012; Kim et al. 2003). Indeed, these may reflect differences between chronic neuropathic pain and inflammatory pain, which arise from different aetiologies, as neuropathic and non-neuropathic chronic pain that similarly differ in aetiologies have been observed to produce different structural changes from one another in the thalamus (Gustin et al. 2011).

*LeBlanc et al.* showed both inflammatory hindlimb capsaicin injection or chronic neuropathic chronic constriction injury (CCI) increased VPL bursting and shifted the cortical oscillatory power towards theta frequencies (4 - 8 Hz), with TRN stimulation of VPL further increasing thalamic bursting but reversing the cortical theta in S1 and the increased mechanical sensitivity observed in both pain conditions (LeBlanc et al. 2017). This suggests a non-linear relationship between amount of VPL bursting and pain perception, though the nature of the burst events may also play a role, as experiments mimicking bursting observe that only stimulations mimicking bursts with at least three spikes, with less than 3 ms intra-burst interval were sufficient to induce anti-nociceptive behaviours (Huh & Cho 2013a).

Thalamocortical dysrhythmia, characterised by a slowing of dominant thalamocortical oscillatory activity from alpha-band frequencies (8 - 12 Hz) to slower theta-band frequencies, is thought to decrease cortical inhibitory activity that may play a role in suppression of nociceptive signalling, therefore facilitating ongoing pain (Schulman et al. 2005; Jones 2010; Alshelh et al. 2016; Llinás et al. 1999). Thalamocortical rhythmicity is thought to underlie the emergence of many brain functions, and concurrently, thalamocortical dysrhythmia has been heavily linked with many pathological conditions, including chronic neuropathic pain (Llinás et al. 1999; Alshelh et al. 2016). Though whether this dysrhythmia is specific to the chronification and is a property of injury vs pain/sensitivity remains to be fully resolved (Gerke et al. 2003) as acute nociceptive stimulation in healthy patients does not seem to invoke dysrhythmia (Alshelh et al. 2016). Potential mechanisms include altered GABAergic transmission in the thalamus, likely from the TRN, which *Zhang et al.* observed switches from a depressing synapse (paired-pulse ratio < 1) to a facilitating synapse after seven days of peripheral inflammation with Complete Freund's adjuvant (CFA), but not after one day (Zhang et al. 2017; Marini et al. 2002; Di Pietro et al. 2018; Gustin et al. 2012; Henderson et al. 2013). *Zhang et al.,* also reported lower thalamic GABA levels seven days after CFA injection compared with after one day, and intriguingly demonstrated that TRN terminal stimulation in VB increased thermal sensitivity in naive mice, but reduced thermal sensitivity in mice seven days post-CFA, as did muscimol infusion in VB (Zhang et al. 2017). This suggests maladaptive changes to both presynaptic and postsynaptic TRN-VB synaptic function as pain undergoes

chronification. Similar switches during prolonged inflammatory pain time courses have been observed in corticofugal pathways, of which the L6CT pathway innervates both the VPL and TRN (Wang et al. 2009; Jurgens et al. 2012; Crandall et al. 2015). Alternatively, thalamocortical dysrhythmia may be partially mediated by thalamic disfacilitation, as the reduction of peripheral input and associated depolarisation may promote the de-inactivation of thalamic T-Type $Ca^{2+}$ channels and activation of hyperpolarisation-activated cation currents, triggering bursts that in conjunction with the TRN mediate slow, rhythmic oscillations (Zhan et al. 1999; Jones 2010; Llinás et al. 1999; McCormick & Pape 1990).

Research where the VPL undergoes chemical ablation does not show an alteration in mechanical and thermal sensitivity until 24 and 48 hours post-insult respectively, calling into question how much VPL is necessary to mediate acute mechanical nociceptive perception (LaBuda et al. 2000). Unlike in the spinal cord, allodynia associated with peripheral inflammation does not lower the neuronal response threshold of NS neurons, suggesting that allodynia is not mediated through increased sensitivity of NS neurons in VPL (Guilbaud et al. 1987; Miraucourt et al. 2007). One recent study also showed that deep brain stimulation in VPL did not alter acute nociceptive thresholds in the naive mouse, but potently reduced thermal and mechanical sensitivity induced by chronic inflammatory and neuropathic pain respectively for the duration of VPL stimulation (Wang et al. 2016). It may be that the VPL, similarly to the role hypothesised for Aβ-mediated signalling, does not play a prominent role in acute nociceptive transduction, but undergoes plastic changes to mediate hyperalgesia associated with chronic neuropathic and inflammatory pain. Studies directly stimulating VPL in pain-free conditions are scarce. Research in humans suggest that direct electrical VPL stimulation can evoke pain sensations, but these sensations occur rarely (~2 %) and are much more commonly evoked (~17 %) in patients with pre-existing chronic pain (Lenz et al. 1993; Davis et al. 1996). Lesions of the lateral thalamus can reduce chronic pain, but also reduce tactile and proprioceptive processing, whereas medial thalamotomies result in reduction of chronic pain and spare non-nociceptive somatosensory processing, suggestive of a somewhat more specific pain-related pathway, and a degree of parallelisation in pain pathways during chronic pain (Mark et al. 1960; Mark et al. 1963; Bettag & Yoshida 1960; Spiegel et al. 1966).

Taken together, VPL as a recipient of STT inputs reliably produces both NS and WDR responses to nociceptive stimulation, undergoing modulation of activity in both acute and chronic pain. Despite this, evidence for its mediation of pain affect in the acute setting remains unsubstantial, and other candidates, both thalamic and non-thalamic, that receive from STT could plausibly mediate acute pain perception (Giesler et al. 1981; Klop et al. 2005; Mouton & Holstege 1998; Al-Khater & Todd 2009). The evidence for VPL playing a causative role in chronic pain is much stronger, though this too is somewhat tempered by similar changes to other thalamic nuclei in chronic pain states, and unspecific interventions (Whitt et al. 2013; Masri et al. 2009; Park et al. 2018; Hains et al. 2006). Indeed, statistical and cross-correlation analyses suggest that chronic pain is associated with reduced communication from VPL to S1 and increased communication from S1 to VPL, with pain-alleviating interventions reversing this activity (LeBlanc et al. 2016; Wang et al. 2007). This research supports the notion that pain, particularly chronic pain, is a percept reliant on cortical activity with thalamic contributions, and implicates cortical output pathways in regulating pain and maintaining pain perception (Kuner & Kuner 2021). Whether VPL is a direct transducer of pain perception, in the way that C fibres could be ascribed, or does so primarily through its influence on S1 and S1-mediated top-down influences on other pain regions remains incompletely resolved and

would be important for the causal understanding of pain mechanisms and the development of non-invasive therapeutic strategies for pain management (Barack et al. 2022; Kim et al. 2021; Folloni et al. 2019; Liu et al. 2021).

## 2.9. The role of the primary somatosensory cortex in pain

The mouse cortex contains ~$10^7$ neurons with ~82 billion synapses in total, resulting in approximately 8,200 synapses per neuron (Schüz & Palm 1989). The sensory cortex is a broadly uniform structure that is segregated into 6 layers (L1 - 6) based on anatomical macro-architecture (Brodmann 1909). It can be viewed as an arrangement of highly interconnected circuits, each receiving sensory data from modality-aligned regions in the thalamus in a largely parallel manner (Ringach 2021). This information arrives primarily in L4, where it is fed to pyramidal cells in L2/3. L2/3 in turn projects to deeper cortical layers 5 and 6, ultimately resulting in pyramidal cells in L5 transmitting the output of cortical circuits subcortically (Adesnik & Naka 2018; Douglas & Martin 2004; Gilbert & Wiesel 1983). There is however a growing body of literature that indicates TC activity can directly excite at least layers 4, 5 and 6 (Gilbert & Wiesel 1979; de Kock et al. 2007; Constantinople & Bruno 2013; Sermet et al. 2019; Mease et al. 2016; Clascá et al. 2012), suggesting that TC communication occurs in parallel streams to a greater extent than previously thought. Projections from sensory cortical regions along a cortical hierarchy to more associational cortical areas tend to reside in upper layers, whereas feedback from these more associational areas tends to be via neurons in deeper layers (Bastos et al. 2012; Markov et al. 2014; Felleman & Van Essen 1991; Van Essen & Maunsell 1983). The routes out of the cortex are through cortical deep layers 5 and 6. Deep layer cortex contains a multitude of different cortical output pathways that possess categorically different synaptic properties, projection patterns, and upstream partners, and until recently it has proved intractable to selectively interrogate these physiologically distinct yet intermingled neuronal populations (Whilden et al. 2021; Hoerder-Suabedissen et al. 2018; Kim et al. 2015; Takahashi et al. 2020; Shipp 2016; Sherman 2017; Shepherd & Yamawaki 2021; Casas-Torremocha et al. 2022; Adesnik & Naka 2018).

The primary somatosensory cortex (S1) is one of a handful of cortical regions whose activity is reliably altered during pain perception and therefore contributes to a so-called ‘neurological pain signature’ that purportedly helps transduce the different qualia we associate with pain (Wager et al. 2013; Coghill 2020; Tan & Kuner 2021). Nociceptive stimuli perceived as more intense are associated with greater S1 activity than those rated as not intense (Timmermann et al. 2001). More specifically, pain is associated with changes in the oscillatory state of S1 (Gross et al. 2007; LeBlanc et al. 2017; Schulman et al. 2005). Neuronal membrane potentials oscillate as a function of ion channel conductances. These fluctuations will occur along a frequency spectrum. When recording extracellularly, the recorded fluctuations with respect to a reference electrode are a composite of all the electric current contributions from the cells in the local vicinity (Buzsáki et al. 2012). As a summation of the electrical activity of neurons, the frequency and amplitude of oscillation will be influenced by the degree of synchrony of the neuronal electrical fluctuations in the recorded population (Poulet & Petersen 2008). As such, changes in oscillatory state correlate with altered neuronal population activity, and may both reflect and influence ongoing neuronal computation and behaviour (Ploner et al. 2006;

Tiemann et al. 2010; Bauer et al. 2014; Llinás et al. 1999; Alshelh et al. 2016; Cardin et al. 2009; Siegle et al. 2014; Miller et al. 2018; Lundqvist et al. 2016; Engel et al. 2001; Shin & Moore 2019). In humans, gamma oscillations between 60 - 95 Hz in S1 vary in amplitude according to perceived pain intensity, whereas stimulus intensity correlates with a drop in the alpha & beta ranges (Ploner et al. 2006; Gross et al. 2007; Heid et al. 2020; Zhang et al. 2012). However, gamma oscillations debatedly reflect attentional demands induced by pain, as visual tasks also elicit gamma oscillations in the occipital lobe, though non-nociceptive stimuli can negatively correlate with gamma (Heid et al. 2020; Tiemann et al. 2010). Gamma oscillations are classified as oscillations between 30 and 80 Hz, with 60 - 95 Hz constituting the higher end of the gamma spectrum (Buzsáki & Draguhn 2004). In rodents, inflammatory pain is associated with both increased gamma and theta in S1 (Tan et al. 2019; LeBlanc et al. 2017; Leblanc et al. 2014). Thalamocortical dysrhythmia, a theoretical framework where resting-state alpha rhythms are replaced by increased theta rhythms, has been proposed to underlie many neuropsychiatric disorders depending on the affected brain circuits, including chronic pain (Llinás et al. 1999; Schulman et al. 2005). This is supported by research reporting a slowing in oscillatory power from alpha to theta in patients with neuropathic vs without neuropathic pain after SCI (Boord et al. 2008). Interestingly, a case-study of a yoga master who claimed not to feel pain during meditation reported increased alpha activity across the somatosensory cortex specifically during meditation (Kakigi et al. 2005). The increased theta power associated with pain is also associated with increased gamma activity due to cross-frequency coupling between low and high frequency oscillations (Llinás et al. 2005). One aforementioned study by *LeBlanc et al.* observed increased theta power in S1 in both inflammatory and neuropathic pain conditions that was reversed along with mechanical sensitivity by stimulation of the TRN that potently altered burst rates in VPL (LeBlanc et al. 2017). Pain associated with thalamocortical dysrhythmia may be mediated through altered thalamic bursting, particularly bursts dependent on T-Type $Ca^{2+}$ channels, as systemic antagonism of T-type $Ca^{2+}$ channels reverses cortical theta shift in S1, as well as thermal hyperalgesia and conditioned place preference (LeBlanc et al. 2016; Walton & Llinás 2011). However, many rescue experiments were not necessarily specific to VPL - S1 pathway, so their anti-nociceptive effects cannot be conclusively attributed to reversed activity in these regions.

Anatomic evidence suggests that VPL is one of 3 distinct pathways that contain ~ 90 % of the STT fibres that will ultimately feed S1, yet these fibres represent less than ¼ of all thalamic projections to S1 (Gingold et al. 1991). Given it's peripheral inputs from somatosensory thalamic nuclei and its acceptance as a hub of somatosensory processing, a longstanding and dominant view has been that S1 mainly processes the sensory-discriminative properties of a painful experience, such as intensity and location (Melzack & Casey 1968; Bushnell et al. 1999). This arguably is not what makes pain such a debilitating and unpleasant experience, indeed it is precisely the brain circuits that mediate unpleasant experiences that are presumably activated and give pain its unpleasant experience. The transduction of the affective emotional experience associated with pain has been ascribed to cortical regions whose activity better correlates with emotional processing more generally, such as the insular or cingulate cortices (Gogolla 2017; Rainville et al. 1997; Han et al. 2003; Meda et al. 2019; Nakata et al. 2014). Indeed, electrical stimulation of the insula and secondary somatosensory cortex (S2) can demonstrably invoke pain sensations, but S1 stimulation almost always invokes somatosensory percepts perceived as not painful (Mazzola et al. 2006; Ostrowsky et al. 2002). This could be due to innervation of S1 and S2 by different regions of VPL, with VPL

shell predominantly projecting to S2, and VPL core projecting to S1, though single VPL cells branch and innervate both (Spreafico et al. 1981; Liao & Yen 2008). Alternatively this can be explained by innervation of S2 and particularly Insula by more medial thalamocortical pathways (Viaene et al. 2011; Lee & Sherman 2008; Kuner & Kuner 2021).

Pain following neuropathic injury, including phantom limb pain, is associated with cortical reorganisation in S1, and the degree of S1 reorganisation correlates highly with subjective pain intensity (Flor et al. 1995; Birbaumer et al. 1997; Lotze et al. 1999; Wrigley et al. 2009; Di Pietro et al. 2018). However, this relationship may be specific to chronic neuropathic pain, as some reports do not observe this relationship in patients with chronic non-neuropathic pain, suggesting that subjective chronic pain *per se* is not a sufficient driver of somatosensory cortical reorganisation, but that pain and cortical reorganisation can both be driven by a common cause (Gustin et al. 2012). Interestingly, the dissociation between subjective pain and the incoming signalling from the periphery mirrors dissociations in non-nociceptive sensations, as somatosensory illusions reveal that S1 activity reflects perceived stimulation rather than actual stimulation (Chen et al. 2003).

The cortex is full of cross-talk between cortical regions, and exerts top-down influences to ongoing sensory processing through cortical outputs (Garner & Keller 2022; Cao et al. 2023; Zhou et al. 2022; Liu et al. 2018; Chen et al. 2018; Tan et al. 2019; Prasad et al. 2020; Markov et al. 2014). So, whilst there is some modularisation with respect to processing of different sensory features, there is ample potential for influence by parallel circuits. For instance, the McGurk effect is a phenomenon where contextual visual information overrides and distorts the perception of a sound, such that the sound perception is inaccurate with respect to the auditory stimulus (self-reported perception changes from correct ‘ba’ to incorrect ‘va’ sound) (McGurk & MacDonald 1976). This example illustrates that integration of sensory information from one modality does not occur independently of other modalities and suggests that the seemingly discrete auditory and visual components of perception are in fact not discrete but can causally influence one another. In short, it is not the case that you decipher an auditory feature in the auditory circuit and a visual feature in the visual circuit only to then combine them for a unified experience containing the two qualia: instead, what you see affects what sound you hear. This phenomenon has recently been ascribed to cross-talk between auditory and visual cortical regions (Garner & Keller 2022), highlighting the potential for one specialised cortical region to heavily influence the processing in another. In the context of pain, *Zhou et al.,* discovered a pathway from the auditory cortex that projected to somatosensory thalamic nuclei and altered nociceptive mechanical sensitivity. In this example, it appears that sound affected how mice felt a nociceptive mechanical stimulus. Intriguingly, the modulation to mechanical sensitivity lasted multiple days, so merely the history of sound was sufficient to induce long-lasting changes in pain thresholds (Zhou et al. 2022). This example also demonstrates not only that cortical regions can influence each other, but that one cortical region can influence what information another cortical region receives with which to perform computations. Indeed, corticospinal neurons project directly to the dorsal horn from prefrontal cortex (PFC), anterior cingulate cortex (ACC), and S1, with activity along one of these pathways likely altering the ascending nociceptive information to many brain regions (Chen et al. 2018; Liu et al. 2018; Galea & Darian-Smith 1994; Moreno-Lopez et al. 2021). The function of top-down modulation of dorsal horn may be to impart associative learning on dorsal horn neurons. Visual cues that predict nociceptive stimuli alter dorsal horn responses to the nociceptive stimulus, and NS neurons in the medullary dorsal horn have even been reported to respond to a visual cue in

the absence of added somatosensory input if the visual cue is highly predictive of a nociceptive stimulus (Duncan et al. 1987; Dubner et al. 1981). Whilst attentional mechanisms are likely involved and have been demonstrated to alter spinal nociceptive responses and pain, this suggests that multimodal associations can influence the earliest possible synapse within the processing of a given modality (Sprenger et al. 2012; Hayes et al. 1981). It is therefore somewhat plausible that although the longstanding purported role of S1 is to resolve sensory-discriminative features of tactile stimuli, prior associations and cross-modal wiring may mean that the somatosensory rendering of a stimulus directly contributes to the emotional weighting associated with it, echoing Sherrington that, "*mind rarely, probably never, perceives any object with absolute indifference, that is, without 'feeling*'" (Sherrington 1900). Research that investigates direct effects of S1 subpopulations on responses to nociception is still in its early infancy, but studies report that S1 projects via the cortico-spinal tract to dorsal horn neurons, and have demonstrated that these neurons contribute to increased mechanical sensitivity during neuropathic allodynia (Liu et al. 2018; Frezel et al. 2020). This corroborates earlier reports that cortico-subcortical disinhibition in S1 facilitates acute inflammatory pain behaviours but inhibits pain behaviours associated with chronic inflammation (Wang et al. 2009). Gamma oscillatory activity in S1 correlates with inflammatory pain, coincides with paw withdrawal from acute nociceptive stimuli, and importantly, when optogenetically induced causes aversive behaviours in naive mice (Tan et al. 2019). This further supports a potential role of S1 modulation of pain affect and displeasure, having been previously established that S1 is reliably activated during nociceptive stimulation (Wager et al. 2013; Gross et al. 2007; Timmermann et al. 2001; Ploner et al. 2000; Wang et al. 2007; Coghill 2020; Tan & Kuner 2021). Whether and to what extent alteration to affect occurs predominantly through cortico-cortical or cortico-subcortical means is not completely resolved. However, it seems plausible and perhaps likely that S1 modulates affective responses to sensory stimuli through its cross-talk and top-down influences.

Taken together, evidence strongly suggests that S1 transduces sensory-discriminative qualia in pain perception, but also implies that S1 can weight affective valence of pain through its influences on the activity of emotion-processing circuitry. Whether it does this predominantly through cortico-cortical routes or through cortico-subcortical routes remains to be fully elucidated, but the research presented here demonstrates a powerful capacity for S1 to modulate pain sensitivity and affect through two distinct cortico-subcortical pathways.

# 3. Methods

## 3.1. Ethics Statement

The local governing body approved all of the following experimental procedures (Regierungspräsidium Karlsruhe, Germany, approval numbers: 35-9185.81/G-29/16, 35-9185.81/G-70/21, T-39-20, 35-9185.82/A-8/20) and procedures were performed to their ethical guidelines.

## 3.2. Animals

Mice (male and female, 7-16 weeks of age) were housed with food and water ad libitum on a 12 h light/dark cycle (housing conditions 20-22 °C, 40-65 % humidity).

### 3.2.1. Mouse lines

#### Layer 6 optogenetic stimulation:

"Ntsr1-Cre" (B6.FVB(Cg)-Tg/(Ntsr1-cre)GN220Gsat/Mmucd)
"Ntsr1-Cre-ChR2-EYFP"; crossbreed between "Ntsr1-cre" x "Ai32" (B6.FVB(Cg)-Tg/(Ntsr1-cre)GN220Sat/Mmucd x B6.129S-Gt(ROSA)26Sortm32(CAG-COP4*H134R/EYFP).

#### Layer 5 optogenetic stimulation:

"Rbp4-Cre" (B6.FVB/CD1-Tg(Rbp4-cre)KL100Gsat/Mmucd)

## 3.3. Virus injection and optical fibre implantation

Katharina Ziegler injected Ntsr1-Cre and Rbp4-Cre mice stereotaxically with an excitatory opsin (AAV2-EF1a DIO-ChR2(H134R)-EYFP-WPRE-pA, 5.7 x $10^{12}$ vg/ml, Zürich vector core), an inhibitory opsin (AAV1-hSyn-SIO-stGtACR2-FusionRed, 2.1 x $10^{13}$ vg/ml, Addgene), or a control virus (AAV2-hSyn-DIO-EGFP, 100 µL at titer ≥ 3 ×$10^{12}$ vg/mL, Addgene). A subset of the optogenetic L6CT experiments involved Ntsr1-Cre-ChR2-EYFP mice, which did not receive virus injections. Analysis revealed no discrepancies between Ntsr1-Cre-ChR2-EYFP mice and virus-injected Ntsr1-Cre experiments, so this data was pooled. The viral expression period spanned 3 to 4 weeks.

During injection and implantation procedures, mice were secured in a stereotaxic frame (Kopf Instruments) and anaesthetised using 1.2-2.0 vol % isoflurane in medical oxygen at a flow rate of 0.8 L/min, whilst maintaining a body temperature of 39 °C. Subcutaneous administration of Carprofen (5 mg/kg, CP-Pharma) and local anaesthesia via Lidocaine injections (Xylocain 1 %, Aspen Pharma) around the scalp and fixation ear bars were administered. Ointment (Bepanthen, Bayer) was applied to shield the eyes from drying during surgery. Upon confirmation of the absence of tail and toe pinch reflexes, a midline incision was made on the skin. The periosteum and aponeurotic galea were removed to expose anatomical reference points (bregma and lambda), and the head was aligned to the stereotaxic frame. Small craniotomies were drilled above the S1-HL, and using calibrated glass micropipettes (Blaubrand; IntraMARK), viral particle solutions were injected into two sites within S1-HL, at specific coordinates relative to bregma (AP, ML) and pia mater (DV):

First injection: ML= +1.4 mm, AP = -0.46 mm; second injection: ML= +1.5 mm, AP = -0.94 mm. Ntsr1-Cre mice were injected at depths of -0.9 and -1.0 mm, whilst Rbp4-Cre mice were injected at depths of -0.7 and -0.8 mm (100 nl at each depth, followed by a 10-minute waiting period before relocating the injecting pipette).

Katharina Ziegler implanted chronic optical fibres (200 µm diameter, numerical aperture of 0.39, Thorlabs GmbH) that were positioned on the dura above the S1-HL (ML = +1.5 mm, AP = -0.94 mm), and the ceramic ferrule housing the optical fibre was affixed to the skull using dental cement. To prevent laser light leakage, the cement was coloured black, and during experiments, the mating sleeve was shielded with black tape. Mice were housed for a period ranging between three and four weeks to ensure optimal viral expression before subsequent experiments.

## 3.4. Histology and immunohistochemistry

My colleagues (for behavioural experiments) and I (electrophysiological experiments) humanely euthanised the mice through transcardial perfusion using a solution of 4 % paraformaldehyde (PFA) in phosphate-buffered saline (PBS). We sliced the brain tissue into 80 µm sections using a vibratome (Thermo Scientific Microm HM 650 V). We treated specific sections with DAPI staining, affixed them with Mowiol mounting medium, and visualised them using an epifluorescent microscope (Leica DM6000).

## 3.5. Behaviour

Behavioural assessments took place within the light cycle, and the animals' experimental identities were blinded to those conducting the experiments. Behaviour was planned as a group, with von Frey performed by Katharina Ziegler and Jan Burghardt, and Antonio Gonzalez performing CPP/CPA and Hargreaves tests.

### 3.5.1. Optogenetic stimulation

The implanted fibre was connected to an optical patch cord from Thorlabs GmbH, linked to a laser output module (473 nm) supplied by Shanghai Laser Optics Century Co., Ltd. The power of the laser at the fibre tip was quantified using a power energy metre from Thorlabs GmbH. Irradiance levels for layers 5 and 6 were approximated based on established measurements in mammalian brain tissue (Deisseroth 2012). With an initial measurement of 10 mW at the fibre tip (fibre NA = 0.39; fibre radius = 100 µm), the calculated irradiance is 318.18 mW/mm². This translates to 3.47 mW/mm² at the depth of L5 (0.75 mm cortical depth) and 1.54 mW/mm² at the depth of L6 (1 mm cortical depth).

### 3.5.2. Laser protocols

Optical stimulation blocks for experiments involving mechanical stimulation were interspersed with at least 30 s non-stimulation blocks. Single laser pulse trial length was 5 s and consisted of continuous laser stimulation. Katharina Ziegler or Jan Burghardt applied mechanical stimuli and Antonio Gonzalez thermal stimuli during laser pulses.

### 3.5.3. Measurements to determine individual paw lifting laser intensity thresholds

Katharina Ziegler administered laser stimuli (continuous for 5 seconds) at intensities of 10, 8, 6, 4, 2, and 0 mW (corresponding to 318.18, 254.55, 190.91, 127.27, 63.64, 0 mW/mm²), conducting five trials at each intensity level and calculating the likelihood of paw lifting for each intensity (refer to **Fig. 2b**). From these trials, she identified, for each mouse, the highest intensity that did not elicit paw lifting. This individualised laser intensity was then employed in sensitivity measurements for mechanical and thermal stimuli. No laser-induced paw lifting was observed for Rbp4-Cre mice injected with DIO-ChR2-EYFP at any of the tested power outputs.

### 3.5.4. Inflammatory pain model

Colleagues or I subcutaneously injected 20 µl of Complete Freund's adjuvant (CFA) into the left hindpaw during isoflurane-induced anaesthesia. The following day, colleagues performed behavioural experiments with the CFA cohorts (von Frey and CPP).

### 3.5.5. von Frey tests

Katharina Ziegler or Jan Burghardt habituated the mice with the von Frey test chamber twice daily for an hour over three consecutive days, absent any von Frey filament stimulation. Each von Frey test session commenced with a 15-minute acclimatisation period. They assessed mechanical sensitivity based on the probability of paw withdrawal upon application of von Frey filaments (Aesthesio Precise Tactile Sensory Evaluator, Ugo Basile S.R.L.) to the plantar surface of the left hindpaw (contralateral to the stimulated HL cortex). They administered eight filaments, ranging from 0.04 to 2.0 grams of force, five times in ascending order, with a minimum 30-second interval between applications. If one filament induced withdrawal responses in all five trials, resulting in a 100 % withdrawal probability, further sensitivity measurements for higher force filaments were ceased. Initial mechanical sensitivity measurements were conducted without laser stimulation (baseline). Subsequently, after a minimum of 1 hour in the home cage, they repeated the test with laser stimulation lasting 5 seconds per trial targeting S1-HL. The mechanical stimulus was delivered within 1 second following the onset of the 5-second laser stimulation. Withdrawal responses were only considered during the 5-second laser stimulation. They performed additional set of tests (baseline and laser) one day post a subcutaneous injection of CFA in the left hindpaw.

### 3.5.6. Thermal tests

Antonio Gonzalez conducted thermal sensitivity evaluations using the Hargreaves apparatus (Ugo Basile Inc., Italy) featuring an infrared heat laser (Model 37370-001, Ugo Basile). The laser targeted the plantar surface of the left hindpaw, emitting increasing levels of radiant heat. To prevent paw damage, the intensity was capped at 35, and a cut-off time of 20 seconds was set. He applied three heat stimulation trials alone, and then in the presence of optogenetic laser stimulation (238.64 mW/mm²), with 3 min of recovery time between trials. He measured the paw withdrawal latency per trial.

### 3.5.7. Conditioned place preference/aversion (CPP/CPA) test

The experimental configuration comprised two chambers, each measuring 15 cm x 15 cm, separated by a neutral chamber of 8 cm x 8 cm dimensions. One chamber was decorated with vertical stripes and a cherry scent, whilst the other horizontal stripes and a honey scent. This

paradigm involved either one session (CPP) or five sessions (CPA) as baseline, succeeded by two conditioning sessions, each lasting 20 minutes. Prior to each session, Antonio Gonzalez gently anaesthetised the mice using isoflurane and secured them to an optic fibre cable, keeping them in a neutral chamber via removable wall slides. Once they recovered from anaesthesia, he removed the wall slides to commence the session. During baseline sessions, no optogenetic stimulus was administered. However, in the conditioning sessions, he applied optogenetic stimulation (8 mW, 254.55 mW/mm$^2$, 20 Hz) when the animal entered the chamber where it previously spent less time (for CPP) or more time (for CPA) during the final baseline session. Pulsed stimulation at 20 Hz was chosen to mitigate potential phototoxic effects from prolonged stimulation necessary for this paradigm. The movement and duration of the animals in each chamber throughout every session were tracked using AnyMaze software (Version 7.1, Stoelting Co., Ireland). To evaluate performance outcomes, he made comparisons between the time spent in the chamber paired with stimulation during the last conditioning session and the time allocated to that same chamber during the last baseline session. Preference indices (PI) were calculated using the following formula: (time in paired chamber - time in unpaired chamber)/(time in paired chamber + time in unpaired chamber).

### 3.5.8. Data and statistical analysis of behaviour

Behavioural data are presented as mean values accompanied by the standard error. Antonio Gonzalez performed statistical analyses using SPSS (Version 28.0.1.0) and R Studio (Version 4.2.0). Unless specifically mentioned, he employed two-way ANOVA for repeated measures with Bonferroni tests for multiple comparisons. Significance was established at a p-value below 0.05. Microscopy images underwent adjustments using Fiji/Image J (Version 1.53c), whilst schematics and figures were collectively crafted using Affinity Designer (Version 1.10.6), GraphPad Prism (Version 9.1.1), and Matlab 2022a by Katharina Ziegler, Jan Burghardt, Antonio Gonzalez and me.

## 3.6. *In vivo* electrophysiology

### 3.6.1. Anaesthetised *in vivo* electrophysiology

I anaesthetised the mice using Urethane (1.4 g/kg, i.p.) and maintained anaesthesia using an oxygen-isoflurane mixture (0.2 %). I securely positioned each mouse with ear bars and levelled the skull. I performed a craniotomy above the well site, and a well, filled with isotonic Ringer's solution, was cemented in place using Paladur. I carefully inserted Silicon probes with 64 sharpened channels (impedance ~50 kOhm) (Cambridge Neurotech) into the S1-HL cortex (ML = +1.67 mm, AP = -1.0 mm, DV = -1.4 mm) and/or VPL (ML = +1.8, AP = -1.3, DV = -4.5) using a micromanipulator (Luigs Neumann 3-axis Motor) at a rate of approximately 2 µm/s. I connected the probes to a RHD2164 headstage amplifier chip (Intan technologies) via a connector (ASSY-77) and an adaptor (A64-Om32x2 Samtec). Signals were amplified and digitised at a sampling rate of 30,030 Hz using an RDH2000 Intan evaluation board through a

USB 2.0 interface. Data acquisition was performed using an Intan Talker module (Cambridge Electronic Devices, Cambridge, UK) with Spike2 (v9.06) software.

### 3.6.2. Awake *in vivo* electrophysiology

I recorded mice aged between 8 to 12 weeks on a cylindrical treadmill composed of a 15 cm diameter foam roller affixed to a custom-made low-friction rotary metal axis linked to two vertical posts. Approximately 2 to 3 weeks prior to these recordings, Katharina Ziegler and I stereotaxically injected Ntsr1-Cre and Rbp4-Cre mice with either an inhibitory opsin (AAV1-hSyn-SIO-stGtACR2-FusionRed, 2.1 x $10^{13}$ vg/ml, Addgene) or an excitatory opsin (AAV2-EF1a DIO-ChR2(H134R)-EYFP-WPRE-pA, 5.7 x $10^{12}$ vg/ml, Zürich vector core), as detailed in the "Virus injection and optical fibre implantation" section,. About a week before recording sessions, I fixed a polycarbonate two-winged head plate onto the skull using dental cement (Super-Bond, Sun Medical Co. LTD). A rubber ring was also cemented around the craniotomy to create a small reservoir for the reference electrode. Post-surgery, mice had a recovery period of 2 days, and I subsequently habituated them to the cylindrical treadmill in a Faraday cage over the following 4 days. During these habituation sessions, which lasted around 60 minutes, the mice freely ambulated on the cylindrical treadmill and were rewarded with sweetened condensed milk. Within 24 hours prior to recording, I performed a craniotomy above the injection sites and sealed the rubber well with silicon elastomer (Kwik-Cast, World Precision Instruments) until the experiment. During the recording session, I removed the protective silicon, and inserted an acute silicon optrode (H3, Cambridge Neurotech) into the S1-HL. I used the recording apparatus and software described in the section "Anaesthetised in vivo electrophysiology" to capture neural activity.

### 3.6.3. Mechanical stimulation during anaesthetised *in vivo* electrophysiology

I determined target regions by applying mechanical stimulation to the hindpaw using either a brush or cotton swab and assessing the resulting evoked activity via the Spike2 visual interface. Mechanical stimulation was automated via a Spike2-prepared stimulation protocol interfaced with hardware (Power1401, Cambridge Electronic Design, Cambridge, UK) controlling stepper controller (Mercury Step C-663 Stepper Motor Controller, PIMikroMove Version 2.25.2.0). For mechanical stimulation I used nine short nylon filaments affixed (Pattex Sekundenkleber) to a force sensor (Single Tact miniature force sensor), connected to a stepper motor. A TTL pulse activated these von Frey filaments, exerting pressure on the paw, and relaying pressure data to the Intan board. A cumulative pressure of 9 grams (9 x 1 gram per filament) was applied for 5-second intervals, repeated every 60 seconds, based on a specified protocol (Hohmann et al. 1995).

### 3.6.4. Optogenetic stimulation during anaesthetised and awake *in vivo* electrophysiology

I placed an optical fibre (Thorlabs GmbH, NA = 0.22; radius = 52.5 µm) 0.5 mm perpendicular to the craniotomy site. Laser power densities overlapped with those used in the behavioural experiments (ranging from ~0.5 to 27 mW at the fibre tip, translating to 57.72 to 3105.34 mW/mm², and 0.26 to 14.16 mW/mm² at the L6 level as per reference (Deisseroth 2012)). Light pulses were automatically triggered via an Omicron Light-Hub2 (wavelength = 488 nm) by a stimulation protocol set up in Spike2 through interface hardware (Power1401, Cambridge

Electronic Design, Cambridge, UK). The number of trial repetitions per condition varied depending on experiments, ranging from 31 to 52 trials for VPL recordings to 10 (in the single case for 5 different laser powers) to 32 for S1 recordings.

### 3.6.5. Stimulation protocol during anaesthetised and awake *in vivo* electrophysiology

I split the experimental design into three distinct stimulus conditions, each lasting 5 seconds: cycling through mechanical stimulation, mechanical stimulation coupled with optogenetic laser activation, and exclusive optogenetic laser stimulation. Between the mechanical and mechanical + laser conditions, a time gap of 60 seconds was maintained, whilst for other conditions, the interval between stimuli was 30 seconds (as depicted in **Fig. 3b**). During awake recordings, the stimulation solely comprised 5 second laser stimuli, occurring every 15 seconds.

### 3.6.6. Spike sorting

Voltage data underwent band-pass filtering upon initial acquisition (0.1-10,000 Hz or 500-5000 Hz). Subsequently, I converted Spike2 data files (.smrx) into binary files through a conversion process that comprised reading the electrophysiology channels within the .smrx file, converting them back to uint16 values from the 16-bit depth analog-to-digital (ADC), and then writing this information into the resulting .bin file. I carried out Spike sorting procedures in a semi-automated manner using Matlab-based Kilosort 2.5, followed by manual curation of resulting clusters in Phy2 (available at https://github.com/cortex-lab/phy). I selected single-units meeting specific criteria - having less than 0.5 % refractory period violations (within 1 ms) and a baseline spike rate greater than 0.1 Hz - for further analysis. I used the following Kilosort 2.5 parameters:

| Parameter | Value | Parameter | Value |
|---|---|---|---|
| ops.fs | 3.003003003003003e+04 | ops.sigmaMask | 30 |
| ops.fshigh | 600 | ops.ThPre | 8 |
| ops.Th | [10 2] | ops.sig | 20 |
| ops.lam | 10 | ops.nblocks | 0 |
| ops.AUCsplit | 0.7 | ops.spkTh | -6 |
| ops.minFR | 1/50 | ops.reorder | 1 |
| ops.momentum | [20 400] | ops.nskip | 35 |
| ops.GPU | 1 | ops.Nfilt | 1024 |
| ops.nfilt_factor | 4 | ops.ntbuff | 64 |

| | | | |
|---|---|---|---|
| ops.NT | 64*1024+ ops.ntbuff | ops.whiteningRange | 32 |
| ops.nSkipCov | 25 | ops.scaleproc | 200 |
| ops.nPCs | 6 | ops.useRAM | 0 |

## 3.6.7. Putative cell-type classification

### 3.6.7.1. Thalamic units:

I identified VPL units based on specific criteria. I verified the probe location within VPL through histological examination. (**Fig. 3a**): The recording process involved the identification of the dorso-lateral channels containing units that exhibited significant responses to either mechanical (M) or mechanical + laser (ML) conditions. All units within this determined range were classified as VPL units.

### 3.6.7.2. Cortical units:

I aligned the recording channels from silicon probes with histological layer demarcations to attribute each unit a specific cortical depth and layer (refer to examples in **Fig. 1a & b**). I identified units presumed to be L6CT and L5 based on their response characteristics to laser light pulses, exhibiting low first-spike latency (< 9.5 ms) and jitter (< 3 ms L5, < 2 ms L6CT) (see **Fig. 1d & e**). I categorised fast-spiking (FS)-like units by their peak-to-second trough latency (< 215 µs (Schmitt et al. 2017)), and consequently excluded them from the optotagged populations. All further electrophysiological analyses encompassed putative FS and RS units.

I verified optotagged units by plotting these units based on their depth along the cortical axis, illustrating the expected positioning of optotagged L5 and L6CT neurons within layers 5 and 6, respectively (refer to **Fig. 1f**).

For the data in **figures 8 - 12**, I did not use waveform parameters to separate units by waveforms: there seems to be no consensus on appropriate parameter values, there is some evidence that waveform features vary between regions, and no ground truth data was collected with which to benchmark any criteria I would employ (Anastassiou et al. 2015; Yu et al. 2019; Schmitt et al. 2017; Barthó et al. 2004; Halassa et al. 2014; Cardin et al. 2009; Madisen et al. 2012).

## 3.6.8. Spike train analysis

Following spike-sorting, Dr. Rebecca Mease and I aligned spike times to stimulus onsets and segregated them into stimulation conditions utilising customised scripts in Matlab 2022a. To enhance clarity in the visual representation presented in **Figs. 3 and 4**, we generated peristimulus time histograms (PSTHs) (with a bin size of 20 ms) and subsequently smoothed them using a Matlab port (https://github.com/iandol/spikes/tree/master/Bars) of the Bayesian Adaptive Regression Splines technique (Wallstrom et al. 2008) using default parameters except for prior_id = 'POISSON'. We conducted all further calculations and analyses on the original, unsmoothed data.

#### 3.6.8.1. Response windows

Dr. Rebecca Mease and I quantified spike counts and timings within a defined time frame of 1.5 seconds following the stimulus onset, augmented by an additional 500 milliseconds to accommodate any delayed activation linked to the mechanical stimulus in relation to the command signal. We measured baseline activity during a period of 1.5 seconds preceding the stimulus onset, as depicted in **Figs. 3b and 4a**. To ensure the elimination of transient effects occurring at stimulus onset (such as the PSTH peak in **Fig. 4d**, L6 - bottom right), and to facilitate a comparison between L and ML conditions, we also examined laser-only trials within the same time windows.

#### 3.6.8.2. Unit modulation

Dr. Rebecca Mease and I considered units in a given stimulus condition as modulated when a significant difference was measured between baseline and stimulus-evoked spiking. We calculated this modulation either based on absolute spike counts (determined through the signed-rank test for paired baseline and stimulus-evoked trials with $p \leq 0.05$) or by evaluating spike timing utilising the ZETA test (Montijn et al. 2021).

#### 3.6.8.3. Response parameters

Dr. Rebecca Mease and I compared single-unit activity across L, M, and ML conditions, utilising both spike counts and inter-spike interval (ISI) statistics to encompass overall spike output and spike timing characteristics. We computed mean spiking rate ($\bar{r}$) as the average spike count per trial, divided by the response window duration of 1.5 s. We computed response probability (RP) as (trial count with at least one spike)/(total trial count), measured within the 1.5 s response window.

#### 3.6.8.4. Spike train statistical analysis

All statistical analysis was done in Matlab 2022a or R, using built-in or custom-written functions. Unless explicitly specified, data was analysed by two-way repeated measures ANOVA with a Bonferroni test. See Supplementary Table 1 for exact statistical tests and test outputs (*F*- and *p*-values). Paired MI and $\bar{r}$ data across conditions (per region) were analysed using the Friedman test, followed by a Wilcoxon signed-rank test. MI and $\bar{r}$ comparisons across regions (Supplementary Table 1) were performed using a mixed-model ANOVA followed by a rank sum test for pairwise differences. To assess the proportion of positively, negatively, or unmodulated units within each stimulation condition, $X^2$ proportions tests were performed, and subsequent Marascuillo procedure for multiple comparisons. Statistical differences in the proportions of responsive units across conditions were evaluated by McNemar's test in cases of paired data or two-proportions $X^2$ tests in cases of unpaired data (custom written), e.g. between cortical layers.

For the modulation index analysis in **Figs. 8d and 9c**, I restricted the considered analysis stimulus windows to the final 2 seconds of each 5 second pulse. I calculated modulation index (MI) as MI = $(\bar{r}_{stimulus}-\bar{r}_{baseline})/(\bar{r}_{stimulus}+\bar{r}_{baseline})$ as in (Onodera & Kato 2022). I classifed high L6CT conditions as laser intensity > 382mW/mm², and low L6CT as laser intensity <= 382mW/mm². I used Wilcoxon signed-rank tests for single-unit MI comparisons between conditions, and Wilcoxon rank sum tests for MI comparisons between groups.

### 3.6.8.5. Population synchrony quantification

After identifying the units belonging to each subpopulation (see **Fig. 2a**), I constructed triggered PSTHs for each condition across the 5 second condition duration. This resulted in a unit-by-bin-by-trial matrix for each condition, with each time bin containing a value of spike counts. The value in each bin denotes that for a given unit during a given trial, the unit spiked n times within a given time period, with a value of 0 denoting that the unit did not spike. By transforming the matrix such that n > 0 = 1, the bins in this 'Coactivity PSTH' now denote whether the unit participated at all for a given time bin in a given trial. The sum of the bins across units constitutes a measure of coactivity for the population at a given time period for a given trial. The coactivity measure for a given PSTH was calculated as the mean coactivity across the bins where at least one unit during that time period was active. The coactivity measure per condition is very sensitive to how many bins each trial is partitioned into and differs between optogenetic stimulation conditions. I leveraged this difference by plotting Coactivity PSTHs for a range of bin sizes from 0.1 ms to 2.048 seconds. The coactivity measures for each condition changed as the bin sizes increased, but the rate of change differed between conditions. This too is still overly sensitive to the choice of bin size, so the final step was to plot the change in coactivity divided by the change in bin size to give a curve where the maximum value is a representation of the increase in bin size necessary to capture the greatest increase in average coactivity. The higher the score the closer a population's neurons tend to spike together.

### 3.6.8.6. Thalamic burst identification

I classified thalamic bursts as 2 or more spikes that each do not exceed 6 ms inter-spike-intervals, which are preceded by at least 50 ms prior silence, and do not exceed 100 ms total duration. These parameters were based on the ones used to study nociceptive signalling in VPL by *Hains et al.* but with a stricter inter-spike interval (ISI) threshold and a pre-burst silence to reflect prior hyperpolarisation necessary for T-Type $Ca^{2+}$ channel availability (Hains et al. 2006; Zhan et al. 1999).

For the determination of burst probability (BP) among single-units in **Fig. 3h & i**, Dr. Rebecca Mease and I considered spikes occurring within an inter-spike-interval of less than 5 milliseconds as part of a burst. BP was then computed as total burst events/(total burst events + total single spike events). Modulation index (MI) was calculated as MI = $(\bar{r}_{stimulus}-\bar{r}_{baseline})/(\bar{r}_{stimulus}+\bar{r}_{baseline})$ as in (Onodera & Kato 2022). Data is presented as (first quartile, median, third quartile) or mean ± S.E.M.

# 4. Cortical Output Layers Modulate Sensory and Affective Nociceptive Perception

## 4.1. Introduction

Cortical output layers 5 and 6 of primary sensory cortices have been implicated in causally altering sensory perception (Takahashi et al. 2020; Voigts et al. 2020; Guo et al. 2017; Ahrens et al. 2015). These studies take advantage of advances in cell-type specific expression of light-activated ion channels to selectively excite or inhibit neuronal populations with sub-millisecond temporal precision (Mahn et al. 2018; Gerfen et al. 2013; Gong et al. 2007; Boyden et al. 2005; Nagel et al. 2003; Nagy 2000). However, selective perturbation of L6CT and L5 populations on sensory perception is rarely co-investigated (Gan et al. 2022; Zhou et al. 2022).

Moreover, S1 L6CT and L5 have not been specifically investigated in the context of pain perception and pathology, of which the neural underpinnings remain incompletely resolved (Kuner & Kuner 2021). Motivated by past work delineating the influence of cortical output pathways on sensory processing across modalities (Wang et al. 2009; Guo et al. 2017; Voigts et al. 2020), my colleagues and I therefore sought to dissect how L6CT and L5 pathways contribute to pain perception.

To experimentally address this question, we combined in vivo electrophysiology, behavioural readouts, and targeted manipulation of L6CT and L5 populations. In brief, we expressed excitatory or inhibitory opsins in L6CT or L5 to either excite or inhibit these neuronal populations during mechanical nociceptive peripheral stimulation or behavioural assays. I recorded extracellular electrophysiological signals to quantify neuronal responses to nociceptive peripheral hindlimb stimulation and how neuronal population activity changed with optogenetic manipulation of these two populations.

## 4.2. Reliable expression and control of ChR2 in S1 L6CT and L5

Transgenic mouse lines in combination with viral vectors are a relatively recent advent and are valuable tools in labelling and dissecting neuronal circuitry with cell-type specificity (Mahn et al. 2018; Gerfen et al. 2013; Gong et al. 2007; Boyden et al. 2005; Nagel et al. 2003; Nagy 2000). To investigate how L6CT and L5 neuronal populations alter pain behaviours and somatosensory neuronal circuitry, the Ntsr1-Cre and Rbp4-Cre mouse lines were employed respectively. Katharina Ziegler induced expression of Channelrhodopsin-2-EYFP in L6CT cells through injection of a AAV-DIO-ChR2-EYFP viral vector in S1 hindlimb cortex (S1-HL) of Ntsr1-Cre mice (**Fig. 1a**), or by cross-breeding Ntsr1-Cre mice with ChR2-EYFP mice. She employed the same approach in Rbp4-Cre mice to attain ChR2-EYFP expression in L5 cells (**Fig. 1b**). To confirm reliable, temporally precise optogenetic excitation of these specific

neuronal populations, I activated ChR2 by administering blue light during 64-channel electrophysiological recordings in S1 of L6-ChR2 or L5-ChR2 mice under low-dose urethane anaesthesia (**Fig 1.c**). I identified putative L6-ChR2 (**Fig. 1d**) and L5-ChR2 (**Fig. 1e**) neurons based on low first-spike latency and low standard deviation of first-spike latency to repeated 10 ms light pulses given in a high-frequency stimulation train. In concordance with the histological stainings, 'tagged' L5-ChR2 units resided at more superficial electrode depths compared with L6-ChR2 units (**Fig. 1f**). Increasing the light intensity emitted from the fibre-optic cable induced increasingly higher sustained firing in these tagged units (**Fig. 1g**), as well as increasing the total number of tagged units (**Fig. 1h**).

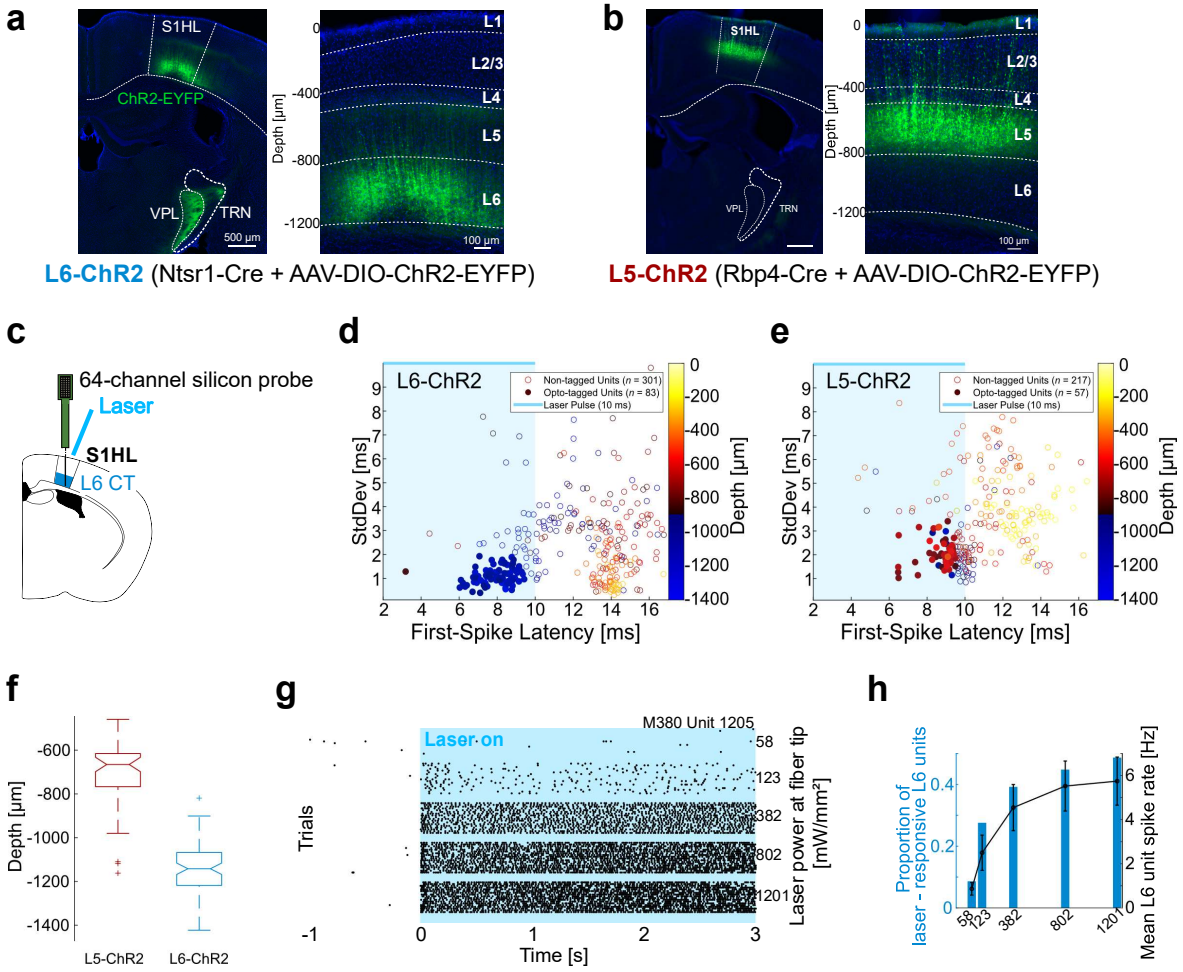


**Figure 1: Transgenic expression of ChR2 enables reliable, specific manipulation of distinct cortical subpopulations with high temporal specificity.**

**(a)** L6-ChR2 mouse showing ChR2-EYFP-expression (green) in S1-HL L6CT neurons and their axons in the ventral posterolateral thalamus (VPL) and thalamic reticular nucleus (TRN). L6CT neurons depth-registered relative to S1-HL layer borders (right panel, dashed lines, estimated based on soma sizes and densities using DAPI signals, blue). Representative example from *n* = 21 mice.

**(b)** S1-HL L5-ChR2 mouse showing ChR2-EYFP-expression (green) in S1 L5 neurons. S1 L5 neurons depth-registered relative to S1-HL layer borders (right panel, dashed lines, estimated based on soma sizes and densities using DAPI signals, blue). Representative example from *n* = 19 mice.

**(c)** Schematic of 64-channel recording and fibre optic optogenetic stimulation in S1-HL.

**(d-f)** 10 Hz optogenetic trains (10 ms pulse length) were given to Ntsr1-Cre-ChR2-EYFP mice (*n* = 3 mice) or Rbp4-Cre-ChR2-EYFP (*n* = 2 mice) as part of a 5 second on 5 second off protocol (> 1000 pulses in total per mouse). Mean first-spike latencies and standard deviations of these first spike latencies to all 10 ms laser pulses were calculated for every single-unit from a pooled dataset of each mouse line.

**(d)** Scatter plot of mean first spike latency and standard deviation of first spike latency in S1-HL of L6-ChR2 mice (*n* = 3). Tagged units (83/384 - filled circles) were assigned by mean latency < 9.5 ms and standard deviation < 2 ms.

**(e)** Scatter plot of mean first spike latency and standard deviation of first spike latency in S1-HL of L5-ChR2 mice (*n* = 2). Tagged units (57/274 - filled circles) were assigned by mean latency < 9.5 ms and standard deviation < 3.5 ms.

**(f)** Box and Whisker plot of Opto-tagged unit depths for L5-ChR2 and L6-ChR2 data in **(d)** and **(e)**. The median L6-ChR2 unit depth was -1157.5 µm (IQR = 150.75 µm), and the median L5-ChR2 unit depth was -665.5 µm (IQR = 151.5 µm).
**(g)** Example raster plots for a laser-responsive L6CT unit (depth = 1205 µm) exposed to increased light intensity.
**(h)** Blue bars: fraction of laser-responsive L6 units (from *n* = 232 L6 units total) as a function of laser power. Black: corresponding mean spike rate (mean ± SEM, *n* = 92 units; mean depth ± SD = 1194 ± 141 µm). Data from a representative experiment (*n* = 3 mice).
Data from Katharina Ziegler, Rebecca Mease, and Ross Folkard. Figure contains panels adapted from *Ziegler et al.* (Ziegler et al. 2023).

## 4.3. S1 L6CT excitation is pro-nociceptive

L6CT modulation is known to alter sensory discrimination and detection thresholds (Guo et al. 2017), and has been studied in the somatosensory system before, but specific manipulation of S1 L6CT cells had never before been investigated in the context of pain. As such, Katharina Ziegler implanted mice with optical fibres (**Fig. 2a**) to assess pain behaviours in freely moving Ntsr1-Cre mice injected with AAV-DIO-ChR2-EYFP in S1-HL. One surprising observation was that high intensity light stimulation induced nocifensive-like behaviours in L6-ChR2 mice absent additional peripheral stimulation of any kind. This paw withdrawal and limb shaking was specific to the limb that corresponded somatotopically with the ChR2 expression, i.e. unilateral ChR2 stimulation in S1-HL induced withdrawal in the contralateral hindlimb (**Fig. 2b**). To assess whether optogenetic stimulation of L6-ChR2 neurons altered mechanical sensitivity, Katharina Ziegler applied a succession of von Frey filaments of increasing filament forces repeatedly to the hindlimb with and without optogenetic stimulation (at an intensity insufficient to induce spontaneous nocifensive behaviours) (**Fig. 2c**). Optogenetic stimulation of L6-ChR2 neurons significantly increased withdrawal probabilities over a range of filament forces (**Fig. 2d**), indicating both an allodynic and a hyperalgesic contribution from L6CT activation. This effect was not seen in control L6-EGFP mice (**supp. Fig. 1a**). To assess the affective response of L6CT stimulation, Antonio Gonzalez performed the real-time conditioned place aversion (CPA) test, under the hypothesis that L6CT stimulation may cause avoidance behaviours (**Fig. 2e**). Once a stable chamber preference was obtained, subsequent sessions involved pairing the preferred chamber with L6CT stimulation. L6CT stimulation induced a statistically significant preference switch in L6-ChR2 mice, but not control mice (**Fig. 2f**), indicating that S1-HL L6CT stimulation is aversive enough for mice to actively avoid.

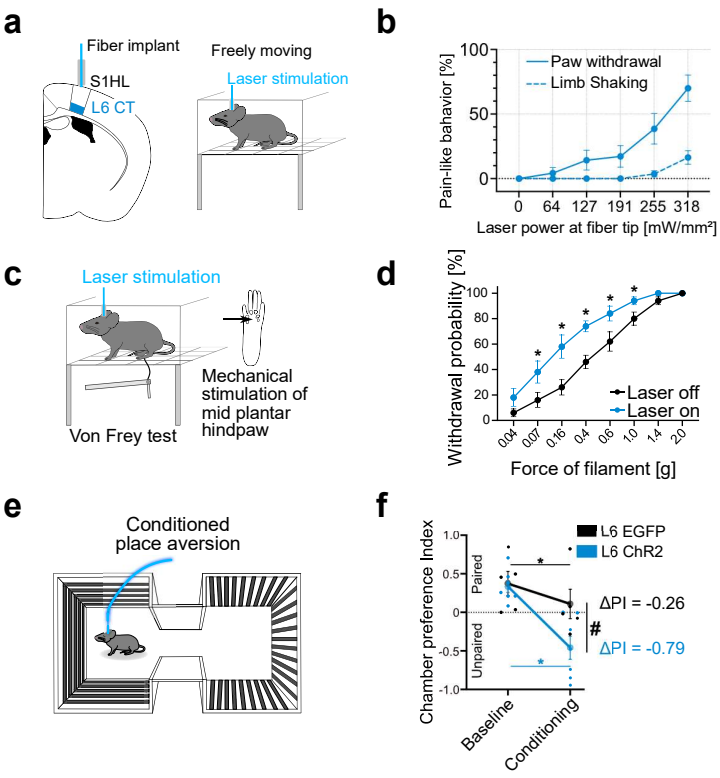


**Figure 2: Layer 6 corticothalamic (L6CT) activation in the S1 hindlimb cortex (S1-HL) increases mechanical sensitivity, exacerbates inflammatory allodynia, and induces aversion.**
**(a)** Schematic of fibre optic implantation and optogenetic L6CT stimulation in freely moving mice.
**(b)** Quantification of pain-like behaviours, paw lifting (blue solid line) and limb shaking (blue dashed line) during 5 s of S1-HL L6CT optogenetic stimulation in the absence of added peripheral sensory stimulation ($n$ = 11 mice).
**(c)** Schematic of von Frey setup used to assess mechanical sensitivity in response to graded force stimulation of the hindpaw with and without L6CT optogenetic stimulation in contralateral S1-HL.
**(d)** Within-animal comparison of paw withdrawal probabilities in response to graded von Frey stimulation of the left hindpaw at baseline (black, Laser off) and during contralateral S1 L6CT optogenetic stimulation (blue, Laser on, 5 s continuous pulse) ($n$ = 10, $p$ < 0.001). L6-EGFP control animals in Supplementary Fig. 1a.
**(e)** Schematic of experimental setup to measure real-time place aversion (CPA) as a function of L6CT optogenetic stimulation in the S1-HL of naive animals.
**(f)** Average chamber preference indices (PI) for L6-ChR2 ($n$ = 7) mice and control L6-EGFP ($n$ = 5). A PI > 0 indicates a preference for whilst a PI < 0 indicates avoidance of the laser-paired chamber. PIs differed significantly between groups during laser stimulation, but not at baseline.
Data from Katharina Ziegler and Antonio Gonzalez. Figure contains panels adapted from *Ziegler et al.* (Ziegler et al. 2023).
Exact $p$ values in Supplementary Table 1.
* and # represent $p$ < 0.05; 2d & f: Two-way repeated measures ANOVA with post-hoc Bonferroni test. Data are shown as mean ± S.E.M.

## 4.4. S1 L6CT excitation increases VPL throughput

S1 L6CT neurons provide monosynaptic excitation and, via the TRN, disynaptic inhibition to VPL cells (Lam & Sherman 2010; Crandall et al. 2015; Landisman & Connors 2007). Given that S1 L6CT excitation induced pro-nociceptive behaviours, it seemed plausible that this might be reflected in altered sensory signalling in VPL neurons. To assess how optogenetic L6CT stimulation alters VPL signalling during nociceptive mechanical stimulation, I performed 64-channel electrophysiological recordings in VPL (**Fig. 3a**) in L6-ChR2 mice under low-dose urethane anaesthesia. An automated mechanical stimulus administered 9 g mechanical pressure dispersed across 9 filaments to mimic nociceptive von Frey stimulation, which was delivered with (ML condition) and without (M condition) L6CT optogenetic stimulation in a cyclical fashion that also included a laser-only condition (L condition) (**Fig. 3b**). The majority of VPL units showed a significant response to at least one of these conditions, with over half responding to all three (**Fig. 3c**). The proportion of responsive VPL units (61 %) increased in the ML condition relative to both M and L conditions (33 % and 54 %) with 12 % of units responding only to this condition. The most prominent spiking increase to mechanical stimulation tended to occur during stimulus onset, correlating more with changes in pressure vs absolute pressure applied (**Fig. 3d**). Optogenetic L6CT stimulation increased spiking in the

VPL population (**Fig. 3e-f**) and response probability per trial (**Fig. 3g**), thereby increasing thalamic throughput to the cortex. L6CT activation approximately doubled mechanically-evoked thalamic spiking in the VPL (~2 AP/stim vs. 1.5 AP/stim vs 1 AP/stim, for ML, L, and M conditions, respectively). Consistent with increased VPL excitation, there was a general decrease in the burst probability of VPL units when mechanical stimulation was paired with L6CT optogenetic stimulation (**Fig. 3h**), with the greatest reduction observed generally in the more bursty units (**Fig. 3i**).

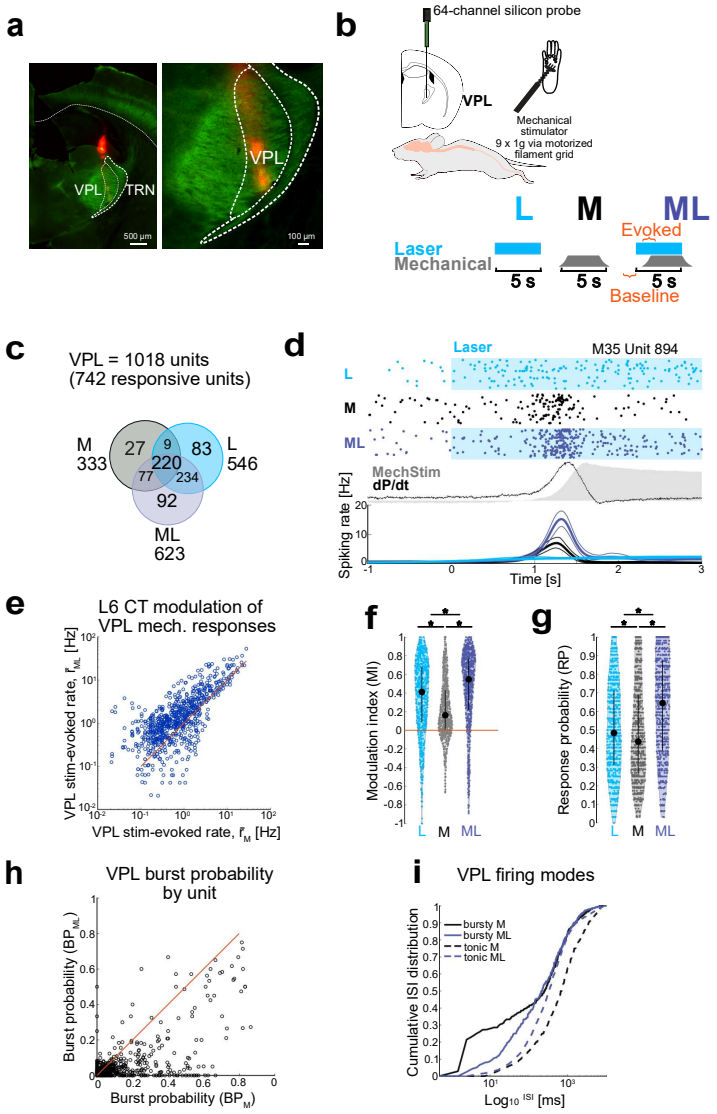


**Figure 3: Layer 6 corticothalamic (L6CT) activation enhances ventral posterolateral thalamus (VPL) spiking output.**
**(a)** ChR2-EYFP-expression (green) in S1-HL of a L6-ChR2 mouse showing fluorescence in L6CT neurons and their axons in the ventral posterolateral thalamus (VPL) and thalamic reticular nucleus (TRN) accompanied by DiI stain (orange) indicating location of probe recording.
**(b)** Left: Schematic of silicon-probe recordings in VPL of anaesthetised mice ($n$ = 4). Right: stimulation protocol for three interleaved stimulation conditions: L6CT activation (L), mechanical hindpaw stimulation (M), and combined L6CT + mechanical stimulation (ML). Analysis windows indicated in orange.
**(c)** Population overlap in L/M/ML conditions. 742/1018 VPL units showed significant modulation in at least one stimulus condition; 92 units were responsive to ML only.
**(d)** Example VPL single-unit responses to L, M, and ML stimulation. Top: raster examples; middle: mechanical pressure (grey shading) and first temporal derivative of pressure (dP/dt, black); bottom: corresponding PSTHs (bin size = 20 ms, smoothed using BARS method (Wallstrom et al. 2008)).
**(e-g)** ML condition enhances VPL responses. **(e)** Comparison of $\bar{r}_{ML}$ vs. $\bar{r}_{M}$ (0.54 **1.14** 2.81) Hz and (0.27 **0.67** 1.71) Hz, respectively, for all VPL units showing modulation in any condition ($n$ = 742). L6CT-evoked difference in spiking rate ($\Delta\bar{r} = \bar{r}_{ML} - \bar{r}_{M}$): (0.02 **0.45** 1.19). Both **(f)** stimulus-evoked modulation index (MI) and **(g)** response probability (RP) per trial varied by condition and were greatest in the ML condition. Black markers and bars show median and IQR. **(f)** $MI_L$ (0.09 **0.41** 0.68), $MI_M$ (0.00 **0.16** 0.43) and $MI_{ML}$ (0.22 **0.55** 0.77) and **(g)** $RP_L$ (0.31 **0.48** 0.71), $RP_M$ (0.27 **0.44** 0.69) and $RP_{ML}$ (0.39 **0.65** 0.87). $MI_{ML} > MI_L > MI_M$ and $RP_{ML} > RP_L > RP_M$.
**(h)** L6CT excitation decreases burst probability (BP) in VPL. For example, BP = 0.1 indicates 10% of spiking events were bursts with 2 or more spikes. Scatter plot: BP of stimulus-evoked spiking, $BP_{ML}$ vs. $BP_M$, for each unit shown in **g** (638/742 units significantly different). $BP_{ML}$ (0 **0.016** 0.047) < $BP_M$ (0 **0.032** 0.144).
**(i)** L6CT activation homogenises stimulus-evoked spike timing in VPL. Cumulative inter-spike interval (ISI) distributions for M and ML conditions for bursty (BP > 0.1, solid line, $n$ = 227) and tonic (BP ≤ 0.1, dashed, $n$ = 515) units. Data shown as the median per 1 ms bin for ISI distributions calculated separately for each unit.
Data from Rebecca Mease and Ross Folkard. * represents $p < 0.05$; 3f & g: Friedman test with post-hoc Wilcoxon signed-rank test. 3h: two-sided McNemar's test (for change in BP) and two-sided Wilcoxon signed-rank test (for comparison of $BP_{ML}$ vs. $BP_M$). Figure contains panels adapted from *Ziegler et al.* (Ziegler et al. 2023).
Exact $p$ values in Supplementary Table 1.

## 4.5. S1 L6CT excitation inhibits S1 L5

Although S1 L6CT acts subcortically, it also synapses locally within S1 through a variety of projections and could therefore alter cortical responses to sensory stimulation. To assess how optogenetic L6CT stimulation alters S1 signalling during nociceptive mechanical stimulation, I administered the same protocol as for VPL recordings except that the 64-channel electrophysiological recording took place in S1 (**Fig. 4a-b**). Cortical layers were putatively assigned based on recording depth. 74 % of units assigned to L6 showed a significant spiking increase to optogenetic L6CT stimulation (**Fig. 4c - left**), whereas mechanical responses were weak or non-existent (**Fig. 4c - middle**). In stark contrast, units putatively assigned to L5, situated above L6, displayed robust mechanical responses that were potently suppressed by L6CT stimulation (**Fig. 4c - right**). This resulted in a near silencing of sensory mechanical transmission in S1 L5 during L6CT stimulation. Upper layers 2/3 and 4 displayed more heterogeneous modulations to both basal and mechanically-evoked activity. Taken together, optogenetic stimulation of L6CT neurons induced heterogeneous modulation of mechanically-induced activity in upper layers, whilst dramatically suppressing mechanically-evoked signalling in L5 (**Fig 4d**).

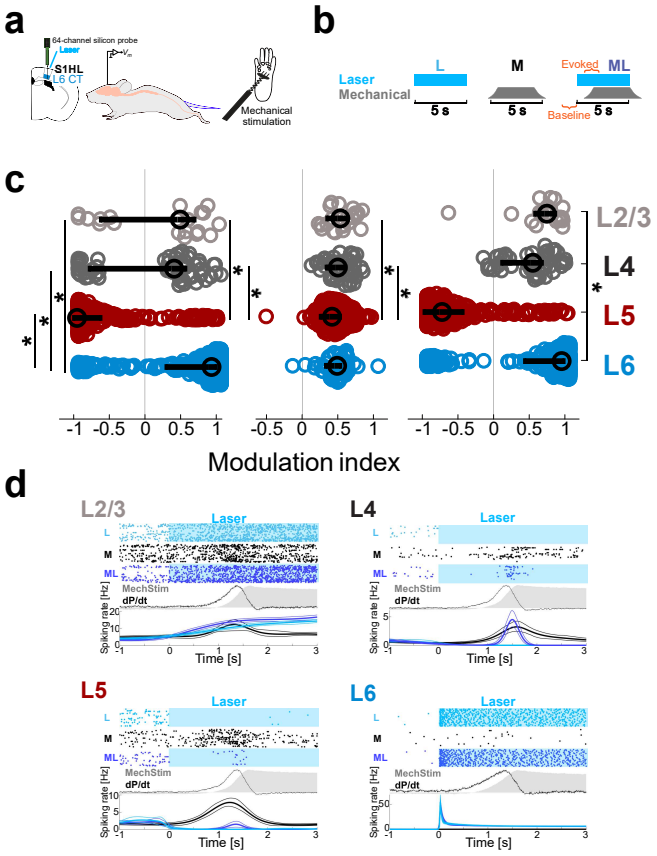


**Figure 4: Layer 6 corticothalamic (L6CT) activation potently suppresses spiking in layer 5 but enhances spiking in superficial layers.**
**(a)** Experimental configuration for silicon-probe recordings in S1-HL of anaesthetised mice ($n$ = 3).
**(b)** Stimulation protocol for three interleaved stimulation conditions: L6CT excitation (L), mechanical hindpaw stimulation (M), and combined L6CT + mechanical simulation (ML). Analysis windows indicated in orange.
**(c)** $MI_L$, $MI_M$, and $MI_{ML}$ distributions with overlaid medians and first and third quartiles for significantly modulated units by layer. Unit counts were $n$ = 25, 62, 323, and 341 for L2/3, L4, L5, and L6 units, respectively, pooled from 3 independent experiments. Data shown as median and interquartile range.
**(d)** Example responses for L, M, and ML conditions in L2/3 (light grey), L4 (grey), L5 (red), and L6 (blue). Top: raster examples; middle: mechanical pressure (grey shading) and first temporal derivative of pressure (dP/dt, black); bottom: corresponding PSTHs (bin size = 20 ms, smoothed using BARS method (Wallstrom et al. 2008)). Data from Rebecca Mease and Ross Folkard. Figure contains panels adapted from *Ziegler et al*. (Ziegler et al. 2023).
* represents $p < 0.05$; 4c: Friedman test with post-hoc two-sided Wilcoxon signed-rank test; Exact $p$ values in Supplementary Table 1.

# 4.6. S1 L5 inhibition increases L6 activity and replicates pro-nociceptive mechanical and aversive effects of L6CT excitation.

Given that the most notable observation of L6CT stimulation subcortically and cortically was suppression of S1 L5, this presented as a potential mechanism contributing to L6CTs pro-nociceptive effect. One implication of this would be that direct S1-HL L5 inhibition should therefore replicate the observed behaviour seen with L6CT excitation. To investigate this, Katharina Ziegler induced expression of the inhibitory opsin stGtACR2 exclusively in S1 L5 by injection of the viral vector AAV-SIO-stGtACR2-FusionRed in Rbp4-Cre mice in S1-HL (**Fig 1a**). Once I had habituated the mice to the roller, I recorded in S1-HL with 64-channel silicon probes and periodically applied light pulses through a fibre-optic cable in the awake mice. For the duration of optogenetic stimulation there was a marked suppression of activity in many units that corresponded to depths of StGt-positive L5 neurons (**Fig. 1c & d-upper**) in **Fig. 1a** as well as to depths of ChR2-positive L5 neurons from previous experiments (**Fig. 1b & h**). This indicated that these were L5 units, and that I was able to reliably suppress L5 activity with StGt optogenetic stimulation for the duration of stimulation. Interestingly, L4 and L6 showed increased activity during optogenetic inhibition of L5 (**Fig. 1d - lower**). Furthermore, L5 inhibition increased mechanical withdrawal probabilities across a range of filament forces during von Frey (**Fig. 1e**) and induced a preference switch in the CPA paradigm (**Fig. 1f**) replicating the effects of S1 L6CT excitation on mechanical sensitivity and avoidance behaviour.

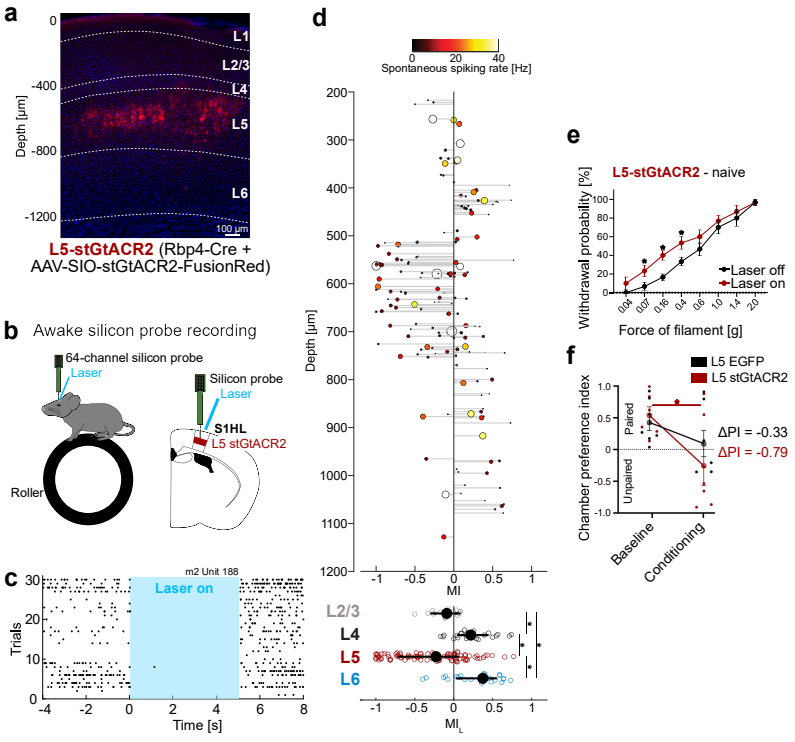


**Figure 5: Layer 5 (L5) inhibition in the S1 hindlimb cortex (S1-HL) replicates mechanical hypersensitivity and avoidance behaviour induced by layer 6 corticothalamic (L6CT) activation.**
**(a)** stGtACR2-FusionRed expression (red) in L5 S1-HL of a Rbp4-Cre mouse. S1-HL layer borders (dashed lines) estimated based on soma sizes and densities using DAPI signals (blue). Representative example from *n* = 15 mice.
**(b)** Schematic of S1-HL silicon probe recordings in a head-fixed awake mouse (upper).
**(c)** Example raster for a laser-suppressed L5 stGtACR2 unit (depth = 589 µm).
**(d)** Upper panel: depth-resolved light modulation indices ($MI_L$) in S1-HL during optogenetic inhibition of L5 (*n* = 3 pooled experiments, 285 units). Each unit is represented by one data point; size and colour of markers are proportional to spontaneous spiking rate (black to yellow: low to high). Depth values are slightly jittered for visibility. Non-significantly modulated units not shown (122/285). Lower panel: $MI_L$ distributions for significantly modulated units by layer.
**(e)** Within-animal comparison of paw withdrawal probabilities in response to graded von Frey stimulation of the hindpaw at baseline (black, laser off) and during contralateral S1-HL L5 optogenetic inhibition (red, laser on, 5 s continuous pulse) (*n* = 6 mice).
**(f)** Average chamber preference indices (PI) for L5-stGtACR2 (*n* = 6) and L5-EGFP (*n* = 7) mice. A PI > 0 indicates a preference for whilst a PI < 0 indicates avoidance of the laser-paired chamber. PIs were not significantly different between groups during laser stimulation or at baseline.
Data from Katharina Ziegler, Jan Burghardt, Antonio Gonzalez, Rebecca Mease, and Ross Folkard.
Exact *p* values in Supplementary Table 1. Figure contains panels adapted from *Ziegler et al.* (Ziegler et al. 2023).

* represents $p < 0.05$; 5d: two-sided Wilcoxon signed-rank test; see Supplementary Table 1 for population medians and first and third quartiles per layer and condition.; 5e & f: Two way repeated measures ANOVA with post-hoc Bonferroni test.

## 4.7. S1 L5 excitation reduces mechanical sensitivity and is sought after to relieve inflammatory pain

Considering that inhibition of baseline L5 activity exacerbated nociceptive behaviours, implying a potential anti-nociceptive influence of baseline L5 firing, increased L5 activity may provide further anti-nociceptive effects. To test this, Katharina Ziegler injected AAV-DIO-ChR2-EYFP into S1-HL of Rbp4-Cre mice so I could record optogenetic excitation specifically of L5 cells. I recorded tagged cells at depths consistent with histologically verified EYFP expression (**Fig. 6a**) observed in **Fig. 1b**. Optogenetic stimulation induced reliable spiking increases for the duration of the light stimulus (**Fig. 6b**). In stark contrast to both S1 L6CT excitation and S1 L5 inhibition, S1 L5 optogenetic excitation induced marked decreases in withdrawal probability across a range of filament forces during von Frey (**Fig 6.c**). Interestingly, L5 excitation in naive mice was aversive in CPA, causing significantly reduced time spent in the laser-paired chamber, an effect not observed in control mice (**supp. Fig. 2f**). To test whether mice might actively seek out S1 L5 excitation as pain relief, Antonio Gonzalez and I injected mice with CFA in the hindlimb contralateral to the S1 L5 injection. Antonio Gonzalez paired S1 L5 excitation with the lesser-preferred chamber in a real time conditioned place preference (CPP) paradigm, where S1 L5 excitation induced a preference switch in L5-ChR2 mice that was not seen in control mice (**Fig. 6d**).

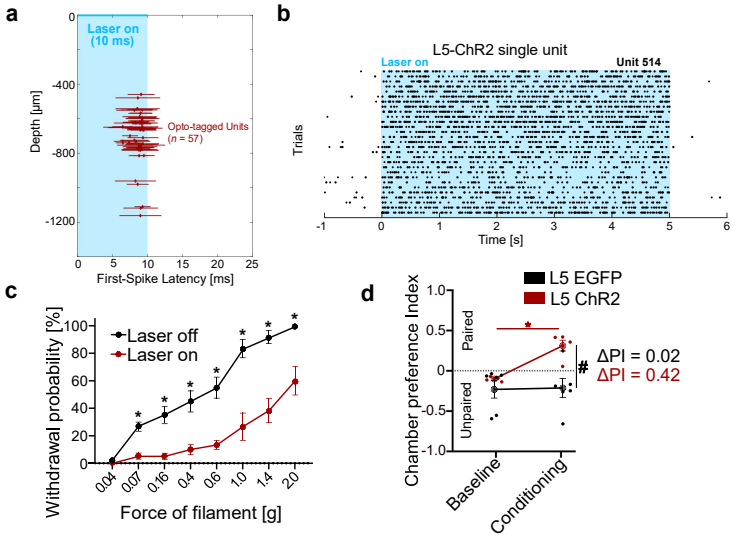


**Figure 6: Layer 5 (L5) activation in the S1 hindlimb cortex (S1-HL) is anti-nociceptive.**
**(a-b)** Representative S1-HL cortex recording from an awake L5-ChR2 mouse demonstrating optogenetic control of the L5 pathway.
**(a)** L5 units were identified based on their short-latency, low jitter response to 10 ms light pulses (1201 mW/mm²). Each marker shows unit depth vs. mean ± SD latency to first evoked spike.
**(b)** Example raster plot of one unit from **a** in response to 5 s laser stimulation (1201 mW/mm² from fibre tip).
**(c)** Within-animal comparison of paw withdrawal probabilities in response to graded von Frey stimulation of the left hindpaw at baseline (black, laser off) and during laser stimulation (red, laser on, 5 s continuous pulse) in the contralateral S1-HL of L5-ChR2 mice ($n = 6$, $p < 0.001$).
**(d)** Average chamber preference indices (PI) for L5-ChR2 ($n = 5$) and L5-EGFP ($n = 6$) mice. A PI > 0 indicates a preference for whilst a PI < 0 indicates avoidance of the laser-paired chamber. PIs were significantly different between groups during laser stimulation, but not at baseline.
Data from Katharina Ziegler, Antonio Gonzalez, and Ross Folkard. Figure contains panels adapted from *Ziegler et al.* (Ziegler et al. 2023). * and # represent $p < 0.05$; 6c & d: Two-way repeated measures ANOVA with post-hoc Bonferroni test. Exact *F* and *p* values in Supplementary Table 1. Data are shown as mean ± S.E.M.

## 4.8. CFA-induced hypersensitivity is modulated by S1 corticofugal outputs and is reflected in increased thalamic bursting

Although L6CT and L5 corticofugal outputs bidirectionally modulate acute nociceptive behaviour, whether they had the same effect in an inflammatory model had yet to be tested. L6CT excitation exacerbated contralateral paw withdrawal probability to the 2 lowest von Frey filament pressures in mice with CFA-induced peripheral hindpaw inflammation (**Fig. 7a**). Consistent with L5-mediated suppression of pain responses, L5 excitation also decreased paw withdrawal probabilities across a range of filament forces in mice with inflamed hindpaws (**Fig. 7b**), even reversing the hypersensitivity induced by CFA-injection, as paw withdrawal probabilities of CFA + L5 excitation were not significantly different from those in naive mice without L5 excitation. To assess how peripheral inflammation may alter activity in the TC - S1 pathway, I performed electrophysiological recordings using 64-channel silicon probe recordings in contralateral VPL in mice that had either undergone CFA or Saline injection in the hindlimb ~24 hours prior to recording (**Fig. 7c)**. Both spike rates and inter-spike intervals (ISIs) were analysed. Thalamic burst firing is thought to be predominantly influenced by low-threshold $Ca^{2+}$ spikes (LTS) caused by T-Type $Ca^{2+}$ channels that cause bursts of action potentials (Jahnsen & Llinás 1984b; Llinás & Jahnsen 1982; Jahnsen & Llinás 1984a). These low threshold currents require approximately 100ms to reset (Zhan et al. 1999). As such, a neuron firing in 'tonic mode' might tend to have a relatively normal (Gaussian) distribution of ISIs, compared with a neuron in 'burst mode' that will have an aggregation of ISIs < 10ms that repeat approximately every 100 ms in a more bi-modal distribution (**Fig. 7d**). When taking the ISI distributions across Saline- and CFA-injected mice, the ISI distributions illustrate that a greater proportion of ISIs in the VPL of CFA-injected mice were < 10 ms (**Fig. 7e**). The Saline and CFA cumulative distributions, which appeared to converge at ~100 ms, were significantly different from one another. This indicates that short-term (~24 hr) peripheral inflammation caused by CFA may increase thalamic bursting. To further quantify thalamic bursting, I defined bursts as 2 or more spikes that each do not exceed 6 ms ISIs, which are preceded by at least 50 ms prior silence, and do not exceed 100 ms duration. This enables identification and quantification of bursting events relative to overall spiking (**Fig. 7f**). Consistent with the ISI distributions, the proportion of bursts relative to overall spikes, as measured by burst-event ratio, was significantly elevated in the CFA group (**Fig. 7g - left**). In contrast, overall spike rates did not differ significantly between Saline and CFA groups (**Fig. 7g - right**), suggesting that whilst CFA-induced peripheral inflammation may cause the VPL to become more bursty, it does not alter total spike rates. Indeed, whilst dissecting the proportion of bursts consisting of various numbers of spikes, CFA mice had a greater proportion of bursts containing > 2 spikes, whereas Saline mice had a significantly greater proportion of bursts consisting of 2 spikes than CFA (**Fig. 7h**). Therefore, in addition to increasing the degree of thalamic bursting, CFA-induced peripheral inflammation also increased the number of spikes within a burst.

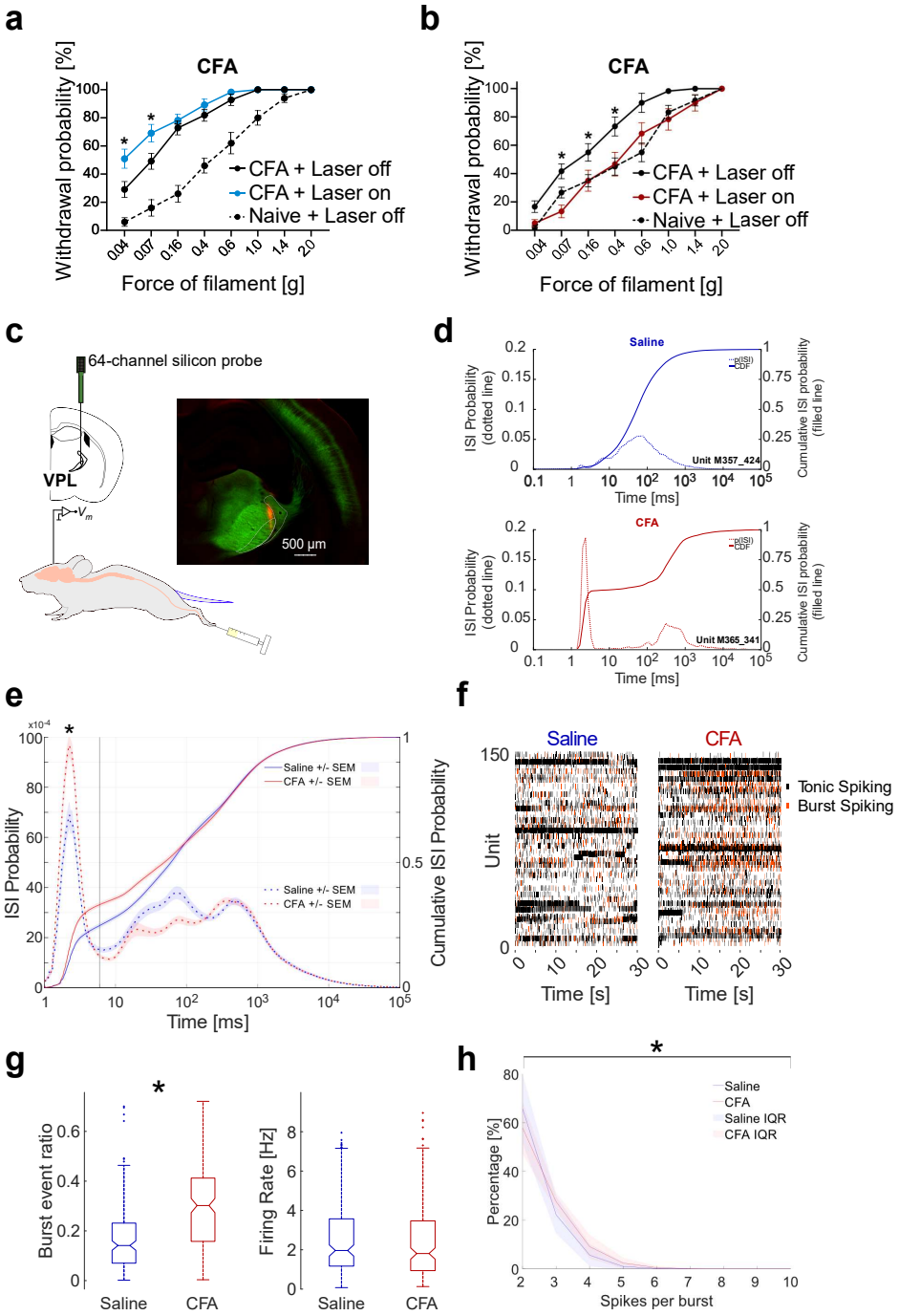


**Figure 7: CFA induces hypersensitivity that is altered by S1 L6CT and S1 L5 and causes increased thalamic bursting.**
**(a)** Within-animal comparison of paw withdrawal probabilities in response to graded von Frey stimulation of the left hindpaw at baseline (black, Laser off) and during L6CT laser stimulation (blue, Laser on, 5 s continuous pulse) in the contralateral S1-HL of L6-ChR2 mice with CFA-induced hindpaw inflammation ($n$ = 10).
**(b)** Same as in **(a)** but in L5-ChR2 mice ($n$ = 12).
**(c)** Left: Schematic of probe recording in the VPL of an anaesthetised mouse. Right: Probe stained in DiI shows recording location in VPL of Ntsr1-Cre-ChR2-EYFP mouse.
**(d)** Example ISI probability distribution (dotted line) and cumulative ISI distribution (filled line) curves for VPL single-units recorded under light anaesthesia in mice injected with Saline (top) or CFA (bottom) ~ 24 hours prior to recording.
**(e)** 177 Saline ($n$ = 3 mice) and 195 CFA ($n$ = 3 mice) mechanically-responsive single-units. Mechanical responses determined with Wilcoxon-signed rank difference in 1.5 seconds pre-trigger vs 1.5 seconds post trigger onset ($p < 0.05$), offset by 0.5 seconds for the mechanical stimulus delay. Mean population ISI (dotted) and cumulative ISI (filled) probability distributions for Saline and CFA plotted on a semi-logarithmic x axis. Vertical black line denotes the max ISI cutoff for burst spikes (6 ms). ISI probability curves (dotted) have been smoothed by the same factor for visualisation purposes only.
**(f)** Random subset of 150 saline (left) and 150 CFA (right) units for the first 30 s elapsed recording time.
**(g) left:** Burst-event ratios for saline vs CFA units. **right:** Firing rates for Saline vs CFA units.
**(h)** Random subset of 177/195 CFA units was selected to compare against 177 Saline activity for probability of 2-11 spikes per burst between conditions. Significant differences were observed in the number of spikes between Saline and CFA groups for probability of 2-10 spikes per burst ($p < 0.005$) in light of a Bonferroni correction for multiple comparisons, with only probability of 11 spikes per burst not significantly different (probability of 11 spikes not shown).
Data from Katharina Ziegler and Ross Folkard. Figure contains panels adapted from *Ziegler et al.* (Ziegler et al. 2023).
* represents $p < 0.05$; 7a & b: Two-way repeated measures ANOVA with post-hoc Bonferroni test. Exact $F$ and $p$ values in Supplementary Table 1. Data are shown as mean ± S.E.M. 7e: Kolmogorov-Smirnov test. 7g: Wilcoxon rank sum test. 7h: Wilcoxon rank sum test.

## 4.9. Discussion

It is commonly thought that pain is a percept created by the cortex with thalamic contributions (Kuner & Kuner 2021). As the major pathways exiting the cortex, corticofugal pathways originating in L5 and L6 have been implicated in causally shaping sensory perceptual experience (Takahashi et al. 2016; Takahashi et al. 2020; Guo et al. 2017). In this study, my colleagues and I showed for the first time that S1 output pathways in L5 and L6 potently alter both the sensory experience, and the affective experience associated with nociceptive signalling. L6CT excitation was potently pro-nociceptive, increasing mechanical and thermal sensitivity, as well as inducing aversion in mice, who actively sought to avoid L6CT stimulation. L6CT increased both basal and mechanically-evoked thalamic throughput to the cortex, shifting the population towards a more tonic-firing profile. This increased thalamic input to S1 was sharply contrasted by silencing of cortical output in L5 induced by L6CT activation. L5 inhibition was sufficient to replicate the mechanical hypersensitivity and avoidance behaviours observed with L6CT excitation, and also increased basal L6 activity. L5 excitation reduced mechanical sensitivity, reversed inflammatory mechanical hypersensitivity, and was sought after in mice with peripheral hindlimb inflammation. Excitation of each cortical layer induced large effects in opposite sign from each other such that mechanical withdrawal thresholds could differ by an order of magnitude depending on the layer stimulated. For example, 60 % withdrawal thresholds, which in control and unstimulated mice hovered at around 0.6 g (**supp. Fig. 1a & b**), were 0.16 g in L6-ChR2 mice and 2 g in L5-ChR2 mice, a tenfold difference. This suggests substantial capacity for nociceptive sensitivity to be modulated by cortical activity in S1, that perception of a peripheral stimulus can be dissociated quite significantly from the actual environmental stimulus - as has been demonstrated in S1 for non-somatosensory representations (Chen et al. 2003), and that perception of a stimulus is heavily dependent on the state of cortical activity to a perhaps somewhat surprisingly large extent (Kok et al. 2016).

The biggest surprise was that L6CT stimulation absent added peripheral stimulation induced spontaneous pain-like behaviours, such as withdrawal and limb shaking, that followed a dose-response relationship with respect to L6CT stimulation intensity. That ChR2 expression was confined to S1 suggests that this might be a motivated motor response to a sensory percept, as opposed to optogenetic stimulation of motor circuitry and a subsequent motor reflex. This was further corroborated by the variability in a mouse's response to a given laser power, and also variability in the motor response (paw withdrawal and limb shaking are distinct motor responses), further indicating that this was not merely a simple motor reflex, which might otherwise be expected to induce more reliable and stereotypic movements. Indeed, at laser powers subthreshold for spontaneous withdrawal, mice would still switch chamber preference to actively avoid L6CT stimulation, indicating a continuum of displeasure. It is also unlikely that the spontaneous withdrawal was a learned association as a result of laser-pairing with von Frey, as none of the control mice nor L5-ChR2 mice showed similar behaviours (**supp. Fig. 1c**). This perhaps controversially indicates that high S1 L6CT activity absent added peripheral input can be sufficient to cause pain perception.

L6CT projects to both VP and POm through numerous modulatory synapses, in contrast to driving inputs these thalamic nuclei receive from the periphery (Whilden et al. 2021; Zhang & Deschênes 1998; Bourassa et al. 1995; Deschênes et al. 1998; Sherman & Guillery 1996; Sherman & Guillery 1998). Along with VPL, reports suggest POm is altered by pain, and that POm projects to S2, a region that can induce pain perception when stimulated (Mazzola et al.

2006; Lee & Sherman 2008; Viaene et al. 2011; Masri et al. 2009; Frandolig et al. 2019). If these thalamic nuclei contain neuronal populations whose activity causally contributes to pain perception and affect, high L6CT activity through optogenetic stimulation might drive these populations, as demonstrated here with increased population spiking in VPL by L6CT excitation, causing pain perception. Ordinarily these thalamic cells may only be driven by temporally coordinated driving inputs from peripheral nociceptive stimulation, but this supports the possibility that the same cells could be driven via L6CT by aberrant cortical activity such as S1 gamma or theta-gamma coupling reported in thalamocortical dysrhythmia (Ploner et al. 2006; Gross et al. 2007; Heid et al. 2020; Zhang et al. 2012; Tan et al. 2019; Tiemann et al. 2010; Llinás et al. 2005).

This L6CT-induced L5 inhibition likely mediated some of the pro-nociceptive phenotype, as direct optogenetic L5 inhibition similarly increased mechanical sensitivity and induced avoidance of optogenetic stimulation, whereas L5 excitation induced behavioural changes in the opposite direction, indicating a negative correlation between pain perception and S1 L5 activity in a physiological range. However, unlike S1 L6CT excitation, neither S1 L5 inhibition nor excitation significantly altered thermal sensitivity (**supp. Fig. 2d & e**). Especially in the case of S1 L5 excitation, optogenetic manipulations resulted in substantial behavioural modulation, indicating that viral efficacy is not the reason behind lack of S1 L5 modulation on thermal sensitivity. L6CT has different local cortical connectivity from L5 (Douglas & Martin 2004; Adesnik & Naka 2018; Gilbert & Wiesel 1983), and unlike L5 projects to FO thalamic structures (Bourassa et al. 1995; Veinante et al. 2000; Deschênes et al. 1994). Whether S1 L6CT projects to VPL cells in a feed-forward loop that targets a different, heat-sensitive cortical region remains to be fully elucidated (Bokiniec et al. 2018). The HO thalamic target of S1 L6CT, the POm, is thought to be much more strongly activated by S1 L5 than L6CT (Usrey & Sherman 2019; Kirchgessner et al. 2021), but is being re-evaluated with respect to its vast heterogeneity, and differences in the distribution of L6CT and L5 inputs to different POm subregions means that a S1 L6CT-POm-mediated modulation of thermal nociception also cannot be completely ruled out, as L6CT seems to innervate the whole POm region, whereas L5 innervation is confined to distinct subregions (Casas-Torremocha et al. 2022).

One potential explanatory route for S1 L5 modulation would be via the spinal cord, as descending CSN neurons from S1 have been shown to synapse in deeper dorsal horn laminae and alter mechanical but not thermal sensitivity (Liu et al. 2018; Frezel et al. 2020). This is congruent with suggestions that nociceptive thermal signals may be comparatively reliant on lamina 1 STT projections that appear less innervated by S1 L5, whereas mechanical nociception can be mediated through projection neurons in deeper laminae (Abrahamsen et al. 2008; Cavanaugh et al. 2009; Braz et al. 2005). Additionally, whereas L6CT excitation was pro-nociceptive across a wide range of mechanical filament forces, L5 inhibition was consistently pro-nociceptive only in the lower pressure filaments, without an obvious ceiling effect, suggestive of allodynia rather than hyperalgesia. It may be the case that mild noxious and low threshold mechanical encoding does not rely on lamina 1 but that encoding of highly noxious stimuli is partially mediated by lamina 1 projection neurons (Mantyh et al. 1997; Abrahamsen et al. 2008). As such, the removal of top-down modulation of deeper laminae in the dorsal horn by S1 L5 inhibition may not modulate lamina 1 signalling and therefore may not alter sensitivity in the highly noxious range, despite contributing to allodynia through altered mechanical signalling in deeper dorsal horn laminae (Liu et al. 2018; Frezel et al. 2020). However, there is likely cross-modulation between the dorsal horn laminae that S1 L5

does innervate (Torsney & MacDermott 2006; Miraucourt et al. 2007; Duan et al. 2014; Peirs et al. 2015; Lu et al. 2013; Cheng et al. 2017), and some disinhibitory mechanisms have been demonstrated in the dorsal horn, so the efficacy of S1 L5 modulation of dorsal horn should be experimentally validated. That S1 L5 inhibition did not cause similar spontaneous pain behaviours to S1 L6CT excitation further indicates that the pro-nociceptive phenotype observed with S1 L6CT stimulation is not solely mediated through its inhibition of S1 L5 output, but also relies on a contribution from L6CT circuitry that is distinct from its direct influence on L5.

S1 L5 inhibition elevates L6 activity, suggesting that L5 may directly or indirectly dampen L6CT signalling. One cannot therefore completely rule out that these two populations mutually inhibit each other, and that the pro-nociceptive phenotype of S1 L5 inhibition was mediated through disinhibition of L6CT. Prior research has yielded heterogeneous results with respect to the sign of L6 modulation induced by L5 inhibition (Kirchgessner et al. 2021; Onodera & Kato 2022), though evidence of L5 projections in L6 has been known for some time (Gilbert & Wiesel 1979). The L6 activity increase with L5 inhibition was lower than that of direct ChR2 excitation of L6CT, which is concordant with a seemingly greater capacity for the latter manipulation to increase pain sensitivity in an experimentally detectable manner, and thus could explain why L6CT excitation, but not S1 L5 inhibition, caused spontaneous pain behaviours and thermal sensitivity. However, inhibition of L6 seems unlikely to be the sole cause of the reduced nociceptive sensitivity observed with L5 excitation, as the magnitude of the effect of L5 excitation was considerable, and many reports suggest L6CT cells are sparsely active under physiological conditions (Vélez-Fort et al. 2014; Crandall et al. 2017; Dash et al. 2022). In this scenario, for L5-mediated inhibition of L6CT cells to cause such a strong effect would have to be the result of a seemingly small change in baseline L6CT activity. This is corroborated by the observation that L6CT inhibition did not decrease, but paradoxically increased mechanical sensitivity by a small amount (**supp. Fig. 2i**). Therefore, whilst a case can be made that the behavioural effects of L6CT are not completely due to its actions on L5, a similar case can be made for the actions of L5 on L6. Given the evidence, I think it is likely that L5 and L6CT pathways have distinct circuitry that each individually and antagonistically mediate pain signalling, alongside a see-saw-esque balance of L5 and L6CT activity enacting a mutually suppressing and potentially potent influence on the severity of pain perception. If both layers suppress each other, then excitation in one layer could result in its own disinhibition through suppression of the other layer, engaging a positive feedback cycle and amplifying its own effects. Intriguingly, L5 is reportedly the most active layer in the cortex (Sakata & Harris 2009; de Kock & Sakmann 2009; O'Connor et al. 2010; de Kock et al. 2021), and L6 thought to be amongst the least active layers (Vélez-Fort et al. 2014; Crandall et al. 2017; Dash et al. 2022; O'Connor et al. 2010). In essence, the two layers may 'compete' with each other, with L5 dominating under basal conditions, and L6CT excitation serving to 'tune-up' sensory salience under certain circumstances. Under what circumstances L6CT can be excited remains a highly important and largely unanswered question.

One unexpected discovery prior to the investigation was the potent anti-nociceptive effect of S1 L5 excitation to both the mechanical sensitivity and the degree of unpleasantness, in that a reason why mice switched chamber preference to 'self-administer' optogenetic S1 L5 excitation might be because it made the inflammation-induced pain subjectively less unpleasant. Other explanations for this behaviour exist: if S1 L5 excitation was independently pleasurable it would also be expected to induce a preference switch. This explanation seems

less plausible, especially considering there was no significant preference for S1 L5 stimulation in naive mice, indeed it induced avoidance behaviours (**supp. Fig 1f**). One explanation for this finding may be that S1 L5 excitation reduces pain perception by inducing an alternative somatosensory sensation that might be preferable to inflammatory pain but not entirely pleasant in and of itself, possibly through facilitation of somatosensory signalling in dorsal horn laminae 3-5 (Liu et al. 2018; Frezel et al. 2020). Attention towards stimuli facilitates sensory signalling in the TC system (Briggs et al. 2013; McAlonan et al. 2008) and modulates spinal cord responses to pain (Sprenger et al. 2012), and attention directed away from noxious and towards non-noxious stimuli has been demonstrated to suppress perceived pain intensity (Quevedo & Coghill 2007). Some studies indicate that 'phantom' percepts or false detections can be generated from certain S1 L5 activity (Takahashi et al. 2016), so perhaps optogenetic stimulation of S1 L5 generates a somatosensory percept that divides attention or occupies attentional bandwidth, inhibiting pain signalling.

That S1 L5 inhibition was an aversive stimulus absent peripheral nociceptive stimulation implies physiological L5 may contribute to an ongoing perceptual state, such that suppression of this activity alters perception sufficiently to alter behaviour. Indeed, this adds to recent literature suggesting that nociceptive thresholds can be altered or 'set' by cortical projections in surprisingly long-lasting and context-dependent ways (Cao et al. 2023; Zhou et al. 2022; Liu et al. 2018). This research may indicate that L5 may be adjusting nociceptive sensitivity and thresholds in a dynamic and ongoing manner, and contexts where S1 L5 outputs are enhanced or reduced might be expected to decrease and increase pain sensitivity respectively. Alterations in S1 L5 basal activity have been implicated in the persistence of chronic neuropathic pain (Cichon et al. 2017). Intriguingly, nociceptive mechanical stimulation increased L5 output, despite L5's anti-nociceptive effects during optogenetic stimulation. S1 L5 projects to many regions that could process pain information, including PAG, POm, MD, and dorsal horn of the spinal cord (Prasad et al. 2020; Frezel et al. 2020). Indeed, S1 L5 predominantly projects to inhibitory interneurons in dorsal horn, which could result in a degree of long-range inhibitory feedback that suppresses further ascending nociceptive signalling, similarly to other mechanisms of negative feedback initiated by noxious inputs (Basbaum & Fields 1978; Basbaum & Fields 1984; Bouhassira et al. 1995; Frezel et al. 2020).

S1 L6CT excitation induced avoidance behaviours, a sign of its unpleasantness, suggesting that S1 has the potential to influence affective pain behaviours and not only sensory-discriminative aspects of pain (Groh et al. 2018; Rainville et al. 1997; Melzack & Casey 1968). Indeed, we are not the first to show changes in affect induced by S1 manipulation (Tan et al. 2019; Wang et al. 2009). The role of VPL and S1 in pain perception has been debated, as both can exhibit specific responses (Apkarian & Shi 1994; Chung et al. 1986; Yen et al. 1991; Apkarian et al. 2000; Patel & Dickenson 2016; Bordi & Quartaroli 2000; Martin et al. 1996) and oscillatory changes in response to pain (Gross et al. 2007; Leblanc et al. 2014; LeBlanc et al. 2017). That the seeking and avoiding behaviours could be modulated by L5 excitation and inhibition respectively may indicate that S1 modulates affective valence through a L5 output pathway. Evidence that the VPL-S1 pathway itself causes an unpleasant valence, in that nociceptive signals in VPL are interpreted with some affective quality by S1, remains lacking, as the S1-induced valence modulation could be mediated through alterations in other ascending pathways, for example via POm to S2, a region that in contrast to S1 can generate pain perception in humans when electrically stimulated (Mazzola et al. 2006).

Both the effects of L6CT and L5 excitation were also manifest in mice with peripheral hindpaw inflammation. However, L6CT excitation appeared not to increase pain sensitivity by the same magnitude in CFA mice compared with naive mice. Indeed, filament forces above 0.07g were not significantly different with vs without L6CT excitation in CFA mice, despite withdrawal probability not approaching the ceiling of 100 %, indicating an absence of the hyperalgesic component of L6CT excitation in mice with CFA-induced inflammation. That the combination of L6CT and CFA does not constitute a full summation of their independent effects on mechanical sensitivity suggests an interaction in the mechanisms underpinning L6CT-mediated and inflammatory-mediated mechanical sensitivity. Interestingly, whilst L6CT excitation increased thalamic firing rates and induced a burst-to-tonic shift in the VPL population, CFA-mediated peripheral inflammation induced a tonic-to-burst shift without increasing firing rates. Both of these shifts cannot simultaneously co-occur, so there is perhaps some antagonism between the two processes that might underlie the reduced efficacy of L6CT excitation in mice with peripheral inflammation. Increased VPL bursting has been implicated both as being nociceptive and anti-nociceptive according to conflicting research (Iwata et al. 2011; LeBlanc et al. 2016; LeBlanc et al. 2017; Saab & Barrett 2016; Hains et al. 2006; Huh & Cho 2013a; Huh et al. 2012; Kim et al. 2003). The devil may be in the details, and this heterogeneous research may homogenise considerably when bifurcated into non-neuropathic vs neuropathic chronic pain conditions (Gustin et al. 2011). VPL undergoes plastic changes that may only manifest after days of peripheral inflammation (Zhang et al. 2017), suggesting time duration of pain may also be a substantial factor influencing the valence of thalamic bursting. However even within a given type of pain model, it is possible that VPL bursting shows an inverse U-shaped relationship with respect to pain perception, as one study noted an increase in VPL bursting in both inflammatory and neuropathic pain models, where TRN stimulation that reduced the mechanical sensitivity associated with these pain conditions further increased VPL bursting (LeBlanc et al. 2017). Given a lack of studies specifically manipulating VPL and assessing pain behaviours in naive mice, the causative mechanisms of how VPL in might contribute to pain perception should arguably be researched further (Huh & Cho 2013a; LaBuda et al. 2000). The fact that VPL undergoes nociception-induced modulation does not guarantee that it is a major causative influence on any of the qualia associated with acute pain perception, though would appear to be a candidate for a L5-independent means of L6CT-induced pro-nociception.

Pain has proved to be resistant to lesions of brain regions whose activity highly correlates with pain perception, leading to theories that pain perception results from distributed networks with considerable parallelisation coupled with a degree of redundancy (Coghill 2020). Studies in split-brain patients report a subjectively different pain experience in each hemisphere from a single nociceptive stimulus, yet highly noxious stimuli resulted in more similar ratings between hemispheres, suggesting that there is a least crude redundancy in pain perception that the corpus callosum has a role in resolving (Stein et al. 1989). Therefore, despite S1 activity correlating with sensory perception better than sensory stimulation, and its role in mediating sensory-discriminative and potentially affective qualia of pain, removal of S1 activity through lesions results in much greater deficits in somatosensory perception than pain perception (Knecht et al. 1996). The redundancy and robust nature of pain suggests that any broad inhibition of one of the core regions in the neurological pain signature may not necessarily result in large anti-nociceptive effects, and that a more targeted approach, where cell-type specific manipulations can recruit cortical subpopulations that engage in newly discovered top-down anti-nociceptive modulations may be an ambitious but ultimately more fruitful therapeutic

endeavour. S1 L5 excitation was sufficiently potent in reversing mechanical sensitivity associated with peripheral hindpaw inflammation such that none of the withdrawal probabilities in the CFA + S1 L5-ChR2 mice under optogenetic stimulation differed significantly from those in naive mice without optogenetic stimulation. This is a notably large effect, as many pharmacological treatments only modestly suppress pain, and/or come with many side effects (Basbaum et al. 2023). S1 L5 could therefore constitute a realistic target for new developments in non-invasive brain stimulation (Folloni et al. 2019; Liu et al. 2021; Kim et al. 2021).

Our research adds to a growing body of literature suggesting that sensory processing in S1 powerfully mediates acute and inflammatory pain perception, and that pain perception is heavily influenced by the balance of excitation between S1 L5 and L6CT pathways. This bolsters a recognition of S1 L5 as an important player in pain conditions (Tan et al. 2019; Cichon et al. 2017) and a possible therapeutic target (Folloni et al. 2019; Liu et al. 2021; Kim et al. 2021), whilst extending research that suggests S1 L5 activity plays an important role in sensory perception by highlighting the role of basal L5 activity contributing to an ongoing conscious, perceptual state (Kim et al. 2021; Liu et al. 2021; Folloni et al. 2019; Tan et al. 2019; Cichon et al. 2017; Takahashi et al. 2020; Takahashi et al. 2016; Mo et al. 2024). My research contributed to the first paper of note to directly implicate S1 L5 in setting acute nociceptive thresholds as well as to specifically demonstrate a role of S1 L6CT in pain perception.

# 5. Corticothalamic Layer 6 Controls Cortical and Thalamic States through Dynamic Modulation of Population Activity and Synchrony

## 5.1. Introduction

A feature of neurons and indeed brain circuits is non-linear input-output (I/O) relationships (Silver 2010). Feedforward inhibition, coupled with pre- and post-synaptic facilitatory/depressive mechanisms, amongst other homeostatic mechanisms, give rise to complex non-linearities in spike transmission. A consequence is that the neuronal activity induced by upstream population activity, whether physiological or optogenetically mediated, may be highly dependent on absolute as well as relative differences in activity. For example, a doubling in upstream population activity may not be reflected in a doubling of spiking output in the downstream population - the spiking output could be more or less than double its previous output. A prominent cause for this can be (although not necessarily) explained by non-linearities in temporal summation that occur within a single depressing synapse (Sherman & Guillery 1998; Swadlow et al. 2002; Swadlow & Gusev 2001; Crochet et al. 2005). However, scenarios exist where nonlinearities that occur at synapses interact to produce the opposite effect on circuit activity, e.g. inducing circuit excitation instead of inhibition (Crandall et al. 2015). Additionally, the relative timings of inputs to the downstream regions will shape the downstream population response. Convergent excitatory inputs spiking at 10 Hz may for example arrive 50 ms from one another yet not overcome feedforward inhibitory influences, yet a population that fires at 10 Hz but with more synchrony (less variability in transmitter release between presynaptic neurons) may excite a postsynaptic neuron to AP threshold before the synaptic delay of feedforward inhibition (Fries 2015). In this example, a downstream population's activity depends less on the upstream population's total activity, and more on the degree of synchrony in the arrival of action potentials from the upstream population.

L6CT exerts monosynaptic excitation and disynaptic inhibition at both TC and cortical synapses, and has been reported to induce a bidirectional modulation of TC excitability depending on L6CT stimulation frequency (Crandall et al. 2015; Jurgens et al. 2012; Lam & Sherman 2010; Whilden et al. 2021; Kim et al. 2014; Frandolig et al. 2019; Olsen et al. 2012; Bortone et al. 2014). In the sensory cortex L6CT has been observed to strongly excite L5 pyramidal neurons and weakly engage L4 excitatory neurons (Kim et al. 2014). Additionally, a number of different L6CT targets provide feed-forward inhibition, from fast-spiking (FS) neurons in L4 and L5, to SOM+ neurons in L5, and FS neurons in L6 that extend translaminarly and inhibit L2-5 (Kim et al. 2014; Frandolig et al. 2019; Olsen et al. 2012; Bortone et al. 2014). Many of these findings have been elucidated through specific optogenetic excitation of L6CT, yet across experiments the effects of continuous L6CT excitation on cortical population activity across different layers has yielded heterogenous observations (Olsen et al. 2012; Guo et al. 2017). Reported differences across sensory modalities could reflect technical discrepancies or real physiological differences in the physiology of different primary sensory cortices.

Emerging theories of brain function suggest that the cortex 'models' the world and the statistics of its environment (Friston 2005; Bastos et al. 2012; Hawkins et al. 2018; Pezzulo et al. 2022). The causes and optimally adaptive responses to light, sound, and touch for an organism might be expected to differ considerably, and these sensory modalities may contain different levels of sensory noise, so it may therefore be expected that this is reflected in differences in the microarchitecture and integration of signals by different sensory cortices (Knill & Pouget 2004; Deneve et al. 2001; Ma et al. 2006; McGurk & MacDonald 1976). However, the few individual studies that examine L6CT across primary cortices of different sensory modalities find more similarities than differences between them (Kim et al. 2014). This comparative evidence is scarce and insufficient to draw strong conclusions, and it remains important to elucidate what are genuine physiological differences between sensory cortices vs differences due to experimental technique, as differences between L6CT methodologies across sensory modalities makes it challenging to aggregate observations in order to give rise to general principles of L6CT function.

The cortex is weakly driven by the thalamus due to sparse connectivity, convergence and low release probability, but TC cells can excite the cortex through synchronous activity, and strong peripheral stimulation can synchronise TC cells (Bruno & Sakmann 2006; Benshalom & White 1986; Ringach 2021). Indeed, thalamic bursts have been reported to dramatically increase the probability of cortical spiking, with the pre-burst silence implicated in a more than doubling of synaptic efficacy (Swadlow & Gusev 2001; Swadlow et al. 2002). This suggests that in driving synapses that have high tonic firing rates, the oscillatory activity where highly synchronised inputs are succeeded by highly synchronised silences may be a more effective means of information transfer to the cortex. In the thalamus, a greater hyperpolarisation will de-inactivate more T-Type $Ca^{2+}$ channels and increase the magnitude of the LTS, which results in more action potentials per burst (Mease et al. 2017; Zhan et al. 1999). Rhythms of synchronous excitation and inhibition may therefore signal with greater efficacy within the TC and CT systems, helping to overcome the many endogenous processes keeping the brain relatively quiet (Shoham et al. 2006; Barth & Poulet 2012). Different neuronal subtypes possess different intrinsic resonant frequencies, and cortical oscillatory state may therefore be influenced by greater or lesser synchronisation in these different neuronal subtypes (Fries 2015; Fries 2005). For example, superficial cortical layers tend to resonate in gamma frequencies, as do inhibitory neurons, whereas deeper cortical neurons show stronger alpha and beta oscillatory power (Maier et al. 2010; Buffalo et al. 2011; Cardin et al. 2009; Siegle et al. 2014). Indeed, strong drive in one cortical layer is capable of synchronising other cortical layers (Adesnik 2018). Recent research has also indicated that L6CT excitation may shape the oscillatory state across A1 such that the timing of tone-evoked activity reaching A1 relative to L6CT activity would result in either its non-linear amplification or suppression across cortical layers, which then biases behavioural detection or discrimination respectively (Guo et al. 2017). Synchrony in action potentials arriving within the postsynaptic membrane time-constant is also influenced by feed-forward inhibitory influences that limit the time-window for excitatory integration (Fries 2015). In this way, neuronal populations can entrain distinct populations to their rhythm. It has even been suggested that the oscillatory frequencies could convey information in and of themselves, as a substrate of neural syntax (Buzsáki & Vöröslakos 2023; Buzsáki 2010; Fries 2015).

In this exploratory study I investigate whether cortical activity is altered by increased L6CT activity in a linear fashion with respect to L6CT activity, and whether this was dependent on

the recipient cortical subpopulation, L6CT activity, and/or L6CT synchrony. I describe that cortical subpopulations are differentially modulated by L6CT activity in a bidirectional fashion dependent on L6CT level of activity, and that L6CT can entrain cortical subpopulations to its firing frequency. Stimulation of L6CT at different frequencies also influenced thalamic firing mode as a function of stimulation frequency, and thalamic firing rate as a function of L6CT activity.

## 5.2. S1 L6CT bidirectionally modulates cortical signalling in an activity-dependent manner

To assess how different L6CT outputs modulated cortical population activity, I recorded activity across the S1 cortical column in lightly anaesthetised Ntsr1-Cre-Chr2-EYFP mice whilst performing optogenetic stimulation of L6CT neurons at increasing light intensities. Increasing the light intensity whilst stimulating at 10 Hz elicited a decrease in the post-pulse first-spike latencies of the cortical populations, with the shift occurring in deepest units at lower light intensities (**Fig. 8a**). Interestingly, at higher laser intensities, units located more superficially showed decreased first-spike latencies, though not to the same extent as the deepest units. I 'optotagged' putative L6CT units based on their short first-spike latencies and low standard deviation of first-spike latencies, which specifically tagged units recorded from the electrodes deepest in the cortex (**Fig. 8b**). After separating the L6CT population from the rest of the S1 population, I could investigate the effect of differing L6CT activity levels on basal firing in S1. At laser intensities too low to sustain elevated L6CT activity, there was no obvious change in S1 activity. However, at low sustained L6CT activity, there was a suppression of S1 activity that persisted for the duration of the light stimulus (**Fig. 8c**). Surprisingly, further increases in the intensity of the light stimulus caused elevated S1 activity compared with baseline that peaked earlier as a function of light intensity and L6CT activity. This population activity could reflect heterogeneous subpopulations within S1 that respond differently to increased L6CT activity, so to track individual unit movements, I calculated modulation indices (MIs) that quantify activity change proportional to baseline activity and tracked single-units between low and high L6CT conditions. Low L6CT activity caused a significant reduction in MIs across the S1 population (**Fig. 8d**). High L6CT activity also induced a significant shift in MI from both low L6CT and baseline activity. 65 % (517/791) of S1 single-units showed an increased MI from low to high L6CT conditions, with ~40 % (316/791) of S1 single-units exhibiting a direction switch from low to high L6CT conditions, whilst only ~10 % (84/791) showed a lower MI for high L6CT than for low L6CT. Taken together, these results indicate that cortical excitability can be bidirectionally modulated based on the magnitude of sustained L6CT activity.

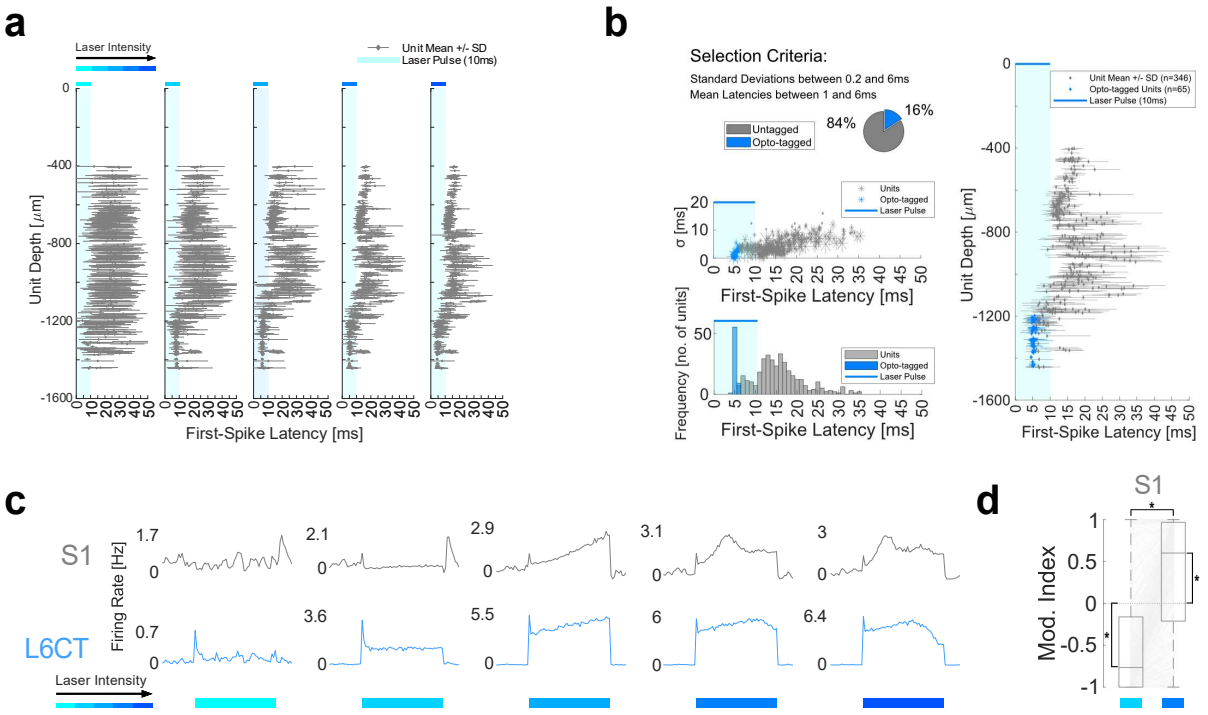


**Figure 8: S1 L6CT bidirectionally modulates cortical signalling in an activity-dependent manner.** 10 Hz laser trains (10 ms pulse length) were applied to S1-HL of Ntsr1-Cre-ChR2-EYFP mice (*n* = 5 mice) as part of a 5 second on 5 second off protocol (> 1000 pulses in total per mouse). The mean first-spike latency and the standard deviation of the first spike latency to all 10 ms laser pulses was calculated per unit from a pooled dataset.
**(a)** Single-unit first-spike latencies plotted against cortical depth for increasing laser stimulation intensities (left to right: 58, 123, 382, 802, 1201 mW/mm$^2$ from fibre tip).
**(b)** Example L6CT 'Optotagging' (802 mW/mm$^2$ from fibre tip) based on first-spike latency and the respective standard deviation results in tagged units registered at the deepest recording depth.
**(c)** Population PSTHs of S1 (non-tagged) (top) and L6CT (bottom) populations for increasing laser stimulation intensities (left to right: 58, 123, 382, 802, 1201 mW/mm$^2$ from fibre tip). As L6 activity increases with increased laser intensity, S1 population activity is initially suppressed, but then increases as L6 activity is increased (Example experiment).
**(d)** Modulation indices for 791 S1 units from *n* = 5 mice showing suppression of S1 activity under low (<= 382mW/mm²) L6CT (215 units) population activity (median MI = -0.76) and increased S1 under high (> 382mW/mm²) L6CT population activity (median MI = 0.6). Lines denote individual unit MI movement between conditions. Increasing the optogenetic stimulation from low to high also induced a switch from suppressed to elevated S1 MIs. * represents $p < 0.05$; 8d: Wilcoxon signed-rank test. Data from Ross Folkard. Exact *p* values in Supplementary Table 1.

It was apparent from **Fig. 8 a & b** that within the S1 population there were two subpopulations that were separable by their respective first-spike latencies and depths. Putative (put.) L4 units had a larger mean first-spike latency and respective standard deviation compared with L6CT units and resided on the upper channels of the recording probe, whereas put. L5 units resided between the L6CT and put. L4 populations and had the largest mean first-spike latency with the largest respective standard deviation (**Fig. 9a**). Both subpopulations seemed to show suppressed activity to low L6CT excitation, though appeared to differ in the rate at which increased L6CT switched their activity from suppressed to excited (**Fig. 9b**). When quantifying the suppressive effect of low L6CT excitation, both put. L4 and L5 subpopulations saw their activity significantly suppressed (**Fig. 9c**). The MI change between populations also differed, with put. L5 units (median MI = -0.96) displaying a more potent suppression than put. L4 (median MI = -0.38). Populations also differed in their basal activity (Put. L4 = 0.27 Hz, Put. L5 = 1.1 Hz). In the high L6CT condition, both put. L4 and put. L5 populations exhibited increased activity that differed significantly between each other, with put. L4 (median MI = 0.98) showing greater enhancement than put. L5 (median MI = 0.30) under high L6CT

excitation. Just over half of put. L4 units exhibited a MI direction switch (82/163) from low to high L6CT conditions, with 76 % showing an increased MI from low to high L6CT (124/163), whereas ~55 % of L5 units switched MI sign (119/218), with 78 % showing an increased MI from low to high L6CT (169/218). Taken together, this analysis indicates that cortical subpopulations at different depths show L6CT-mediated activity switches, though the extent of inhibition or excitation L6CT activity exerts on single-units differs based on which subpopulation they belong to (**Fig. 9d**).

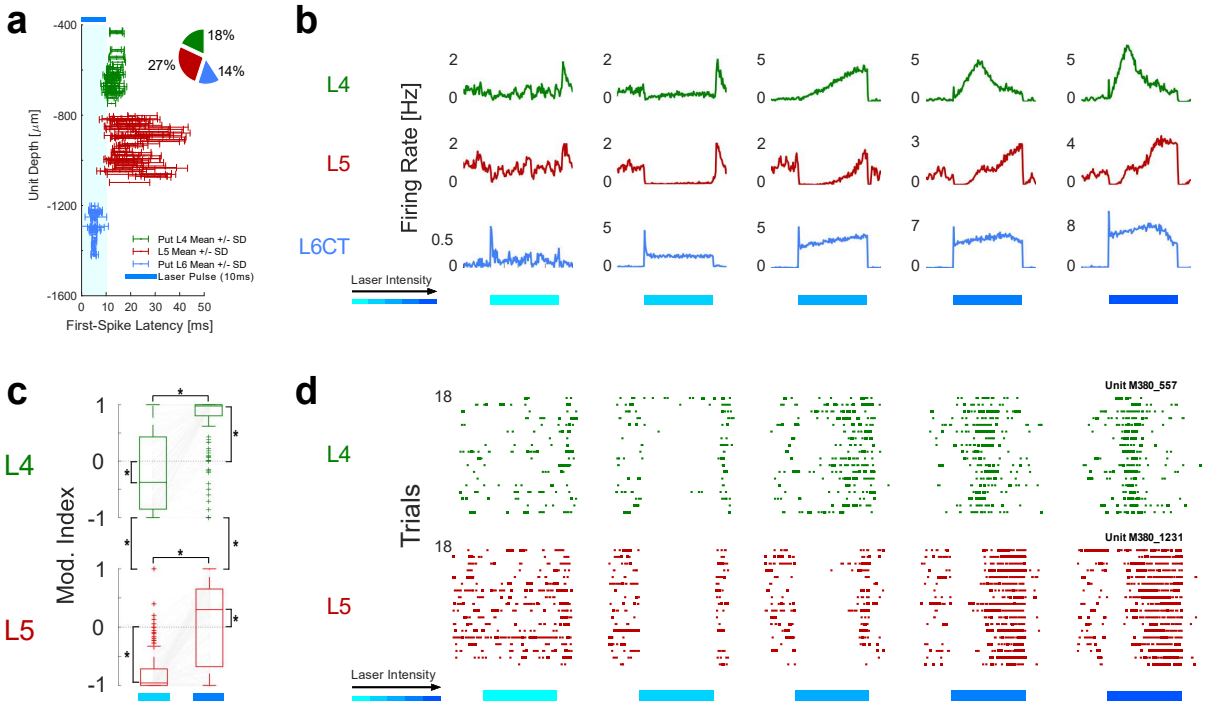


**Figure 9: L6CT activity switch modulates distinct cortical subpopulations differently.**
**(a)** Example latency vs depth plot showing optotagged L6CT units (58 units, blue), as well as distinct cortical subpopulations (*n* = 75 units, green; 112 units, red) that show different L6CT evoked first-spike latencies and latency variability, as well as different cortical depths.
**(b)** Example population activity under increasing L6CT activity for the putative L4 (green) and L5 (red) subpopulations. L6CT activity seems to influence the direction of population activity in both subpopulations.
**(c)** Box and Whisker plots showing modulation indices for putative L4 (green) and L5 (red) under lower (light blue) and higher (dark blue) L6CT activity (median L6 low = 0.83Hz, median L6 high = 3.77Hz) for *n* = 5 mice. Low (<= 382mW/mm²) L6CT activity induced significantly lower L4 activity (*n* = 163 units, median MI = -0.38) as well as L5 suppression (*n* = 219 units, median MI = - 0.95). In contrast, high (> 382mW/mm²) L6CT activity increased L4 (median MI = 0.98) and L5 activity (median MI = 0.3). Increasing L6CT stimulation from low to high also induced a switch from suppressed to elevated MIs in both L4 and L5 populations. L5 was suppressed more than L4 under low L6CT activity, and L4 was excited more than L5 under high L6CT activity.
**(d)** Single-unit raster plots showing putative L4 (green) and L5 (red) single-unit responses to increasing light intensities of optogenetic L6CT stimulation. Data from Ross Folkard. * represents $p < 0.05$; 9c: Wilcoxon signed-rank test (within-group differences), Wilcoxon rank sum (between-group differences). Exact *p* values in Supplementary Table 1.

## 5.3. S1 L6CT stimulation induces frequency-dependent facilitation in upper cortical layers.

The bidirectional activity switch exhibited by L4 and L5 populations to increased L6CT activity indicates non-linear responses to increased L6CT spiking. A potential mechanism for this is

frequency-dependent facilitation, the summation of EPSCs due to multiple presynaptic action potentials occurring in quick succession. As L6CT activity is increased, the probability of such events occurring may also increase and could therefore be reflected in a greater spiking output across a population. The L6-L4 synapse has previously been demonstrated to exhibit paired-pulse facilitation (Lee & Sherman 2008). To test whether L4 and L5 populations underwent increases in activity depending on the frequency of L6CT activation, I performed 64-channel electrophysiological S1 cortical recordings where Ntsr1-Cre-Chr2-EYFP mice were stimulated with 10 ms light pulses at different frequencies. This elicited reliable spiking in L6CT units that could then serve to examine frequency-dependent responses to L6CT in cortical subpopulations (**Fig. 10a**). The typical L4 response to low frequency L6CT stimulation was an increase in activity relative to baseline that increased in a frequency-dependent manner (**Fig. 10b**). In contrast, low frequency L6CT stimulation suppressed L5 activity for at least 50 ms after the light stimulus onset. As the frequency of L6CT stimulation increased however, the magnitude of post-L6CT suppression seemingly decreased, and higher frequency stimulation even induced an increase in L5 activity in the 50 ms following optogenetic stimulation, although an initial inhibition always seemed present. To investigate whether frequency-dependent facilitation occurred, I compared responses in 50 ms post optogenetic stimulation between 1st and 3rd pulses in both the 1 Hz and 10 Hz conditions (**Fig. 10c**). Intriguingly, L4 units showed an increased response to the 3rd stimulus compared with the 1st stimulus in both the 1 Hz and 10 Hz conditions, though 10 Hz exerted greater facilitation than 1 Hz. In contrast, only 10 Hz caused significantly increased responses in L5 units to the 3rd pulse (**Fig. 10d**). When assessing the change in responses between 1st and 3rd pulses across conditions, 10Hz showed a larger increase in MI vs 1 Hz in both L4 and L5, and when compared under the same timepoints to continuous L6CT stimulation, continuous stimulation induced negative MIs in the majority of L4 and L5 units (**Fig. 10e**). Thus, for the same time-periods during L6CT stimulation, L4 and L5 can be both facilitated or suppressed depending on the nature of L6CT stimulation.

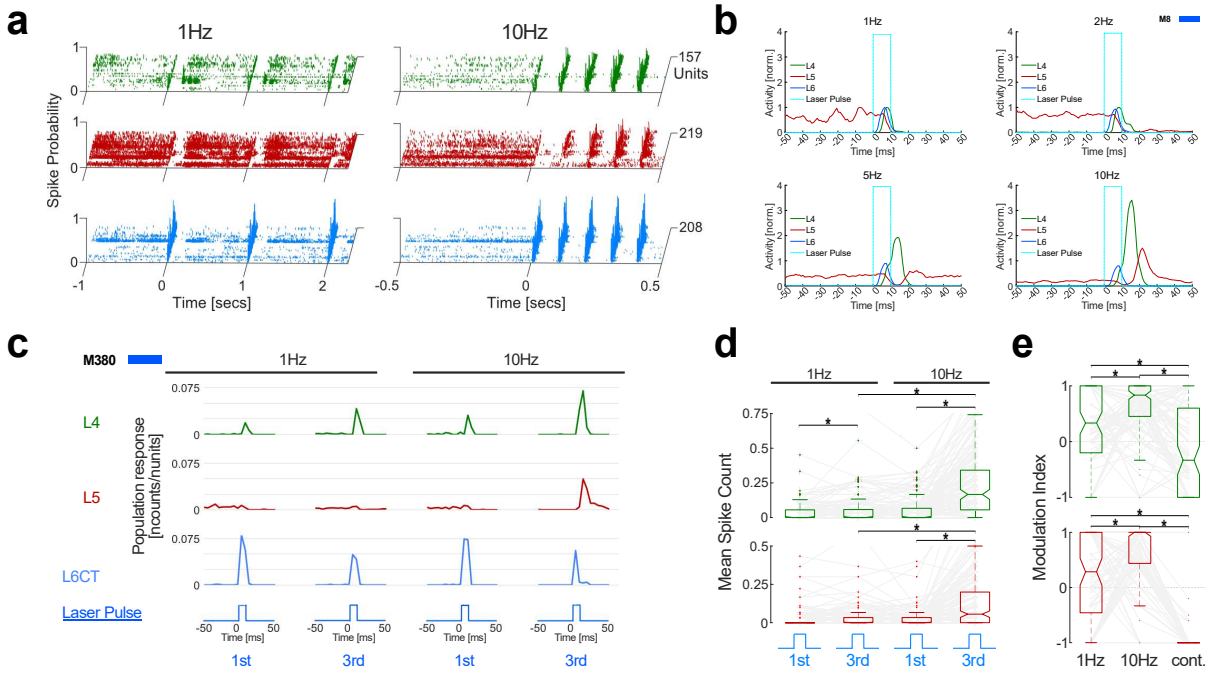


**Figure 10: L6CT excitation causes frequency-dependent facilitation in L4 and L5.**

**(a)** Unit PSTHs across trials for 1 Hz (left) and 10 Hz (right) stimulation of L6CT neurons across trials. *n* = 5 mice. High frequency pulses of high L6CT stimulation tends to increase the probability of spiking per laser pulse per unit. Spike probability of 1 = 1 spike per trial per bin for a given unit. Bin size = 1ms.
**(b)** Example population PSTH of 50ms pre and post onset of optogenetic stimulation (laser pulse - light blue dotted line) for 1 Hz (top left), 2 Hz (top right), 5 Hz (bottom left) and 10 Hz (bottom right) frequencies. Normalised with respect to max. subpopulation response to 1Hz stimulus*. Units from a representative experiment: L4 = 15, L5 = 31, L6CT = 39.
**(c)** Example PSTHs of L4 and L5 population responses (split into 5ms bins) to 1st and 3rd 10ms optogenetic pulses in a stimulus train in a 1 Hz and 10 Hz condition. Data from representative experiment: L4 = 75, L5 = 112, L6CT = 58.
**(d)** Mean spike counts for L4 and L5 units in response to the 1st and 3rd optogenetic pulse in the 1 Hz and 10 Hz stimulus trains. 10Hz causes greater facilitation in L4 than 1 Hz, and similarly causes facilitation in L5 unit responses. Units pooled from *n* = 5 experiments: L4 = 157, L5 = 219, L6CT = 208.
**(e)** Modulation indices for the difference in responses between 1st and 3rd pulses for the 1 Hz and 10 Hz conditions and the equivalent time periods of continuous pulses as for 10Hz. MIs for 10 Hz are greater than for 1 Hz in L4 and L5, whereas MIs for continuous L6CT stimulation are lower than both 10 Hz and 1 Hz in L4 and L5. Units pooled from *n* = 5 experiments: L4 = 157, L5 = 219, L6CT = 208. Data from Ross Folkard. * represents $p < 0.05$; 10d & e: Wilcoxon signed-rank test. Exact *p* values in Supplementary Table 1. *PSTH = units x bins summed over trials. PSTH./ntrials. popPSTH = sum(PSTH,1). Max = max(popPSTH) for 1Hz condition. For every condition, follow the same procedure but divide by this max. value rather than max. for that condition. Laser power at fibre tip exceeded 382mW/mm² for the data in this figure.

## 5.4. S1 L6CT entrains subpopulations in upper cortical layers through regulation of cortical synchrony.

Given the contrasting effects of cortical responses to 10 Hz vs continuous L6CT stimulation, despite elevated L6CT activity in both conditions (**Fig. 11a & b**), I speculated about whether a dominant determinant of cortical responses was the synchrony of L6CT independent of overall L6CT activity. To derive a measure of cortical synchrony independent from activity, I binned the activity during the stimulation trains of the different conditions into PSTHs of different bin sizes. I could then determine the average population coactivity (how many active units there are on average in a given bin for a given trial) as a function of bin size. Because this coactivity measure is heavily dependent on bin sizes (larger bins tend to contain activity from more units), I then assessed the degree to which L6CT coactivity changes as a function of bin size (for a given condition, how much does coactivity change when the bin size is increased by x ms), with the largest differences between conditions arising over bin size increases within 5 ms (**Fig. 11c**). I used the maximum value as the measure of population synchrony for that condition. When these synchrony measures were plotted against the total L6CT population activity during the stimulation per condition, both the slope gradient and the $r^2$ were close to zero, suggesting little correlation between the synchrony measure and the recorded measures of L6CT activity across conditions (**Fig. 11d**). At high laser intensities, the low frequency stimulation conditions tended to produce L6CT activity that was comparatively high in synchrony and low in activity, whereas continuous stimulation produced the inverse (**supp. Fig. 3a**).
When separating the activity and synchrony of the other cortical subpopulations, L6CT activity predicted the activity of L4 only, and was not a significant predictor of L5 activity (**Fig. 11e**). Neither L4 activity nor L5 activity were correlated significantly with L6CT synchrony. In contrast, L6CT synchrony significantly predicted L4 and L5 synchrony, and L4 synchrony was further correlated significantly with L6CT activity (**Fig. 11f**). Taken together, L6CT spiking exerts a strong influence on L4 spiking, with its activity shaping both L4 activity and synchrony. Additionally, L6CT entrains both L4 and L5 spiking through its influence on population spiking synchrony whilst in the case of L5 not necessarily altering overall activity. Intriguingly, L5 activity, though not correlated with L6CT activity, was significantly correlated with L4 activity

(**supp. Fig. 3b**), and coupled with the temporal sequence of population activity (L6CT → L4 → L5; **Fig. 9a & 10b**) may further support this sequence of information flow.

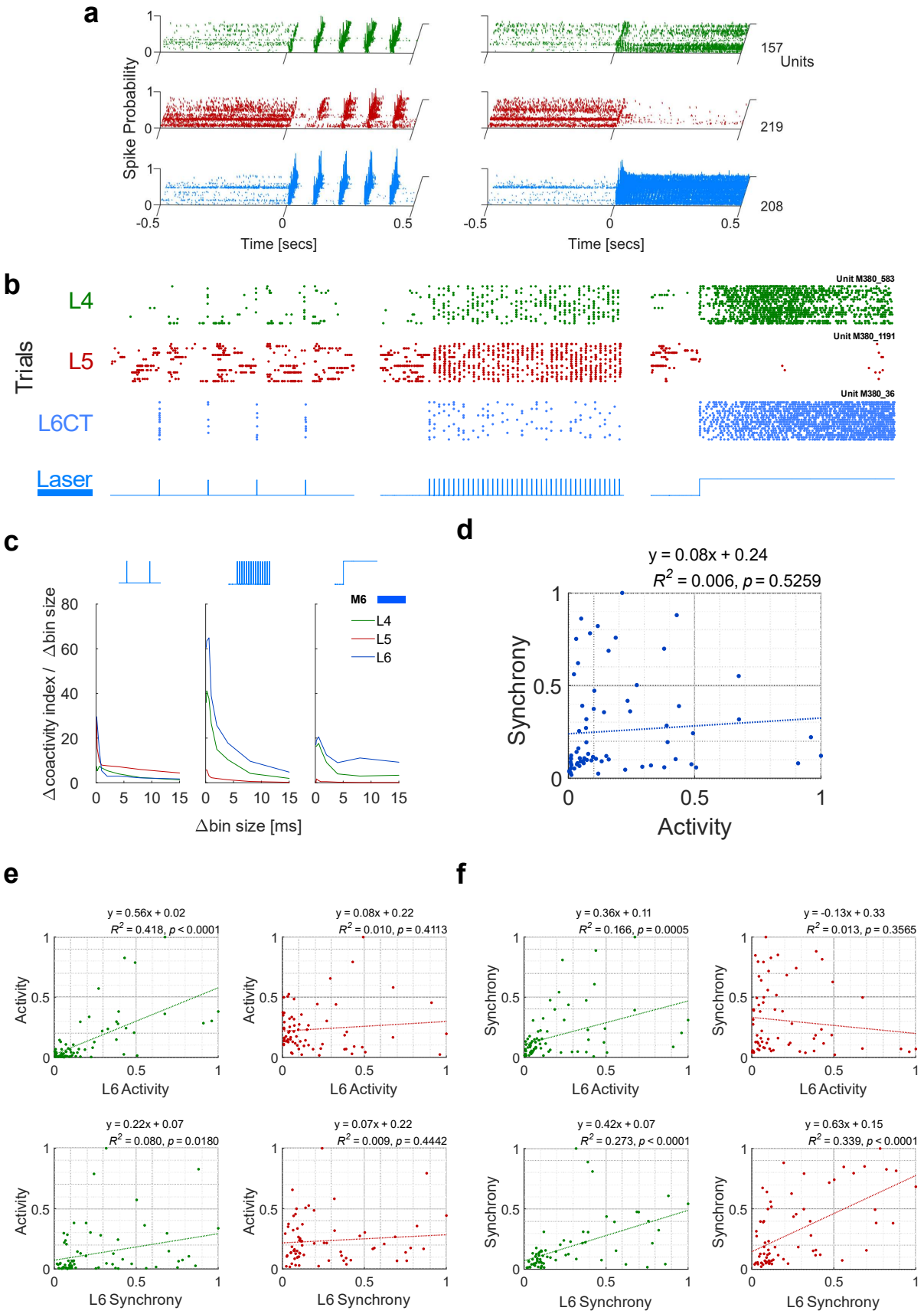

**Figure 11: L6CT entrains L4 and L5 subpopulations by influencing population firing synchrony.**
**(a)** Unit PSTHs across trials for 10Hz (left) and continuous (right) stimulation of L6CT neurons across trials. *n* = 5 mice. Spike probability of 1 = 1 spike per trial per bin for a given unit. Bin size = 1ms.
**(b)** Example single-unit raster plots displaying responses of L6CT, L4 and L5 populations to optogenetic stimulation under different conditions (1 Hz, 10 Hz, continuous).
**(c)** Example synchrony plot. Synchrony measure calculated as max increase in coactive units as a function of bin size increase, normalised to the max of all conditions (*n* = 70) across experiments. *n* units: L4 = 20, L5 = 15, L6 = 29.
**(d)** Normalised Activity vs Synchrony scatter plot for L6CT pooled across experiments demonstrating little covariance between measures, indicating sufficient extraction of independent measures of synchrony and activity.
**(e)** Effect of L6CT activity (top) and synchrony (bottom) on activity in L4 (green) and L5 (red). L6CT activity predicts > 40% of L4 activity variability.
**(f)** Effect of L6CT activity (top) and synchrony (bottom) on synchrony in L4 (green) and L5 (red).
A-d calculated with response windows 0-5 seconds. B-d: 70 data points across 5 experiments.
Data from Ross Folkard.

## 5.5. S1 L6CT activity patterns bidirectionally influence thalamic firing mode

Having observed how L6CT activity affected cortical dynamics, it remained to be tested how different L6CT spiking patterns shape thalamic states. I performed recordings of VPL in Ntsr1-Cre-Ch2-EYFP mice during different patterns of light stimulation to activate ChR2 in L6CT neurons and in turn observe changes in VPL activity. In one instance, I performed a dual recording in S1 and VPL to observe activity in both L6CT and VPL populations simultaneously (**Fig. 12a, b, & c**). The L6-TC synapse has been shown previously *in vitro* to undergo paired-pulse facilitation (Crandall et al. 2015; Jurgens et al. 2012). To address this *in vivo*, I calculated the probability of spiking in response to 1st and 3rd optogenetic pulses of either a 1 Hz or a 10 Hz stimulus train **(Fig.12c**). Consistent with this, 3 optogenetic light pulses delivered at 10 Hz, but not 1 Hz, was sufficient to induce an increased probability of spiking in VPL units (**Fig. 12d**) Previous studies have demonstrated that continuous L6CT excitation induces a switch in neurons from burst to tonic mode (Mease et al. 2014; Ziegler et al. 2023). However, other stimulation protocols have been less comprehensively studied, and different L6CT stimulation frequencies have non-linear effects in S1 (**Fig. 11**). I stimulated VPL units with 1 Hz, 10 Hz and continuous optogenetic excitation of L6CT cells. To quantify bursting, I defined burst spikes in a manner identical to **Fig. 7** (2 or more spikes that each do not exceed 6 ms inter-spike-intervals, which are preceded by at least 50 ms prior silence, and do not exceed 100 ms duration). This enabled conservative classification of bursts and identification of burst spikes (**Fig. 12e**). As reported in previous literature, I found that continuous stimulation of L6CT indeed decreased the burst-event ratio, a measure of the proportion of bursts relative to total activity, suggesting a shift in the population towards tonic-firing mode (**Fig. 12f**). In contrast, both 1 Hz and 10 Hz L6CT stimulation induced an increase in burst-event ratios, indicative of elevated burst-mode activity, with 10 Hz inducing a greater shift than 1 Hz. All L6CT stimulation patterns induced an increased number of bursts (**Fig. 12g**), with 10 Hz inducing the greatest increase in total burst number, whereas 1 Hz and continuous stimulation did not differ significantly from one another. All L6CT stimulation patterns induced an increase in total spike rate, which seemingly correlated with total amount of optogenetic stimulation and L6CT activity (**supp. Fig. 3a**) in that 1 Hz elicited the smallest increase in spike rate and continuous stimulation the largest (**Fig. 12h**). Taken together, these results suggest that L6CT excitation

serves to increase thalamic throughput in a manner proportional to the amount of L6CT stimulation, but the dynamics of L6CT stimulation influences the firing-mode with which the thalamic signalling is transmitted.

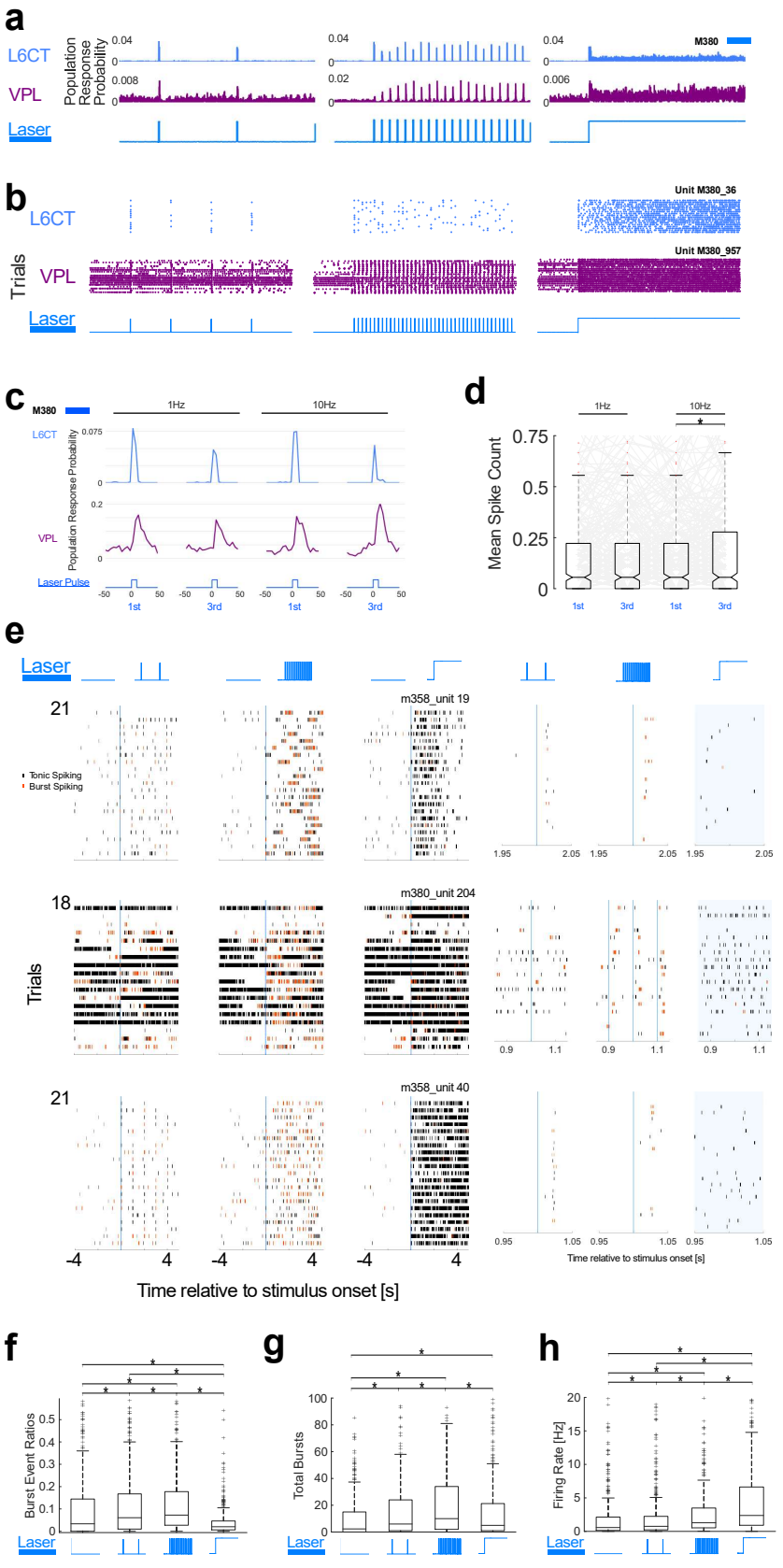


**Figure 12: L6CT stimulation patterns shape spike rates and firing modes in VPL.**
**(a)** Example Population PSTHs for L6CT (top) and VPL (middle) populations simultaneously recorded during 1 Hz (left), 10 Hz (middle), and continuous (right) optogenetic stimulation of L6CT neurons.
**(b)** Example Raster plots of L6CT (top) and VPL (middle) single-units simultaneously recorded during 1 Hz (left), 10 Hz (middle), and continuous (right) optogenetic stimulation of L6CT neurons.
**(c)** Example dual recording in S1 and VPL demonstrating increased VPL activity to the 3rd pulse of 10 Hz condition.
**(d)** VPL population shows increased response to 3rd pulse of a 10 Hz train, but not 3rd pulse of a 1 Hz train. 439 units, *n* = 4 mice.
**(f)** Frequency stimulation conditions increased burst event ratios relative to baseline in a dose-response manner (10 Hz > 1 Hz), whereas continuous stimulation decreased burst event ratios relative to baseline. 439 units, *n* = 4 mice.
**(g)** L6CT stimulation increased total burst number relative to baseline, with the greatest increase observed for 10 Hz L6CT stimulation. 439 units, *n* = 4 mice.
**(h)** L6CT stimulation increased total firing rate relative to baseline, displaying a dose-response relationship with respect to total optogenetic stimulation. 439 units, *n* = 4 mice. Data from Ross Folkard. * represents $p < 0.05$; 12d & f-h: Wilcoxon signed-rank test. Exact *p* values in Supplementary Table 1.

## 5.6. Discussion

I demonstrated in S1 that L6CT excitation can modulate cortical activity not just in a non-linear fashion, but also in an opposite direction. Whilst these experiments did not specifically test which mechanisms were at play for this bidirectional modulation of activity, this bidirectional switch occurred in at least two distinct cortical subpopulations, and to different extents, suggesting that this switch can occur at different types of synapses, and that a bidirectional switch is in principle not narrowly limited to finely tuned synaptic and circuit configurations. Therefore, although the bidirectional switch was surprising, L6CT is unlikely the only cell-type with the necessary circuitry to induce a bidirectional switch based on its activity level. Indeed, a similar bidirectional switch has been observed in the thalamus in response to varying degrees of L6CT activity (Crandall et al. 2015). Given that the aforementioned study implicated feed-forward inhibition as a key factor in the switch, this opens up the possibility that other neuronal circuits with feed-forward inhibitory circuitry may display activity switches where the downstream population is inhibited at one level of upstream population activity, and excited under upstream population activity at another level. Further investigation of circuitry utilising optogenetic excitation might reveal non-linear population effects by exciting the target population at a range of stimulus intensities to investigate neuronal circuit activity over a range of population firing rates. Additionally, this invites investigation into circuits previously dissected with optogenetic manipulation that may show greater context-dependence and non-linearity than originally recognised.

L5 activity triggered by L6CT activation produced consistently longer first spike latencies that were more variable than L4 activity, suggesting that L5 excitatory responses at high L6CT activity or frequency may have arisen through multiple synapses. This is corroborated by population PSTHs that even under high frequencies show initial L5 inhibition followed by rebound elevated activity above baseline. This suggests that L5 might be inhibited by L6CT and subsequently receive sufficient excitation through an intermediary in the higher frequency conditions that is not present in the lower frequency conditions, and that these facilitatory responses are not mediated predominantly through direct ionotropic mechanisms in the L6CT-L5 synapse. That L4 activity was a much stronger predictor of L5 activity than L6CT activity may also indicate that L4 is an intermediate cause of L5 excitatory responses under high L6CT activity. L5 dendritic arbours have been observed close to L4/L5 border, though the more observed route of L4 to L5 communication is thought to be predominantly via L2/3 (Adesnik & Naka 2018; Douglas & Martin 2004; Gilbert & Wiesel 1983; Gilbert & Wiesel 1979). This could also explain why excitation is not seen at lower L6CT activity levels, as L4 is not as active under low L6CT and is indeed itself mildly inhibited under these circumstances. I show that L4 also undergoes frequency-dependent facilitation to L6CT activity, which could partially explain the frequency-dependent L5 facilitation observed, through an increased excitatory drive. Unlike L5, L4 has not been shown to be strongly excited by single L6CT spikes, and L4 cells possess metabotropic glutamate receptors that reportedly hyperpolarise the cell membrane (Kim et al. 2014; Lee & Sherman 2012; Lee & Sherman 2009). Despite this, there was a notable positive correlation between L6CT activity and L4 activity as well as frequency-dependent facilitation in L4 units to repeated pulses of L6CT excitation, possibly due to direct facilitatory effects overcoming metabotropic suppressive modulation (Lee & Sherman 2008; Kim et al. 2014; Lee & Sherman 2012; Lee & Sherman 2009).

The frequency-dependent facilitation of L4 could aid in amplifying sensory inputs from thalamic regions, which are thought to predominantly terminate in L4 (Gilbert & Wiesel 1979; Douglas & Martin 2004; Adesnik & Naka 2018; Constantinople & Bruno 2013; Sherman & Guillery 2002; Clascá et al. 2012). A flurry of L6CT activity prior to arrival of TC input should increase the probability of postsynaptic spiking in L4, as it does under basal conditions in this study, which in turn may increase the cortical output in L5. One surprising finding was the facilitation observed in L4 to 1 Hz L6CT stimulation, something that was absent in L5. This suggests that L4 may integrate information from L6CT over much longer time windows than L5 does; in essence L4 has a longer 'memory' of L6CT activity compared with L5. The exact mechanisms behind this remain unknown, and whilst metabotropic glutamatergic activation may work within these timescales, such metabotropic receptors so far identified in L4 signalling seem predominantly to suppress L4 activity (Lee & Sherman 2009; Lee & Sherman 2012).

I also constructed a computational tool for separating neuronal population synchrony from activity, which was validated on L6CT population data, and was able to independently investigate the role of activity and synchrony on downstream neuronal spiking responses. This approach is somewhat similar to the one by *Russo et al.* but was tailored to measure population synchrony rather than to identify neuronal ensembles (Russo & Durstewitz 2017). This enabled dissociation of L6CT population synchrony from activity, such that both were independent parameters with little correlation. As a result, this enabled more detailed analysis investigating how L6CT influenced downstream cortical subpopulations. Whilst L6CT activity was a strong predictor of L4 activity, that in turn influenced and preceded L5 activity, L6CT activity did not strongly predict L5 activity, in that changes in total L5 output did not significantly correlate with changes in L6CT population activity. However, L6CT synchrony was a strong predictor of both L4 and L5 synchrony. So, in the case of L5 population activity, L6CT influenced the time when a L5 unit was active, and whether it was active in tandem with other L5 units, but not necessarily how active it was. Therefore, if one hypothesises that there is information transfer along L6CT→L4→L5, it would appear that L6CT neuronal synchrony is preserved more robustly than its total spiking output, and that L6CT synchrony and activity could represent distinct channels during information transfer (Buzsáki & Vöröslakos 2023; Buzsáki 2010). The differing contributions from L6CT synchrony vs activity to cortical signalling additionally provided a useful validation of the synchrony measure and the methodological tool.

By modulating cortical synchrony, L6CT may shape integration windows for arrival of sensory information that may influence how that sensory information is processed. *Guo et al.* reported that auditory tones presented within 50 ms of optogenetic L6CT stimulation cessation in primary auditory cortex (A1) were better discriminated against tones of similar frequencies, though were less likely to be detected. The opposite effect followed a 150 ms delay between L6CT stimulation cessation and tone, where detection of stimuli improved, but discrimination between stimuli was impaired (Guo et al. 2017). Similar research suggests that sensory signals may be either enhanced or suppressed depending on which phase of a cortical oscillation they arrive during (Cardin et al. 2009; Siegle et al. 2014). S1 L6CT through entrainment of cortical activity to specific periods may perform a similar action on sensory signals, which may bias the cortex towards stimulus detection or discrimination. Subsequent research reports that L6CT cells in primary auditory cortex (A1) increase activity prior to self-initiated sounds in a reward setting, but not during regular self-generated sounds caused by locomotion (Clayton et al. 2021). My research suggests that L6CT is able to impart its

synchrony to other cortical layers, such that depending on the timing of the sensory input relative to the cortical oscillatory phase, the sensory input may be either amplified or suppressed. It has been previously demonstrated that L6CT continuous stimulation can induce translaminar modulation in the cortex, but my findings suggest L6CT at physiological frequencies can entrain cortical signalling in upper layers to specific L6CT rhythms.

Neuronal rhythms have been postulated as a possible neural syntax with which messages, in the form of spikes, are conveyed throughout the brain (Buzsáki & Vöröslakos 2023; Buzsáki 2010). L6CT manipulation was capable of altering periods of L5 population excitation and inhibition in an oscillatory manner, without altering its total excitability. In terms of a message passing scheme, it might prove beneficial to be able to alter the syntactic structure of a message - in this case the oscillatory activity - without drastically altering the incoming sensory information - the total spiking activity. Mechanisms for generating multiple messages through different parsing of the underlying information occurs in biological systems; perhaps the most famous example being alternative ribonucleic acid (RNA) splicing that gives rise to expression of functionally different messenger-RNA (mRNA) molecules (Berget et al. 1977). This alteration to the cortical rhythm without altering the long-term firing rate of the cortical output in the absence of added peripheral input may additionally aid in avoiding saturation/distortion of neuronal signalling during sensory input from L6CT cells that receive comparatively little direct sensory input: i.e. maintaining bandwidth for firing rates to encode differences in peripheral inputs (Bastos et al. 2012; Markov et al. 2014; Felleman & Van Essen 1991; Vélez-Fort et al. 2014).

Within L5 are the major output pathways from the cortex. Therefore, one would expect consequential effects from altering L5 output so drastically (for example, see **Fig. 5** and **Fig. 6**). That L6CT can gate L5 output through purely its own activity levels warrants further investigation into how L6CT behaves in response to different environmental circumstances. As a modulator, and a highly non-linear transformer, of both cortical inputs and outputs, it seemingly has huge potential to sculpt what sensory information gets attended to by the cortex, and what processed information leaves the cortex. A major question pertains to how physiologically relevant the L6CT manipulation is in the studies above and optogenetic manipulations in general. Perhaps these results merely constitute a proof of principle that L6CT could potentially under unknown, yet extreme circumstances behave in a manner similarly to this, but in practice seldom does?
Firstly, it has so far proved experimentally challenging to record from and interpret the activity of numerous L6CT units simultaneously during behaviour. Whilst the typical L6CT cell appears most of the time to be virtually silent, L6 is the cortical layer with most cells, and it seems implausible that these cells have no function, even if the function is still not fully known (Vélez-Fort et al. 2014; Crandall et al. 2017; Dash et al. 2022; Molnár 2019; Meyer et al. 2010). Additionally, alterations to synaptic properties of the L6-TRN pathway, essentially converting L6-TRN from a modulatory to a driving synapse, have been shown to improve sensory learning of relevant tones amongst distractors tones, but impair the discounting of a previously reward-predictive but now irrelevant tone when presented alongside a predictive visual stimulus (Ahrens et al. 2015). This research implies a potent but nuanced role for endogenous L6CT activity in goal-oriented sensory discrimination, because if L6CT was not active, then alteration to the synaptic properties would not be expected to substantially modulate behaviour, and no additional exogenous L6CT excitation was evoked in this study. A plausible explanation for the reportedly low L6CT activity despite the marked influence of endogenous L6CT on

behaviour is that L6CT is active under certain circumstances, and as possibly the most populated layer of the cortex, there is capacity for cells to be more finely–tuned to specific features or contexts than cells in other layers (Meyer et al. 2010). As such, L6CT cells individually have a lower likelihood of firing compared to other cortical cell-types, possibly explaining why correlations between L6CT activity and single stimuli may not be as robust as for other cell-types in the cortex (Vélez-Fort et al. 2014; Dash et al. 2022). Additionally, L6CT cells receive a comparatively large proportion of their inputs from higher cortical areas (Bastos et al. 2012; Markov et al. 2014; Felleman & Van Essen 1991; Vélez-Fort et al. 2014). One study reported that V1 L6CT activity approximates the arithmetic sum of visual and vestibular signals, suggesting complex integrative capacities for L6CT cells (Vélez-Fort et al. 2018). Considering that state of the art recording and clustering technologies can isolate ~750 neurons from a 384-electrode probe, this represents a minority of L6CT cells in ~1.15 $mm^3$ section of cortex, even with the assumption that all electrodes reside in L6 (Steinmetz et al. 2019; Jun et al. 2017; Meyer et al. 2010). These reasons coupled with a selection bias for large, high-firing units in many extracellular *in vivo* electrophysiological recording techniques may partially explain the apparent dearth of L6CT activity, despite tangible effects from L6CT manipulation (Ahrens et al. 2015; Andolina et al. 2013; Andolina et al. 2007; Murphy & Sillito 1987; Vélez-Fort et al. 2014; Crandall et al. 2017; Dash et al. 2022; Molnár 2019; Meyer et al. 2010).

Secondly, L6CT neurons have been observed *in vivo* to fire between 0 and > 10 Hz (O'Connor et al. 2010), which in this study was a sufficient range of population firing rates to induce both inhibition and excitation of L4 and L5 neurons. Whilst it may not be the case that hundreds of L6CT cells reach this firing rate simultaneously under physiological conditions, it seems plausible that a few L6CT cells could suffice in inhibiting or exciting downstream L4 and L5 targets in a microcircuit.

Not only did L6CT flexibly modulate cortical activity, it also altered thalamic activity and firing mode. When L6CT was entrained to 1 Hz or 10 Hz frequencies, thalamic activity shifted towards burst-firing mode, whereas continuous L6CT activity shifted thalamic activity towards tonic firing. When comparing the different conditions with respect to their synchrony and activity, the frequency stimulations were previously demonstrated to have a greater synchrony/activity ratio than continuous stimulation for L6CT units (e.g. 10 Hz shows greater L6CT synchrony and lower total activity compared to continuous stimulation) (**supp. Fig. 3a**). Whilst the total spike rate seems to correlate best with overall L6CT activity for a given optogenetic manipulation, the firing mode seems to reflect conditions that tend to induce more L6CT synchrony. More simultaneous recordings of S1 and VPL would allow this to be quantifiably tested, as although L6CT synchrony and VPL activity were investigated under the same optogenetic frequencies and intensities, there are not enough VPL recordings where L6CT activity is simultaneously recorded to make concrete conclusions about how L6CT synchrony alters VPL firing mode. However, given the evidence above, it seems plausible that L6CT could modulate VPL activity, where VPL spike output could be influenced by the amount of L6CT activity, and the VPL firing mode influenced more by the L6CT synchrony.

Whilst e.g. 10 Hz optogenetic L6CT stimulation produced rhythmic activity across multiple cortical layers, the synchrony of the L6CT activity was most likely higher than would be expected from endogenous oscillatory activity at 10 Hz, in that the vast majority of L6CT units spiked within 10 ms of each other. This drawback of optogenetic stimulation may also have

knock-on effects in the modulation of L4 and L5 populations, as they also spiked with relatively high synchrony. As such, the modulations observed in this study may arguably reflect levels of L6CT synchrony more associated with endogenous gamma oscillations rather than alpha oscillations.

Optogenetic stimulation gives little control over the shape of population neuronal activity, i.e. how large the standard distribution and the coefficient of variation of stimulated cells are. Much of neuronal computation likely relies on high variability in activity within a population, and in populations with feed-forward inhibition this may paradoxically result in higher population activity needed to record non-linearities in neuronal systems (Ma et al. 2006). For example, the activity switch in a single cortical target may not require such high mean activity in the L6CT population if the population coefficient of variation is greater, as there may be less feed-forward inhibition to overcome than if all cells in L6CT population were excited to the same extent and therefore triggering lots of feed-forward inhibition. The outcome of this would be that bidirectional modulation of cortical firing may occur physiologically at lower L6CT activity levels than reported here.

Urethane anaesthesia has been shown to alter TC signalling and influence TC firing mode (Huh & Cho 2013b). Whilst cortical and thalamic effect sizes have been often normalised with respect to baseline in this study to account for the suppressive effect of anaesthesia and to emphasise relative changes in activity, one cannot rule out that urethane transforms I/O curves in a non-linear fashion, such that the relative changes may be greater or lesser in the awake mouse. Intuitively, anaesthesia would be assumed to more likely dampen rather than accentuate the relative effects of manipulations on neuronal activity, as otherwise the implication would seemingly be that the anaesthetised brain has a higher capacity than the awake brain for information encoding. However, these findings should still be validated in the awake mouse, particularly when cortical responses to thalamic spiking have been demonstrated to be enhanced by a preceding absence of spiking (Swadlow & Gusev 2001; Swadlow et al. 2002).

In summary, my research demonstrated that L6CT activity at different optogenetic stimulation intensities induces distinct modulations to activity in cortical subpopulations in opposite sign. This poses broad questions regarding the circuit functions of many neuronal populations and whether they too have both suppressive and excitatory effects dependent on activity levels. My research also suggests mono- and multi-synaptic facilitatory effects from repetitive L6CT activity, that in the case of L4 can possibly be integrated over seconds. I developed a method to dissociate population activity from synchrony, which was used to demonstrate that L6CT can entrain multiple cortical subpopulations to its rhythms in a manner that is distinct from its effect on their firing activity. Additionally, I observed that L6CT activity exerts bidirectional modulation of thalamic bursting probability as a function of its stimulation frequency, with potential roles for L6CT activity and synchrony mediating TC firing rate and mode respectively, though this awaits further validation. Investigation into the effects of L6CT manipulation during sensory perception in the awake mouse will go a long way to answering some of the questions raised from this research. Taken together, this research suggests that L6CT can ‘tune up’ or ‘tune down’ signalling in S1 and can independently shape cortical rhythmicity, whilst altering the emphasis of the type of information S1 receives from the thalamus.

# 6. Contributions

Figures 1-6 were adapted from *Ziegler et al.* (Ziegler et al. 2023). The experiments in *Ziegler et al.,* were planned primarily by: Prof. Dr. Alexander Groh, Dr. Rebecca Mease, Katharina Ziegler, Antonio Gonzalez, Jan Burghardt, and me, with contributions from Dr Sailaja Goda, Emilio Isaias-Camacho, and Dr. Jesus Martin-Cortecero. I contributed directly to the electrophysiological experiments throughout the thesis. Antonio Gonzalez assisted me in some electrophysiological experiments. Analysis and data presentation (figures) of electrophysiological data was performed by Dr. Rebecca Mease and me for figures 1-6. I helped plan the behavioural experiments, analysis and data presentation, but did not perform these directly myself, and none of the behavioural data I directly collected is presented in this thesis. von Frey data was acquired and analysed by Katharina Ziegler and Jan Burghardt, with Antonio Gonzalez performing CPA, CPP, and Hargreaves behaviour and analysis. Behavioural statistical analysis and presentation was discussed in group meetings and performed by Katharina Ziegler and Antonio Gonzalez.

For Figures 7 - 12 planning, acquisition, analysis, and data presentation was performed by me. Synchrony analysis was planned by Emilio Isaias-Camacho and me and was implemented by me in the programming language MATLAB with some use of functions written by Emilio Isaias-Camacho. MATLAB scripts and functions made by Emilio Isaias-Camacho and me were used in the electrophysiological data analysis throughout the thesis.

My work was funded predominantly through the B10 project in the DFG SFB1158 2nd round.

# 7. Bibliography


Abrahamsen, B. et al., 2008. The cell and molecular basis of mechanical, cold, and inflammatory pain. *Science*, 321(5889), pp.702–705.

Abraira, V.E. et al., 2017. The Cellular and Synaptic Architecture of the Mechanosensory Dorsal Horn. *Cell*, 168(1-2), pp.295–310.e19.

Abraira, V.E. & Ginty, D.D., 2013. The sensory neurons of touch. *Neuron*, 79(4), pp.618–639.

Adesnik, H., 2018. Layer-specific excitation/inhibition balances during neuronal synchronization in the visual cortex. *The Journal of physiology*, 596(9), pp.1639–1657.

Adesnik, H. & Naka, A., 2018. Cracking the Function of Layers in the Sensory Cortex. *Neuron*, 100(5), pp.1028–1043.

Ahrens, S. et al., 2015. ErbB4 regulation of a thalamic reticular nucleus circuit for sensory selection. *Nature neuroscience*, 18(1), pp.104–111.

Akopian, A.N. et al., 1999. The tetrodotoxin-resistant sodium channel SNS has a specialized function in pain pathways. *Nature neuroscience*, 2(6), pp.541–548.

Al-Khater, K.M. & Todd, A.J., 2009. Collateral projections of neurons in laminae I, III, and IV of rat spinal cord to thalamus, periaqueductal gray matter, and lateral parabrachial area. *The Journal of comparative neurology*, 515(6), pp.629–646.

Alshelh, Z. et al., 2016. Chronic Neuropathic Pain: It's about the Rhythm. *The Journal of neuroscience: the official journal of the Society for Neuroscience*, 36(3), pp.1008–1018.

Anastassiou, C.A. et al., 2015. Cell type- and activity-dependent extracellular correlates of intracellular spiking. *Journal of neurophysiology*, 114(1), pp.608–623.

Andolina, I.M. et al., 2007. Corticothalamic feedback enhances stimulus response precision in the visual system. *Proceedings of the National Academy of Sciences of the United States of America*, 104(5), pp.1685–1690.

Andolina, I.M., Jones, H.E. & Sillito, A.M., 2013. Effects of cortical feedback on the spatial properties of relay cells in the lateral geniculate nucleus. *Journal of neurophysiology*, 109(3), pp.889–899.

Apkarian, A.V. et al., 2000. Segregation of Nociceptive and Non-Nociceptive Networks in the Squirrel Monkey Somatosensory Thalamus. *Journal of neurophysiology*, 84(1), pp.484–494.

Apkarian, A.V. & Hodge, C.J., 1989. Primate spinothalamic pathways: II. The cells of origin of the dorsolateral and ventral spinothalamic pathways. *The Journal of comparative neurology*, 288(3), pp.474–492.

Apkarian, A.V. & Shi, T., 1994. Squirrel monkey lateral thalamus. I. Somatic nociresponsive neurons and their relation to spinothalamic terminals. *The Journal of neuroscience: the official journal of the Society for Neuroscience*, 14(11 Pt 2), pp.6779–6795.

Baliki, M.N. & Apkarian, A.V., 2015. Nociception, pain, negative moods, and behavior

selection. *Neuron*, 87(3), pp.474–491.

Barack, D.L. et al., 2022. A call for more clarity around causality in neuroscience. *Trends in neurosciences*, 45(9), pp.654–655.

Barth, A.L. & Poulet, J.F.A., 2012. Experimental evidence for sparse firing in the neocortex. *Trends in neurosciences*, 35(6), pp.345–355.

Barthó, P. et al., 2004. Characterization of neocortical principal cells and interneurons by network interactions and extracellular features. *Journal of neurophysiology*, 92(1), pp.600–608.

Basbaum, A.I. et al., 2009. Cellular and molecular mechanisms of pain. *Cell*, 139(2), pp.267–284.

Basbaum, A.I. & Fields, H.L., 1978. Endogenous pain control mechanisms: review and hypothesis. *Annals of neurology*, 4(5), pp.451–462.

Basbaum, A.I. & Fields, H.L., 1984. Endogenous pain control systems: brainstem spinal pathways and endorphin circuitry. *Annual review of neuroscience*, 7(1), pp.309–338.

Basbaum, A.I., Jensen, T.S. & Keefe, F.J., 2023. Fifty years of pain research and clinical advances: highlights and key trends. *Pain*, 164(11S), pp.S11–S15.

Bastos, A.M. et al., 2012. Canonical microcircuits for predictive coding. *Neuron*, 76(4), pp.695–711.

Bauer, M. et al., 2014. Attentional Modulation of Alpha/Beta and Gamma Oscillations Reflect Functionally Distinct Processes. *The Journal of neuroscience: the official journal of the Society for Neuroscience*, 34(48), pp.16117–16125.

Bennett, D.L. et al., 2019. The Role of Voltage-Gated Sodium Channels in Pain Signaling. *Physiological reviews*, 99(2), pp.1079–1151.

Bennett, G.J. et al., 1980. Physiology and morphology of substantia gelatinosa neurons intracellularly stained with horseradish peroxidase. *The Journal of comparative neurology*, 194(4), pp.809–827.

Benshalom, G. & White, E.L., 1986. Quantification of thalamocortical synapses with spiny stellate neurons in layer IV of mouse somatosensory cortex. *The Journal of comparative neurology*, 253(3), pp.303–314.

Berget, S.M., Moore, C. & Sharp, P.A., 1977. Spliced segments at the 5’ terminus of adenovirus 2 late mRNA. *Proceedings of the National Academy of Sciences of the United States of America*, 74(8), pp.3171–3175.

Berkley, K.J., 1983. Spatial relationships between the terminations of somatic sensory motor pathways in the rostral brainstem of cats and monkeys. II. Cerebellar projections compared with those of the ascending somatic sensory pathways in lateral diencephalon. *The Journal of comparative neurology*, 220(2), pp.229–251.

Bettag, W. & Yoshida, T., 1960. Stereotaxic operations for pain relief. *Acta neurochir*, 8.

Bice, T.N. & Beal, J.A., 1997. Quantitative and neurogenic analysis of neurons with supraspinal projections in the superficial dorsal horn of the rat lumbar spinal cord. *The Journal of comparative neurology*, 388(4), pp.565–574.

Birbaumer, N. et al., 1997. Effects of regional anesthesia on phantom limb pain are mirrored in changes in cortical reorganization. *The Journal of neuroscience: the official journal of the Society for Neuroscience*, 17(14), pp.5503–5508.

Boivie, J., 1971. The termination in the thalamus and the zona incerta of fibres from the dorsal column nuclei (DCN) in the cat. an experimental study with silver impregnation methods. *Brain research*, 28(3), pp.459–490.

Bokiniec, P. et al., 2018. The neural circuits of thermal perception. *Current opinion in neurobiology*, 52, pp.98–106.

Boord, P. et al., 2008. Electroencephalographic slowing and reduced reactivity in neuropathic pain following spinal cord injury. *Spinal cord*, 46(2), pp.118–123.

Bordi, F. & Quartaroli, M., 2000. Modulation of nociceptive transmission by NMDA/glycine site receptor in the ventroposterolateral nucleus of the thalamus. *Pain*, 84(2-3), pp.213–224.

Bortone, D.S., Olsen, S.R. & Scanziani, M., 2014. Translaminar inhibitory cells recruited by layer 6 corticothalamic neurons suppress visual cortex. *Neuron*, 82(2), pp.474–485.

Bouhassira, D. et al., 1995. Dorsal horn convergent neurones: negative feedback triggered by spatial summation of nociceptive afferents. *Pain*, 62(2), pp.195–200.

Bourassa, J., Pinault, D. & Deschênes, M., 1995. Corticothalamic projections from the cortical barrel field to the somatosensory thalamus in rats: a single-fibre study using biocytin as an anterograde tracer. *The European journal of neuroscience*, 7(1), pp.19–30.

Boyden, E.S. et al., 2005. Millisecond-timescale, genetically targeted optical control of neural activity. *Nature neuroscience*, 8(9), pp.1263–1268.

Braz, J. et al., 2014. Transmitting pain and itch messages: a contemporary view of the spinal cord circuits that generate gate control. *Neuron*, 82(3), pp.522–536.

Braz, J.M. et al., 2005. Parallel “pain” pathways arise from subpopulations of primary afferent nociceptor. *Neuron*, 47(6), pp.787–793.

Briggs, F., Mangun, G.R. & Usrey, W.M., 2013. Attention enhances synaptic efficacy and the signal-to-noise ratio in neural circuits. *Nature*, 499(7459), pp.476–480.

Brodmann, K., 1909. *Vergleichende Lokalisationslehre der Grosshirnrinde in ihren Prinzipien dargestellt auf Grund des Zellenbaues*, Leipzig: Barth.

Brown-Séquard, C.E., 1869. Lectures ON THE PHYSIOLOGY AND PATHOLOGY OF THE NERVOUS SYSTEM; AND ON THE TREATMENT OF ORGANIC NERVOUS AFFECTIONS. *The Lancet*, 93(2372), pp.219–220.

Bruno, R.M. & Sakmann, B., 2006. Cortex is driven by weak but synchronously active thalamocortical synapses. *Science*, 312(5780), pp.1622–1627.

Buffalo, E.A. et al., 2011. Laminar differences in gamma and alpha coherence in the ventral stream. *Proceedings of the National Academy of Sciences of the United States of America*, 108(27), pp.11262–11267.

Bushnell, M.C. et al., 1999. Pain perception: is there a role for primary somatosensory cortex? *Proceedings of the National Academy of Sciences of the United States of*

*America*, 96(14), pp.7705–7709.

Bushnell, M.C. & Duncan, G.H., 1989. Sensory and affective aspects of pain perception: is medial thalamus restricted to emotional issues? *Experimental brain research. Experimentelle Hirnforschung. Experimentation cerebrale*, 78(2), pp.415–418.

Buzsáki, G., 2010. Neural syntax: cell assemblies, synapsembles, and readers. *Neuron*, 68(3), pp.362–385.

Buzsáki, G., Anastassiou, C.A. & Koch, C., 2012. The origin of extracellular fields and currents—EEG, ECoG, LFP and spikes. *Nature reviews. Neuroscience*. Available at: https://www.nature.com/articles/nrn3241.

Buzsáki, G. & Draguhn, A., 2004. Neuronal oscillations in cortical networks. *Science*, 304(5679), pp.1926–1929.

Buzsáki, G. & Vöröslakos, M., 2023. Brain rhythms have come of age. *Neuron*, 111(7), pp.922–926.

Cao, P. et al., 2023. Green light induces antinociception via visual-somatosensory circuits. *Cell reports*, 42(4), p.112290.

Cardin, J.A. et al., 2009. Driving fast-spiking cells induces gamma rhythm and controls sensory responses. *Nature*, 459(7247), pp.663–667.

Casas-Torremocha, D. et al., 2022. A combinatorial input landscape in the “higher-order relay” posterior thalamic nucleus. *The Journal of neuroscience: the official journal of the Society for Neuroscience*. Available at: http://dx.doi.org/10.1523/JNEUROSCI.0698-22.2022.

Casey, K.L. & Morrow, T.J., 1983. Ventral Posterior Thalamic Neurons Differentially Responsive to Noxious Stimulation of the Awake Monkey. *Science*, 221(4611), pp.675–677.

Castro-Alamancos, M.A. & Oldford, E., 2002. Cortical sensory suppression during arousal is due to the activity-dependent depression of thalamocortical synapses. *The journal of physiology*, 541(Pt 1), pp.319–331.

Caterina, M.J. et al., 1997. The capsaicin receptor: a heat-activated ion channel in the pain pathway. *Nature*, 389(6653), pp.816–824.

Cavanaugh, D.J. et al., 2009. Distinct subsets of unmyelinated primary sensory fibers mediate behavioral responses to noxious thermal and mechanical stimuli. *Proceedings of the National Academy of Sciences of the United States of America*, 106(22), pp.9075–9080.

Cheah, M., Fawcett, J.W. & Andrews, M.R., 2017. Assessment of Thermal Pain Sensation in Rats and Mice Using the Hargreaves Test. *Bio-protocol*, 7(16). Available at: http://dx.doi.org/10.21769/BioProtoc.2506.

Cheng, L. et al., 2017. Identification of spinal circuits involved in touch-evoked dynamic mechanical pain. *Nature neuroscience*, 20(6), pp.804–814.

Chen, L.M., Friedman, R.M. & Roe, A.W., 2003. Optical imaging of a tactile illusion in area 3b of the primary somatosensory cortex. *Science (New York, N.Y.)*, 302(5646), pp.881–885.

Chen, T. et al., 2018. Top-down descending facilitation of spinal sensory excitatory transmission from the anterior cingulate cortex. *Nature communications*, 9(1), p.1886.

Christensen, B.N. & Perl, E.R., 1970. Spinal neurons specifically excited by noxious or thermal stimuli: marginal zone of the dorsal horn. *Journal of neurophysiology*, 33(2), pp.293–307.

Chung, J.M. et al., 1979. Excitation of primate spinothalamic neurons by cutaneous C-fiber volleys. *Journal of neurophysiology*, 42(5), pp.1354–1369.

Chung, J.M. et al., 1986. Response characteristics of neurons in the ventral posterior lateral nucleus of the monkey thalamus. *Journal of neurophysiology*, 56(2), pp.370–390.

Chung, S., Li, X. & Nelson, S.B., 2002. Short-term depression at thalamocortical synapses contributes to rapid adaptation of cortical sensory responses in vivo. *Neuron*, 34(3), pp.437–446.

Cichon, J. et al., 2017. Activation of cortical somatostatin interneurons prevents the development of neuropathic pain. *Nature neuroscience*, 20(8), pp.1122–1132.

Clascá, F., Rubio-Garrido, P. & Jabaudon, D., 2012. Unveiling the diversity of thalamocortical neuron subtypes. *The European journal of neuroscience*, 35(10), pp.1524–1532.

Clayton, K.K. et al., 2021. Auditory Corticothalamic Neurons Are Recruited by Motor Preparatory Inputs. *Current biology: CB*, 31(2), pp.310–321.e5.

Coghill, R.C., 2020. The Distributed Nociceptive System: A Framework for Understanding Pain. *Trends in neurosciences*, 43(10), pp.780–794.

Constantinople, C.M. & Bruno, R.M., 2013. Deep cortical layers are activated directly by thalamus. *Science*, 340(6140), pp.1591–1594.

Cook, A.J. et al., 1987. Dynamic receptive field plasticity in rat spinal cord dorsal horn following C-primary afferent input. *Nature*, 325(7000), pp.151–153.

Craig, A.D. et al., 1994. A thalamic nucleus specific for pain and temperature sensation. *Nature*, 372(6508), pp.770–773.

Craig, A.D., Jr, Linington, A.J. & Kniffki, K.D., 1989. Cells of origin of spinothalamic tract projections to the medial and lateral thalamus in the cat. *The Journal of comparative neurology*, 289(4), pp.568–585.

Crandall, S.R. et al., 2017. Infrabarrels Are Layer 6 Circuit Modules in the Barrel Cortex that Link Long-Range Inputs and Outputs. *Cell reports*, 21(11), pp.3065–3078.

Crandall, S.R., Cruikshank, S.J. & Connors, B.W., 2015. A corticothalamic switch: controlling the thalamus with dynamic synapses. *Neuron*, 86(3), pp.768–782.

Crochet, S. et al., 2005. Modulation of synaptic transmission in neocortex by network activities: Properties of single-axon EPSPs in vivo. *The European journal of neuroscience*, 21(4), pp.1030–1044.

Cruikshank, S.J. et al., 2010. Pathway-Specific Feedforward Circuits between Thalamus and Neocortex Revealed by Selective Optical Stimulation of Axons. *Neuron*, 65(2), pp.230–245.

Dash, S., Autio, D.M. & Crandall, S.R., 2022. State-dependent modulation of activity in distinct layer 6 corticothalamic neurons in barrel cortex of awake mice. *The Journal of neuroscience: the official journal of the Society for Neuroscience*. Available at: http://dx.doi.org/10.1523/JNEUROSCI.2219-21.2022.

Davis, K.D. et al., 1996. Thalamic stimulation-evoked sensations in chronic pain patients and in nonpain (movement disorder) patients. *Journal of neurophysiology*, 75(3), pp.1026–1037.

Deisseroth, K., 2012. Predicted irradiance values: model based on direct measurements in mammalian brain tissue.

Deleuze, C. et al., 2012. T-Type Calcium Channels Consolidate Tonic Action Potential Output of Thalamic Neurons to Neocortex. *The Journal of neuroscience: the official journal of the Society for Neuroscience*, 32(35), pp.12228–12236.

Deneve, S., Latham, P.E. & Pouget, A., 2001. Efficient computation and cue integration with noisy population codes. *Nature neuroscience*, 4(8), pp.826–831.

Deschênes, M., Bourassa, J. & Pinault, D., 1994. Corticothalamic projections from layer V cells in rat are collaterals of long-range corticofugal axons. *Brain research*, 664(1-2), pp.215–219.

Deschênes, M., Veinante, P. & Zhang, Z.W., 1998. The organization of corticothalamic projections: reciprocity versus parity. *Brain research. Brain research reviews*, 28(3), pp.286–308.

Di Pietro, F. et al., 2018. The relationship between thalamic GABA content and resting cortical rhythm in neuropathic pain. *Human brain mapping*, 39(5), pp.1945–1956.

Dougherty, P.M. et al., 1993. Combined application of excitatory amino acids and substance P produces long-lasting changes in responses of primate spinothalamic tract neurons. *Brain research. Brain research reviews*, 18(2), pp.227–246.

Douglas, R.J. & Martin, K.A.C., 2004. Neuronal circuits of the neocortex. *Annual review of neuroscience*, 27, pp.419–451.

Douglass, D.K., Carstens, E. & Watkins, L.R., 1992. Spatial summation in human thermal pain perception: comparison within and between dermatomes. *Pain*, 50(2), pp.197–202.

Duan, B. et al., 2014. Identification of spinal circuits transmitting and gating mechanical pain. *Cell*, 159(6), pp.1417–1432.

Dubin, A.E. & Patapoutian, A., 2010. Nociceptors: the sensors of the pain pathway. *The Journal of clinical investigation*, 120(11), pp.3760–3772.

Dubner, R., Hoffman, D.S. & Hayes, R.L., 1981. Neuronal activity in medullary dorsal horn of awake monkeys trained in a thermal discrimination task. III. Task-related responses and their functional role. *Journal of neurophysiology*, 46(3), pp.444–464.

Duncan, G.H. et al., 1987. Task-related responses of monkey medullary dorsal horn neurons. *Journal of neurophysiology*, 57(1), pp.289–310.

Engel, A.K., Fries, P. & Singer, W., 2001. Dynamic predictions: oscillations and synchrony in top-down processing. *Nature reviews. Neuroscience*, 2(10), pp.704–716.

Familtsev, D. et al., 2016. Ultrastructure of geniculocortical synaptic connections in the tree

shrew striate cortex: Geniculocortical synaptic connections in tree shrew striate cortex. *The Journal of comparative neurology*, 524(6), pp.1292–1306.

Fanselow, M.S., 1994. Neural organization of the defensive behavior system responsible for fear. *Psychonomic bulletin & review*, 1(4), pp.429–438.

Felleman, D.J. & Van Essen, D.C., 1991. Distributed hierarchical processing in the primate cerebral cortex. *Cerebral cortex* , 1(1), pp.1–47.

Fernandes, E.C. et al., 2020. Primary afferent-driven presynaptic inhibition of C-fiber inputs to spinal lamina I neurons. *Progress in neurobiology*, 188, p.101786.

Fields, H., 2004. State-dependent opioid control of pain. *Nature reviews. Neuroscience*, 5(7), pp.565–575.

Flor, H. et al., 1995. Phantom-limb pain as a perceptual correlate of cortical reorganization following arm amputation. *Nature*, 375(6531), pp.482–484.

Folloni, D. et al., 2019. Manipulation of subcortical and deep cortical activity in the primate brain using transcranial focused ultrasound stimulation. *Neuron*, 101(6), pp.1109–1116.e5.

Frandolig, J.E. et al., 2019. The Synaptic Organization of Layer 6 Circuits Reveals Inhibition as a Major Output of a Neocortical Sublamina. *Cell reports*, 28(12), pp.3131–3143.e5.

Frezel, N. et al., 2020. In-Depth Characterization of Layer 5 Output Neurons of the Primary Somatosensory Cortex Innervating the Mouse Dorsal Spinal Cord. *Cerebral cortex communications*, 1(1), p.tgaa052.

Fries, P., 2005. A mechanism for cognitive dynamics: neuronal communication through neuronal coherence. *Trends in cognitive sciences*, 9(10), pp.474–480.

Fries, P., 2015. Rhythms for Cognition: Communication through Coherence. *Neuron*, 88(1), pp.220–235.

Friston, K., 2005. A theory of cortical responses. *Philosophical transactions of the Royal Society of London. Series B, Biological sciences*, 360(1456), pp.815–836.

Galea, M.P. & Darian-Smith, I., 1994. Multiple corticospinal neuron populations in the macaque monkey are specified by their unique cortical origins, spinal terminations, and connections. *Cerebral cortex (New York, N.Y.: 1991)*, 4(2), pp.166–194.

Gan, Z. et al., 2022. Layer-specific pain relief pathways originating from primary motor cortex. *Science*, 378(6626), pp.1336–1343.

Garner, A.R. & Keller, G.B., 2022. A cortical circuit for audio-visual predictions. *Nature neuroscience*, 25(1), pp.98–105.

Gauriau, C. & Bernard, J.-F., 2004. A comparative reappraisal of projections from the superficial laminae of the dorsal horn in the rat: the forebrain. *The Journal of comparative neurology*, 468(1), pp.24–56.

Gerfen, C.R., Paletzki, R. & Heintz, N., 2013. GENSAT BAC cre-recombinase driver lines to study the functional organization of cerebral cortical and basal ganglia circuits. *Neuron*, 80(6), pp.1368–1383.

Gerke, M.B. et al., 2003. Thalamic neuronal activity in rats with mechanical allodynia

following contusive spinal cord injury. *Neuroscience*, 117(3), pp.715–722.

Giesler, G.J., Jr et al., 1981. Spinothalamic tract neurons that project to medial and/or lateral thalamic nuclei: evidence for a physiologically novel population of spinal cord neurons. *Journal of neurophysiology*, 46(6), pp.1285–1308.

Gilbert, C.D. & Wiesel, T.N., 1983. Functional organization of the visual cortex. *Progress in brain research*, 58, pp.209–218.

Gilbert, C.D. & Wiesel, T.N., 1979. Morphology and intracortical projections of functionally characterised neurones in the cat visual cortex. *Nature*, 280(5718), pp.120–125.

Gingold, S.I., Greenspan, J.D. & Apkarian, A.V., 1991. Anatomic evidence of nociceptive inputs to primary somatosensory cortex: relationship between spinothalamic terminals and thalamocortical cells in squirrel monkeys. *The Journal of comparative neurology*, 308(3), pp.467–490.

Gogolla, N., 2017. The insular cortex. *Current biology: CB*, 27(12), pp.R580–R586.

Gong, S. et al., 2007. Targeting Cre recombinase to specific neuron populations with bacterial artificial chromosome constructs. *The Journal of neuroscience: the official journal of the Society for Neuroscience*, 27(37), pp.9817–9823.

Greenspan, J.D., Vierck, C.J., Jr & Ritz, L.A., 1986. Sensitivity to painful and nonpainful electrocutaneous stimuli in monkeys: effects of anterolateral chordotomy. *The Journal of neuroscience: the official journal of the Society for Neuroscience*, 6(2), pp.380–390.

Groh, A. et al., 2018. Acute and Chronic Pain Processing in the Thalamocortical System of Humans and Animal Models. *Neuroscience*, 387, pp.58–71.

le Gros Clark, W.E., 1936. The termination of ascending tracts in the thalamus of the macaque monkey. *Journal of anatomy*, 71(Pt 1), pp.7–40.

Gross, J. et al., 2007. Gamma oscillations in human primary somatosensory cortex reflect pain perception. *PLoS biology*, 5(5), p.e133.

Guido, W. et al., 1995. Receiver operating characteristic (ROC) analysis of neurons in the cat's lateral geniculate nucleus during tonic and burst response mode. *Visual neuroscience*, 12(4), pp.723–741.

Guilbaud, G. et al., 1980. Neurones responding to noxious stimulation in VB complex and caudal adjacent regions in the thalamus of the rat. *Pain*, 8(3), pp.303–318.

Guilbaud, G. et al., 1986. The organization of spinal pathways to ventrobasal thalamus in an experimental model of pain (the arthritic rat). An electrophysiological study. *Pain*, 26(3), pp.301–312.

Guilbaud, G. et al., 1987. Thresholds and encoding of neuronal responses to mechanical stimuli in the ventro-basal thalamus during carrageenin-induced hyperalgesic inflammation in the rat. *Experimental brain research. Experimentelle Hirnforschung. Experimentation cerebrale*, 68(2), pp.311–318.

Guillery, R.W., 1995. Anatomical evidence concerning the role of the thalamus in corticocortical communication: a brief review. *Journal of anatomy*, 187 ( Pt 3), pp.583–592.

Guo, W. et al., 2017. A Corticothalamic Circuit for Dynamic Switching between Feature

Detection and Discrimination. *Neuron*, 95(1), pp.180–194.e5.

Gustin, S.M. et al., 2011. Different pain, different brain: thalamic anatomy in neuropathic and non-neuropathic chronic pain syndromes. *The Journal of neuroscience: the official journal of the Society for Neuroscience*, 31(16), pp.5956–5964.

Gustin, S.M. et al., 2012. Pain and plasticity: is chronic pain always associated with somatosensory cortex activity and reorganization? *The Journal of neuroscience: the official journal of the Society for Neuroscience*, 32(43), pp.14874–14884.

Hains, B.C., Saab, C.Y. & Waxman, S.G., 2006. Alterations in burst firing of thalamic VPL neurons and reversal by Na(v)1.3 antisense after spinal cord injury. *Journal of neurophysiology*, 95(6), pp.3343–3352.

Hains, B.C., Saab, C.Y. & Waxman, S.G., 2005. Changes in electrophysiological properties and sodium channel Nav1.3 expression in thalamic neurons after spinal cord injury. *Brain: a journal of neurology*, 128(Pt 10), pp.2359–2371.

Halassa, M.M. et al., 2014. State-dependent architecture of thalamic reticular subnetworks. *Cell*, 158(4), pp.808–821.

Han, C.J. et al., 2003. Trace but not delay fear conditioning requires attention and the anterior cingulate cortex. *Proceedings of the National Academy of Sciences of the United States of America*, 100(22), pp.13087–13092.

Han, Z.S., Zhang, E.T. & Craig, A.D., 1998. Nociceptive and thermoreceptive lamina I neurons are anatomically distinct. *Nature neuroscience*, 1(3), pp.218–225.

Hawkins, J. et al., 2018. A Framework for Intelligence and Cortical Function Based on Grid Cells in the Neocortex. *Frontiers in neural circuits*, 12, p.121.

Hayes, R.L., Dubner, R. & Hoffman, D.S., 1981. Neuronal activity in medullary dorsal horn of awake monkeys trained in a thermal discrimination task. II. Behavioral modulation of responses to thermal and mechanical stimuli. *Journal of neurophysiology*, 46(3), pp.428–443.

Head, H. & Holmes, G., 1911. SENSORY DISTURBANCES FROM CEREBRAL LESIONS. *Brain: a journal of neurology*, 34(2-3), pp.102–254.

Heid, C. et al., 2020. Early gamma-oscillations as correlate of localized nociceptive processing in primary sensorimotor cortex. *Journal of neurophysiology*, 123(5), pp.1711–1726.

Henderson, L.A. et al., 2013. Chronic pain: lost inhibition? *The Journal of neuroscience: the official journal of the Society for Neuroscience*, 33(17), pp.7574–7582.

Hoerder-Suabedissen, A. et al., 2018. Subset of Cortical Layer 6b Neurons Selectively Innervates Higher Order Thalamic Nuclei in Mice. *Cerebral cortex* , 28(5), pp.1882–1897.

Hohmann, A.G. et al., 1995. Inhibition of noxious stimulus-evoked activity of spinal cord dorsal horn neurons by the cannabinoid WIN 55,212-2. *Life sciences*, 56(23-24), pp.2111–2118.

Honda, C.N., Mense, S. & Perl, E.R., 1983. Neurons in ventrobasal region of cat thalamus selectively responsive to noxious mechanical stimulation. *Journal of neurophysiology*, 49(3), pp.662–673.

Horch, K.W., Tuckett, R.P. & Burgess, P.R., 1977. A key to the classification of cutaneous mechanoreceptors. *The Journal of investigative dermatology*, 69(1), pp.75–82.

Hughes, D.I. et al., 2003. Lack of evidence for sprouting of Abeta afferents into the superficial laminas of the spinal cord dorsal horn after nerve section. *The Journal of neuroscience: the official journal of the Society for Neuroscience*, 23(29), pp.9491–9499.

Hu, H. & Agmon, A., 2016. Differential Excitation of Distally versus Proximally Targeting Cortical Interneurons by Unitary Thalamocortical Bursts. *The Journal of neuroscience: the official journal of the Society for Neuroscience*, 36(26), pp.6906–6916.

Huh, Y. et al., 2012. Interactive responses of a thalamic neuron to formalin induced lasting pain in behaving mice. *PloS one*, 7(1), p.e30699.

Huh, Y. & Cho, J., 2013a. Discrete pattern of burst stimulation in the ventrobasal thalamus for anti-nociception. *PloS one*, 8(6), p.e67655.

Huh, Y. & Cho, J., 2013b. Urethane anesthesia depresses activities of thalamocortical neurons and alters its response to nociception in terms of dual firing modes. *Frontiers in behavioral neuroscience*, 7, p.141.

Hunt, S.P. et al., 1997. Peptide- and non-peptide-containing unmyelinated primary afferents: the parallel processing of nociceptive information. *Philosophical transactions of the Royal Society of London. Series B, Biological sciences*, 308(1136), pp.283–289.

Iwata, K. et al., 1992. Diencephalic projections from the superficial and deep laminae of the medullary dorsal horn in the rat. *The Journal of comparative neurology*, 321(3), pp.404–420.

Iwata, M. et al., 2011. High-frequency stimulation in the ventral posterolateral thalamus reverses electrophysiologic changes and hyperalgesia in a rat model of peripheral neuropathic pain. *Pain*, 152(11), pp.2505–2513.

Jahnsen, H. & Llinás, R., 1984a. Electrophysiological properties of guinea-pig thalamic neurones: an in vitro study. *The Journal of physiology*, 349, pp.205–226.

Jahnsen, H. & Llinás, R., 1984b. Voltage-dependent burst-to-tonic switching of thalamic cell activity: an in vitro study. *Archives italiennes de biologie*, 122(1), pp.73–82.

Jasmin, L. et al., 1997. Transneuronal labeling of a nociceptive pathway, the spino-(trigemino-)parabrachio-amygdaloid, in the rat. *The Journal of neuroscience: the official journal of the Society for Neuroscience*, 17(10), pp.3751–3765.

Jones, E.G., 2010. Thalamocortical dysrhythmia and chronic pain. *Pain*, 150(1), pp.4–5.

Jones, E.G., 2001. The thalamic matrix and thalamocortical synchrony. *Trends in neurosciences*, 24(10), pp.595–601.

Jones, E.G., 2007. *The Thalamus 2 Volume Hardback Set* 2nd ed., Cambridge, England: Cambridge University Press.

Jones, E.G., 1998. Viewpoint: the core and matrix of thalamic organization. *Neuroscience*, 85(2), pp.331–345.

Jones, M.W. et al., 1987. The spinothalamic tract: an examination of the cells of origin of the dorsolateral and ventral spinothalamic pathways in cats. *The Journal of comparative*

*neurology*, 260(3), pp.349–361.

Julius, D. & Basbaum, A.I., 2001. Molecular mechanisms of nociception. *Nature*, 413(6852), pp.203–210.

Jun, J.J. et al., 2017. Fully integrated silicon probes for high-density recording of neural activity. *Nature*, 551(7679), pp.232–236.

Jurgens, C.W.D. et al., 2012. Optogenetic stimulation of the corticothalamic pathway affects relay cells and GABAergic neurons differently in the mouse visual thalamus. *PloS one*, 7(9), p.e45717.

Kakigi, R. et al., 2005. Intracerebral pain processing in a Yoga Master who claims not to feel pain during meditation. *European journal of pain* , 9(5), pp.581–589.

Kenshalo, D.R., Jr et al., 1982. Facilitation of the response of primate spinothalamic cells to cold and to tactile stimuli by noxious heating of the skin. *Pain*, 12(2), pp.141–152.

Kenshalo, D.R., Jr et al., 1980. Responses of neurons in primate ventral posterior lateral nucleus to noxious stimuli. *Journal of neurophysiology*, 43(6), pp.1594–1614.

Kim, D. et al., 2003. Thalamic control of visceral nociception mediated by T-type Ca2+ channels. *Science*, 302(5642), pp.117–119.

Kim, E.J. et al., 2015. Three Types of Cortical Layer 5 Neurons That Differ in Brain-wide Connectivity and Function. *Neuron*, 88(6), pp.1253–1267.

Kim, J. et al., 2014. Layer 6 corticothalamic neurons activate a cortical output layer, layer 5a. *The Journal of neuroscience: the official journal of the Society for Neuroscience*, 34(29), pp.9656–9664.

Kim, S. et al., 2021. Transcranial focused ultrasound stimulation with high spatial resolution. *Brain stimulation*, 14(2), pp.290–300.

Kirchgessner, M.A., Franklin, A.D. & Callaway, E.M., 2021. Distinct “driving” versus “modulatory” influences of different visual corticothalamic pathways. *Current biology: CB*. Available at: https://www.sciencedirect.com/science/article/pii/S0960982221012653.

Klit, H., Finnerup, N.B. & Jensen, T.S., 2009. Central post-stroke pain: clinical characteristics, pathophysiology, and management. *Lancet neurology*, 8(9), pp.857–868.

Klop, E.M. et al., 2005. In cat four times as many lamina I neurons project to the parabrachial nuclei and twice as many to the periaqueductal gray as to the thalamus. *Neuroscience*, 134(1), pp.189–197.

Klop, E.M., Mouton, L.J. & Holstege, G., 2004. Less than 15% of the spinothalamic fibers originate from neurons in lamina I in cat. *Neuroscience letters*, 360(3), pp.125–128.

Knecht, S., Kunesch, E. & Schnitzler, A., 1996. Parallel and serial processing of haptic information in man: effects of parietal lesions on sensorimotor hand function. *Neuropsychologia*, 34(7), pp.669–687.

Kniffki, K.D. & Mizumura, K., 1983. Responses of neurons in VPL and VPL-VL region of the cat to algesic stimulation of muscle and tendon. *Journal of neurophysiology*, 49(3), pp.649–661.

Knill, D.C. & Pouget, A., 2004. The Bayesian brain: the role of uncertainty in neural coding and computation. *Trends in neurosciences*, 27(12), pp.712–719.

de Kock, C.P.J. et al., 2021. High-frequency burst spiking in layer 5 thick-tufted pyramids of rat primary somatosensory cortex encodes exploratory touch. *Communications Biology*, 4(1), pp.1–14.

de Kock, C.P.J. et al., 2007. Layer- and cell-type-specific suprathreshold stimulus representation in rat primary somatosensory cortex. *The Journal of physiology*, 581(Pt 1), pp.139–154.

de Kock, C.P.J. & Sakmann, B., 2009. Spiking in primary somatosensory cortex during natural whisking in awake head-restrained rats is cell-type specific. *Proceedings of the National Academy of Sciences of the United States of America*, 106(38), pp.16446–16450.

Kok, P. et al., 2016. Selective Activation of the Deep Layers of the Human Primary Visual Cortex by Top-Down Feedback. *Current biology: CB*, 26(3), pp.371–376.

Kuner, R., 2015. Spinal excitatory mechanisms of pathological pain. *Pain*, 156 Suppl 1, pp.S11–S17.

Kuner, R. & Flor, H., 2016. Structural plasticity and reorganisation in chronic pain. *Nature reviews. Neuroscience*, 18(1), pp.20–30.

Kuner, R. & Kuner, T., 2021. Cellular Circuits in the Brain and Their Modulation in Acute and Chronic Pain. *Physiological reviews*, 101(1), pp.213–258.

LaBuda, C.J. et al., 2000. Mechanical and thermal hypersensitivity develops following kainate lesion of the ventral posterior lateral thalamus in rats. *Neuroscience letters*, 290(1), pp.79–83.

Lam, Y.-W. & Sherman, S.M., 2010. Functional organization of the somatosensory cortical layer 6 feedback to the thalamus. *Cerebral cortex* , 20(1), pp.13–24.

Landisman, C.E. & Connors, B.W., 2007. VPM and PoM nuclei of the rat somatosensory thalamus: intrinsic neuronal properties and corticothalamic feedback. *Cerebral cortex* , 17(12), pp.2853–2865.

Lawson, S.N., Crepps, B.A. & Perl, E.R., 1997. Relationship of substance P to afferent characteristics of dorsal root ganglion neurones in guinea-pig. *The Journal of physiology*, 505 ( Pt 1)(Pt 1), pp.177–191.

Leblanc, B.W. et al., 2014. Cortical theta is increased while thalamocortical coherence is decreased in rat models of acute and chronic pain. *Pain*, 155(4), pp.773–782.

LeBlanc, B.W. et al., 2017. Thalamic Bursts Down-regulate Cortical Theta and Nociceptive Behavior. *Scientific reports*, 7(1), p.2482.

LeBlanc, B.W. et al., 2016. T-type calcium channel blocker Z944 restores cortical synchrony and thalamocortical connectivity in a rat model of neuropathic pain. *Pain*, 157(1), pp.255–263.

Lee, C.C. & Sherman, S.M., 2009. Glutamatergic inhibition in sensory neocortex. *Cerebral cortex* , 19(10), pp.2281–2289.

Lee, C.C. & Sherman, S.M., 2012. Intrinsic modulators of auditory thalamocortical

transmission. *Hearing research*, 287(1-2), pp.43–50.

Lee, C.C. & Sherman, S.M., 2008. Synaptic properties of thalamic and intracortical inputs to layer 4 of the first- and higher-order cortical areas in the auditory and somatosensory systems. *Journal of neurophysiology*, 100(1), pp.317–326.

Lee, H. & Caterina, M.J., 2005. TRPV channels as thermosensory receptors in epithelial cells. *Pflugers Archiv: European journal of physiology*, 451(1), pp.160–167.

Lenz, F.A. et al., 1989. Characteristics of the bursting pattern of action potentials that occurs in the thalamus of patients with central pain. *Brain research*, 496(1-2), pp.357–360.

Lenz, F.A. et al., 1993. Thermal and pain sensations evoked by microstimulation in the area of human ventrocaudal nucleus. *Journal of neurophysiology*, 70(1), pp.200–212.

Lesica, N.A. et al., 2006. Dynamic Encoding of Natural Luminance Sequences by LGN Bursts. *PLoS biology*, 4(7), p.e209.

Liao, C.-C. & Yen, C.-T., 2008. Functional connectivity of the secondary somatosensory cortex of the rat. *Anatomical record (Hoboken, N.J.: 2007)*, 291(8), pp.960–973.

Lidierth, M., 2007. Long-range projections of Adelta primary afferents in the Lissauer tract of the rat. *Neuroscience letters*, 425(2), pp.126–130.

Light, A.R. & Perl, E.R., 1979. Spinal termination of functionally identified primary afferent neurons with slowly conducting myelinated fibers. *The Journal of comparative neurology*, 186(2), pp.133–150.

Li, L. et al., 2011. The functional organization of cutaneous low-threshold mechanosensory neurons. *Cell*, 147(7), pp.1615–1627.

Liu, C. et al., 2021. Transcranial focused ultrasound enhances sensory discrimination capability through somatosensory cortical excitation. *Ultrasound in medicine & biology*, 47(5), pp.1356–1366.

Liu, X.B., Honda, C.N. & Jones, E.G., 1995. Distribution of four types of synapse on physiologically identified relay neurons in the ventral posterior thalamic nucleus of the cat. *The Journal of comparative neurology*, 352(1), pp.69–91.

Liu, X.B. & Jones, E.G., 1999. Predominance of corticothalamic synaptic inputs to thalamic reticular nucleus neurons in the rat. *The Journal of comparative neurology*, 414(1), pp.67–79.

Liu, Y. et al., 2018. Touch and tactile neuropathic pain sensitivity are set by corticospinal projections. *Nature*, 561(7724), pp.547–550.

Llinás, R. et al., 2005. Rhythmic and dysrhythmic thalamocortical dynamics: GABA systems and the edge effect. *Trends in neurosciences*, 28(6), pp.325–333.

Llinás, R. & Jahnsen, H., 1982. Electrophysiology of mammalian thalamic neurones in vitro. *Nature*, 297(5865), pp.406–408.

Llinás, R.R. et al., 1999. Thalamocortical dysrhythmia: A neurological and neuropsychiatric syndrome characterized by magnetoencephalography. *Proceedings of the National Academy of Sciences of the United States of America*, 96(26), pp.15222–15227.

Lotze, M. et al., 1999. Does use of a myoelectric prosthesis prevent cortical reorganization

and phantom limb pain? *Nature neuroscience*, 2(6), pp.501–502.

Lozsádi, D.A., Gonzalez-Soriano, J. & Guillery, R.W., 1996. The course and termination of corticothalamic fibres arising in the visual cortex of the rat. *The European journal of neuroscience*, 8(11), pp.2416–2427.

Lundqvist, M. et al., 2016. Gamma and Beta Bursts Underlie Working Memory. *Neuron*, 90(1), pp.152–164.

Lu, Y. et al., 2013. A feed-forward spinal cord glycinergic neural circuit gates mechanical allodynia. *The Journal of clinical investigation*, 123(9), pp.4050–4062.

Lu, Y. & Perl, E.R., 2005. Modular organization of excitatory circuits between neurons of the spinal superficial dorsal horn (laminae I and II). *The Journal of neuroscience: the official journal of the Society for Neuroscience*, 25(15), pp.3900–3907.

Madisen, L. et al., 2012. A toolbox of Cre-dependent optogenetic transgenic mice for light-induced activation and silencing. *Nature neuroscience*, 15(5), pp.793–802.

Mahn, M. et al., 2018. High-efficiency optogenetic silencing with soma-targeted anion-conducting channelrhodopsins. *Nature communications*, 9(1), p.4125.

Maier, A. et al., 2010. Distinct superficial and deep laminar domains of activity in the visual cortex during rest and stimulation. *Frontiers in systems neuroscience*, 4. Available at: http://journal.frontiersin.org/article/10.3389/fnsys.2010.00031/abstract.

Malmberg, A.B. et al., 1997. Preserved acute pain and reduced neuropathic pain in mice lacking PKCgamma. *Science*, 278(5336), pp.279–283.

Mantyh, P.W. et al., 1997. Inhibition of hyperalgesia by ablation of lamina I spinal neurons expressing the substance P receptor. *Science*, 278(5336), pp.275–279.

Maren, S., 2001. Neurobiology of Pavlovian fear conditioning. *Annual review of neuroscience*, 24(1), pp.897–931.

Marini, G., Ceccarelli, P. & Mancia, M., 2002. Thalamocortical dysrhythmia and the thalamic reticular nucleus in behaving rats. *Clinical neurophysiology: official journal of the International Federation of Clinical Neurophysiology*, 113(7), pp.1152–1164.

Markov, N.T. et al., 2014. Anatomy of hierarchy: feedforward and feedback pathways in macaque visual cortex. *The Journal of comparative neurology*, 522(1), pp.225–259.

Mark, V.H., Ervin, F.R. & Hackett, T.P., 1960. Clinical aspects of stereotactic thalamotomy in the human. Part I. The treatment of chronic severe pain. *Archives of neurology*, 3, pp.351–367.

Mark, V.H., Ervin, F.R. & Yakovlev, P.I., 1963. Stereotactic Thalamotomy: III. The Verification of Anatomical Lesion Sites in the Human Thalamus. *Archives of neurology*, 8(5), pp.528–538.

Marshall, G.E. et al., 1996. Neurokinin-1 receptors on lumbar spinothalamic neurons in the rat. *Neuroscience*, 72(1), pp.255–263.

Martin, R.J., Apkarian, A.V. & Hodge, C.J., Jr, 1990. Ventrolateral and dorsolateral ascending spinal cord pathway influence on thalamic nociception in cat. *Journal of neurophysiology*, 64(5), pp.1400–1412.

Martin, W.J., Hohmann, A.G. & Walker, J.M., 1996. Suppression of noxious stimulus-evoked activity in the ventral posterolateral nucleus of the thalamus by a cannabinoid agonist: correlation between electrophysiological and antinociceptive effects. *The Journal of neuroscience: the official journal of the Society for Neuroscience*, 16(20), pp.6601–6611.

Masri, R. et al., 2009. Zona incerta: a role in central pain. *Journal of neurophysiology*, 102(1), pp.181–191.

Ma, W.J. et al., 2006. Bayesian inference with probabilistic population codes. *Nature neuroscience*, 9(11), pp.1432–1438.

Mayer, D.J., Price, D.D. & Becker, D.P., 1975. Neurophysiological characterization of the anterolateral spinal cord neurons contributing to pain perception in man. *Pain*, 1(1), pp.51–58.

Mazzola, L., Isnard, J. & Mauguière, F., 2006. Somatosensory and pain responses to stimulation of the second somatosensory area (SII) in humans. A comparison with SI and insular responses. *Cerebral cortex* , 16(7), pp.960–968.

McAlonan, K., Cavanaugh, J. & Wurtz, R.H., 2008. Guarding the gateway to cortex with attention in visual thalamus. *Nature*, 456(7220), pp.391–394.

McCormick, D.A. & Pape, H.C., 1990. Properties of a hyperpolarization-activated cation current and its role in rhythmic oscillation in thalamic relay neurones. *The Journal of physiology*, 431, pp.291–318.

McGurk, H. & MacDonald, J., 1976. Hearing lips and seeing voices. *Nature*, 264(5588), pp.746–748.

McKemy, D.D., Neuhausser, W.M. & Julius, D., 2002. Identification of a cold receptor reveals a general role for TRP channels in thermosensation. *Nature*, 416(6876), pp.52–58.

Mease, R.A. et al., 2017. Multiplexed Spike Coding and Adaptation in the Thalamus. *Cell reports*, 19(6), pp.1130–1140.

Mease, R.A., Krieger, P. & Groh, A., 2014. Cortical control of adaptation and sensory relay mode in the thalamus. *Proceedings of the National Academy of Sciences of the United States of America*, 111(18), pp.6798–6803.

Mease, R.A., Metz, M. & Groh, A., 2016. Cortical Sensory Responses Are Enhanced by the Higher-Order Thalamus. *Cell reports*, 14(2), pp.208–215.

Meda, K.S. et al., 2019. Microcircuit mechanisms through which mediodorsal thalamic input to anterior cingulate cortex exacerbates pain-related aversion. *Neuron*, 102(5), pp.944–959.e3.

Melzack, R. & Casey, K.L., 1968. Sensory, motivational, and central control determinants of pain: a new conceptual model. *The skin senses*, 1, pp.423–443.

Melzack, R. & Loeser, J.D., 1977. Phantom body pain in paraplegics: Evidence for a central “pattern generating mechanism” for pain. *Pain*, 4, pp.195–210.

Melzack, R. & Wall, P.D., 1965. Pain mechanisms: a new theory. *Science*, 150(3699), pp.971–979.

Mendell, L.M., 1966. Physiological properties of unmyelinated fiber projection to the spinal cord. *Experimental neurology*, 16(3), pp.316–332.

Merskey, H. & Bogduk, N. eds., 2011. Part 3: Pain terms, A Current List with Definitions and Notes on Usage. In *IASP Task Force on Taxonomy*. Seattle: IASP Press, pp. 209–214.

Meyer, H.S. et al., 2010. Number and laminar distribution of neurons in a thalamocortical projection column of rat vibrissal cortex. *Cerebral cortex* , 20(10), pp.2277–2286.

Miller, E.K., Lundqvist, M. & Bastos, A.M., 2018. Working Memory 2.0. *Neuron*, 100(2), pp.463–475.

Miraucourt, L.S., Dallel, R. & Voisin, D.L., 2007. Glycine inhibitory dysfunction turns touch into pain through PKCgamma interneurons. *PloS one*, 2(11), p.e1116.

Mishra, S.K. et al., 2011. TRPV1-lineage neurons are required for thermal sensation: TRPV1-lineage neurons. *The EMBO journal*, 30(3), pp.582–593.

Mo, C., McKinnon, C. & Murray Sherman, S., 2024. A transthalamic pathway crucial for perception. *Nature communications*, 15(1), p.6300.

Molliver, D.C. et al., 1997. IB4-Binding DRG Neurons Switch from NGF to GDNF Dependence in Early Postnatal Life. *Neuron*, 19(4), pp.849–861.

Molnár, Z., 2019. Cortical layer with no known function. *The European journal of neuroscience*, 49(7), pp.957–963.

Montijn, J.S. et al., 2021. A parameter-free statistical test for neuronal responsiveness. *eLife*, 10. Available at: http://dx.doi.org/10.7554/eLife.71969.

Moqrich, A. et al., 2005. Impaired thermosensation in mice lacking TRPV3, a heat and camphor sensor in the skin. *Science (New York, N.Y.)*, 307(5714), pp.1468–1472.

Moreno-Lopez, Y. et al., 2021. The corticospinal tract primarily modulates sensory inputs in the mouse lumbar cord. *eLife*, 10. Available at: http://dx.doi.org/10.7554/eLife.65304.

Mouton, L.J. & Holstege, G., 1998. Three times as many lamina I neurons project to the periaqueductal gray than to the thalamus: a retrograde tracing study in the cat. *Neuroscience letters*, 255(2), pp.107–110.

Murphy, P.C. & Sillito, A.M., 1987. Corticofugal feedback influences the generation of length tuning in the visual pathway. *Nature*, 329(6141), pp.727–729.

Nagel, G. et al., 2003. Channelrhodopsin-2, a directly light-gated cation-selective membrane channel. *Proceedings of the National Academy of Sciences of the United States of America*, 100(24), pp.13940–13945.

Nagy, A., 2000. Cre recombinase: the universal reagent for genome tailoring. *Genesis* , 26(2), pp.99–109.

Nakata, H., Sakamoto, K. & Kakigi, R., 2014. Meditation reduces pain-related neural activity in the anterior cingulate cortex, insula, secondary somatosensory cortex, and thalamus. *Frontiers in psychology*, 5, p.1489.

Neumann, S. et al., 2008. Innocuous, not noxious, input activates PKCgamma interneurons of the spinal dorsal horn via myelinated afferent fibers. *The Journal of neuroscience: the official journal of the Society for Neuroscience*, 28(32), pp.7936–7944.

Nichols, M.L. et al., 1999. Transmission of chronic nociception by spinal neurons expressing the substance P receptor. *Science (New York, N.Y.)*, 286(5444), pp.1558–1561.

O'Connor, D.H. et al., 2010. Neural activity in barrel cortex underlying vibrissa-based object localization in mice. *Neuron*, 67(6), pp.1048–1061.

Olsen, S.R. et al., 2012. Gain control by layer six in cortical circuits of vision. *Nature*, 483(7387), pp.47–52.

Onodera, K. & Kato, H.K., 2022. Translaminar recurrence from layer 5 suppresses superficial cortical layers. *Nature communications*, 13(1), pp.1–16.

Ostrowsky, K. et al., 2002. Representation of pain and somatic sensation in the human insula: a study of responses to direct electrical cortical stimulation. *Cerebral cortex* , 12(4), pp.376–385.

Owens, C.M., Zhang, D. & Willis, W.D., 1992. Changes in the response states of primate spinothalamic tract cells caused by mechanical damage of the skin or activation of descending controls. *Journal of neurophysiology*, 67(6), pp.1509–1527.

Park, A. et al., 2018. Pain After Spinal Cord Injury Is Associated With Abnormal Presynaptic Inhibition in the Posterior Nucleus of the Thalamus. *The journal of pain: official journal of the American Pain Society*, 19(7), pp.727.e1–727.e15.

Patel, R. & Dickenson, A.H., 2016. Neuronal hyperexcitability in the ventral posterior thalamus of neuropathic rats: modality selective effects of pregabalin. *Journal of neurophysiology*, 116(1), pp.159–170.

Peier, A.M. et al., 2002. A TRP channel that senses cold stimuli and menthol. *Cell*, 108(5), pp.705–715.

Peirs, C. et al., 2015. Dorsal Horn Circuits for Persistent Mechanical Pain. *Neuron*, 87(4), pp.797–812.

Peirs, C., Dallel, R. & Todd, A.J., 2020. Recent advances in our understanding of the organization of dorsal horn neuron populations and their contribution to cutaneous mechanical allodynia. *Journal of neural transmission* , 127(4), pp.505–525.

Perl, E.R. & Whitlock, D.G., 1961. Somatic stimuli exciting spinothalamic projections to thalamic neurons in cat and monkey. *Experimental neurology*, 3, pp.256–296.

Peschanski, M. et al., 1980. Encoding of noxious heat messages in neurons of the ventrobasal thalamic complex of the rat. *Brain research*, 197(2), pp.401–413.

Pezzulo, G., Parr, T. & Friston, K., 2022. The evolution of brain architectures for predictive coding and active inference. *Philosophical transactions of the Royal Society of London. Series B, Biological sciences*, 377(1844), p.20200531.

Pinault, D. & Deschênes, M., 1998. Anatomical evidence for a mechanism of lateral inhibition in the rat thalamus. *The European journal of neuroscience*, 10(11), pp.3462–3469.

Ploner, M. et al., 2000. Differential organization of touch and pain in human primary somatosensory cortex. *Journal of neurophysiology*, 83(3), pp.1770–1776.

Ploner, M. et al., 2006. Pain suppresses spontaneous brain rhythms. *Cerebral cortex (New York, N.Y.: 1991)*, 16(4), pp.537–540.

Polgár, E. et al., 1999. GABAergic neurons that contain neuropeptide Y selectively target cells with the neurokinin 1 receptor in laminae III and IV of the rat spinal cord. *The Journal of neuroscience: the official journal of the Society for Neuroscience*, 19(7), pp.2637–2646.

Poulet, J.F.A. & Petersen, C.C.H., 2008. Internal brain state regulates membrane potential synchrony in barrel cortex of behaving mice. *Nature*, 454(7206), pp.881–885.

Prasad, J.A., Carroll, B.J. & Sherman, S.M., 2020. Layer 5 Corticofugal Projections from Diverse Cortical Areas: Variations on a Pattern of Thalamic and Extrathalamic Targets. *The Journal of neuroscience: the official journal of the Society for Neuroscience*, 40(30), pp.5785–5796.

Price, D.D. et al., 1979. Functional relationships between neurons of marginal and substantia gelatinosa layers of primate dorsal horn. *Journal of neurophysiology*, 42(6), pp.1590–1608.

Price, D.D. et al., 1978. Spatial and temporal transformations of input to spinothalamic tract neurons and their relation to somatic sensations. *Journal of neurophysiology*, 41(4), pp.933–947.

Price, D.D. & Dubner, R., 1977. Neurons that subserve the sensory-discriminative aspects of pain. *Pain*, 3(4), pp.307–338.

Price, D.D., Greenspan, J.D. & Dubner, R., 2003. Neurons involved in the exteroceptive function of pain. *Pain*, 106(3), pp.215–219.

Price, D.D. & Mayer, D.J., 1975. Neurophysiological characterization of the anterolateral quadrant neurons subserving pain in M. mulatta. *Pain*, 1(1), pp.59–72.

Quevedo, A.S. & Coghill, R.C., 2007. Attentional modulation of spatial integration of pain: evidence for dynamic spatial tuning. *The Journal of neuroscience: the official journal of the Society for Neuroscience*, 27(43), pp.11635–11640.

Rainville, P. et al., 1997. Pain affect encoded in human anterior cingulate but not somatosensory cortex. *Science*, 277(5328), pp.968–971.

Raja, S.N. et al., 2020. The revised International Association for the Study of Pain definition of pain: concepts, challenges, and compromises. *Pain*, 161(9), pp.1976–1982.

Ralston, H.J., 3rd & Ralston, D.D., 1994. Medial lemniscal and spinal projections to the macaque thalamus: an electron microscopic study of differing GABAergic circuitry serving thalamic somatosensory mechanisms. *The Journal of neuroscience: the official journal of the Society for Neuroscience*, 14(5 Pt 1), pp.2485–2502.

Reichova, I. & Sherman, S.M., 2004. Somatosensory corticothalamic projections: distinguishing drivers from modulators. *Journal of neurophysiology*, 92(4), pp.2185–2197.

Rexed, B., 1952. The cytoarchitectonic organization of the spinal cord in the cat. *The Journal of comparative neurology*, 96(3), pp.414–495.

Ringach, D.L., 2021. Sparse thalamocortical convergence. *Current biology: CB*. Available at: http://dx.doi.org/10.1016/j.cub.2021.02.032.

Rodriguez-Moreno, J. et al., 2020. Area-Specific Synapse Structure in Branched Posterior Nucleus Axons Reveals a New Level of Complexity in Thalamocortical Networks. *The*

*Journal of neuroscience: the official journal of the Society for Neuroscience*, 40(13), pp.2663–2679.

Russo, E. & Durstewitz, D., 2017. Cell assemblies at multiple time scales with arbitrary lag constellations. *eLife*, 6, p.e19428.

Saab, C.Y. & Barrett, L.F., 2016. Thalamic Bursts and the Epic Pain Model. *Frontiers in computational neuroscience*, 10, p.147.

Sakata, S. & Harris, K.D., 2009. Laminar structure of spontaneous and sensory-evoked population activity in auditory cortex. *Neuron*, 64(3), pp.404–418.

Schmitt, L.I. et al., 2017. Thalamic amplification of cortical connectivity sustains attentional control. *Nature*, 545(7653), pp.219–223.

Schulman, J.J. et al., 2005. Thalamocortical dysrhythmia syndrome: MEG imaging of neuropathic pain. *Thalamus & related systems*, 3(1), pp.33–39.

Schüz, A. & Palm, G., 1989. Density of neurons and synapses in the cerebral cortex of the mouse. *The Journal of comparative neurology*, 286(4), pp.442–455.

Sermet, B.S. et al., 2019. Pathway-, layer- and cell-type-specific thalamic input to mouse barrel cortex. *eLife*, 8. Available at: http://dx.doi.org/10.7554/eLife.52665.

Shepherd, G.M.G. & Yamawaki, N., 2021. Untangling the cortico-thalamo-cortical loop: cellular pieces of a knotty circuit puzzle. *Nature reviews. Neuroscience*. Available at: http://dx.doi.org/10.1038/s41583-021-00459-3.

Sherman, S.M., 2017. Functioning of Circuits Connecting Thalamus and Cortex. *Comprehensive Physiology*, 7(2), pp.713–739.

Sherman, S.M., 2001a. Thalamic relay functions. *Progress in brain research*, 134, pp.51–69.

Sherman, S.M., 2007. The thalamus is more than just a relay. *Current opinion in neurobiology*, 17(4), pp.417–422.

Sherman, S.M., 2001b. Tonic and burst firing: dual modes of thalamocortical relay. *Trends in neurosciences*, 24(2), pp.122–126.

Sherman, S.M. & Guillery, R.W., 1996. Functional organization of thalamocortical relays. *Journal of neurophysiology*, 76(3), pp.1367–1395.

Sherman, S.M. & Guillery, R.W., 1998. On the actions that one nerve cell can have on another: distinguishing “drivers” from “modulators.” *Proceedings of the National Academy of Sciences of the United States of America*, 95(12), pp.7121–7126.

Sherman, S.M. & Guillery, R.W., 2002. The role of the thalamus in the flow of information to the cortex. *Philosophical transactions of the Royal Society of London. Series B, Biological sciences*, 357(1428), pp.1695–1708.

Sherman, S.M. & Koch, C., 1986. The control of retinogeniculate transmission in the mammalian lateral geniculate nucleus. *Experimental brain research. Experimentelle Hirnforschung. Experimentation cerebrale*, 63(1), pp.1–20.

Sherrington, C.S., 1900. Cutaneous sensations. In E. A. Schäfer, ed. *Text-book of Physiology, Volume 2*. Harvard University: Y. J. Pentland, 1900, pp. 920–941.

Shin, H. & Moore, C.I., 2019. Persistent Gamma Spiking in SI Nonsensory Fast Spiking Cells Predicts Perceptual Success. *Neuron*, 0(0). Available at: http://www.cell.com/article/S0896627319305641/abstract [Accessed July 19, 2019].

Shipp, S., 2016. Neural Elements for Predictive Coding. *Frontiers in psychology*, 7, p.1792.

Shoham, S., O'Connor, D.H. & Segev, R., 2006. How silent is the brain: is there a "dark matter" problem in neuroscience? *Journal of comparative physiology. A, Neuroethology, sensory, neural, and behavioral physiology*, 192(8), pp.777–784.

Siegle, J.H., Pritchett, D.L. & Moore, C.I., 2014. Gamma-range synchronization of fast-spiking interneurons can enhance detection of tactile stimuli. *Nature neuroscience*, 17(10), pp.1371–1379.

Silver, R.A., 2010. Neuronal arithmetic. *Nature reviews. Neuroscience*, 11(7), pp.474–489.

Snider, W.D. & McMahon, S.B., 1998. Tackling pain at the source: new ideas about nociceptors. *Neuron*, 20(4), pp.629–632.

Spiegel, E.A. et al., 1966. Medial and basal thalamotomy in so-called intractable pain. *Pain*.

Spike, R.C. et al., 2003. A quantitative and morphological study of projection neurons in lamina I of the rat lumbar spinal cord. *The European journal of neuroscience*, 18(9), pp.2433–2448.

Spiller, W.G., 1912. The treatment of persistent pain of organic origin in the lower part of the body by division of the anterolateral column of the spinal cord. *Journal of the American Medical Association*, LVIII(20), p.1489.

Spreafico, R., Hayes, N.L. & Rustioni, A., 1981. Thalamic projections to the primary and secondary somatosensory cortices in cat: single and double retrograde tracer studies. *The Journal of comparative neurology*, 203(1), pp.67–90.

Sprenger, C. et al., 2012. Attention modulates spinal cord responses to pain. *Current biology: CB*, 22(11), pp.1019–1022.

Stein, B.E., Price, D.D. & Gazzaniga, M.S., 1989. Pain perception in a man with total corpus callosum transection. *Pain*, 38(1), pp.51–56.

Steinmetz, N.A. et al., 2019. Distributed coding of choice, action and engagement across the mouse brain. *Nature*, 576(7786), pp.266–273.

Sugiura, Y. et al., 1993. Quantitative analysis of central terminal projections of visceral and somatic unmyelinated (C) primary afferent fibers in the guinea pig. *The Journal of comparative neurology*, 332(3), pp.315–325.

Sugiura, Y., Lee, C.L. & Perl, E.R., 1986. Central projections of identified, unmyelinated (C) afferent fibers innervating mammalian skin. *Science*, 234(4774), pp.358–361.

Sugiura, Y., Terui, N. & Hosoya, Y., 1989. Difference in distribution of central terminals between visceral and somatic unmyelinated (C) primary afferent fibers. *Journal of neurophysiology*, 62(4), pp.834–840.

Suminaite, D., Lyons, D.A. & Livesey, M.R., 2019. Myelinated axon physiology and regulation of neural circuit function. *Glia*, 67(11), pp.2050–2062.

Swadlow, H.A. & Gusev, A.G., 2001. The impact of "bursting" thalamic impulses at a

neocortical synapse. *Nature neuroscience*, 4(4), pp.402–408.

Swadlow, H.A., Gusev, A.G. & Bezdudnaya, T., 2002. Activation of a cortical column by a thalamocortical impulse. *The Journal of neuroscience: the official journal of the Society for Neuroscience*, 22(17), pp.7766–7773.

Takahashi, N. et al., 2016. Active cortical dendrites modulate perception. *Science*, 354(6319), pp.1587–1590.

Takahashi, N. et al., 2020. Active dendritic currents gate descending cortical outputs in perception. *Nature neuroscience*, 23(10), pp.1277–1285.

Tan, L.L. et al., 2019. Gamma oscillations in somatosensory cortex recruit prefrontal and descending serotonergic pathways in aversion and nociception. *Nature communications*, 10(1), p.983.

Tan, L.L. & Kuner, R., 2021. Neocortical circuits in pain and pain relief. *Nature reviews. Neuroscience*, 22(8), pp.458–471.

Tan, L.L., Oswald, M.J. & Kuner, R., 2021. Neurobiology of brain oscillations in acute and chronic pain. *Trends in neurosciences*, 44(8), pp.629–642.

Tiemann, L. et al., 2010. Gamma oscillations as a neuronal correlate of the attentional effects of pain. *Pain*, 150(2), pp.302–308.

Timmermann, L. et al., 2001. Differential coding of pain intensity in the human primary and secondary somatosensory cortex. *Journal of neurophysiology*, 86(3), pp.1499–1503.

Todd, A.J., 2017. Identifying functional populations among the interneurons in laminae I-III of the spinal dorsal horn. *Molecular pain*, 13, p.1744806917693003.

Todd, A.J., 2010. Neuronal circuitry for pain processing in the dorsal horn. *Nature reviews. Neuroscience*, 11(12), pp.823–836.

Todd, A.J. et al., 2002. Projection neurons in lamina I of rat spinal cord with the neurokinin 1 receptor are selectively innervated by substance p-containing afferents and respond to noxious stimulation. *The Journal of neuroscience: the official journal of the Society for Neuroscience*, 22(10), pp.4103–4113.

Todd, A.J., McGill, M.M. & Shehab, S.A., 2000. Neurokinin 1 receptor expression by neurons in laminae I, III and IV of the rat spinal dorsal horn that project to the brainstem. *The European journal of neuroscience*, 12(2), pp.689–700.

Tominaga, M. et al., 1998. The cloned capsaicin receptor integrates multiple pain-producing stimuli. *Neuron*, 21(3), pp.531–543.

Torsney, C. & MacDermott, A.B., 2006. Disinhibition opens the gate to pathological pain signaling in superficial neurokinin 1 receptor-expressing neurons in rat spinal cord. *The Journal of neuroscience: the official journal of the Society for Neuroscience*, 26(6), pp.1833–1843.

Traub, R.J., Sedivec, M.J. & Mendell, L.M., 1986. The rostral projection of small diameter primary afferents in Lissauer's tract. *Brain research*, 399(1), pp.185–189.

Treede, R.-D. et al., 2015. A classification of chronic pain for ICD-11. *Pain*, 156(6), pp.1003–1007.

Trevino, D.L., Coulter, J.D. & Willis, W.D., 1973. Location of cells of origin of spinothalamic tract in lumbar enlargement of the monkey. *Journal of neurophysiology*, 36(4), pp.750–761.

Usrey, W.M. & Sherman, S.M., 2019. Corticofugal circuits: Communication lines from the cortex to the rest of the brain. *The Journal of comparative neurology*, 527(3), pp.640–650.

Vallbo, A.B. & Johansson, R.S., 1984. Properties of cutaneous mechanoreceptors in the human hand related to touch sensation. *Human neurobiology*, 3(1), pp.3–14.

Van Essen, D.C. & Maunsell, J.H.R., 1983. Hierarchical organization and functional streams in the visual cortex. *Trends in neurosciences*, 6, pp.370–375.

Van Horn, S.C., Erişir, A. & Sherman, S.M., 2000. Relative distribution of synapses in the A-laminae of the lateral geniculate nucleus of the cat. *The Journal of comparative neurology*, 416(4), pp.509–520.

Vartiainen, N. et al., 2016. Thalamic pain: anatomical and physiological indices of prediction. *Brain: a journal of neurology*, 139(Pt 3), pp.708–722.

Veinante, P., Lavallée, P. & Deschênes, M., 2000. Corticothalamic projections from layer 5 of the vibrissal barrel cortex in the rat. *The Journal of comparative neurology*, 424(2), pp.197–204.

Vélez-Fort, M. et al., 2018. A Circuit for Integration of Head- and Visual-Motion Signals in Layer 6 of Mouse Primary Visual Cortex. *Neuron*, 98(1), pp.179–191.e6.

Vélez-Fort, M. et al., 2014. The stimulus selectivity and connectivity of layer six principal cells reveals cortical microcircuits underlying visual processing. *Neuron*, 83(6), pp.1431–1443.

Viaene, A.N., Petrof, I. & Sherman, S.M., 2011. Properties of the thalamic projection from the posterior medial nucleus to primary and secondary somatosensory cortices in the mouse. *Proceedings of the National Academy of Sciences of the United States of America*, 108(44), pp.18156–18161.

Vierck, C.J., Jr & Luck, M.M., 1979. Loss and recovery of reactivity to noxious stimuli in monkeys with primary spinothalamic cordotomies, followed by secondary and tertiary lesions of other cord sectors. *Brain: a journal of neurology*, 102(2), pp.233–248.

Voigts, J., Deister, C.A. & Moore, C.I., 2020. Layer 6 ensembles can selectively regulate the behavioral impact and layer-specific representation of sensory deviants. *eLife*, 9. Available at: http://dx.doi.org/10.7554/eLife.48957.

Wager, T.D. et al., 2013. An fMRI-based neurologic signature of physical pain. *The New England journal of medicine*, 368(15), pp.1388–1397.

Wallstrom, G., Liebner, J. & Kass, R.E., 2008. An Implementation of Bayesian Adaptive Regression Splines (BARS) in C with S and R Wrappers. *Journal of statistical software*, 26(1), pp.1–21.

Walton, K.D. & Llinás, R.R., 2011. Central Pain as a Thalamocortical Dysrhythmia: A Thalamic Efference Disconnection? In L. Kruger & A. R. Light, eds. *Translational Pain Research: From Mouse to Man*. Boca Raton, FL: CRC Press/Taylor & Francis.

Wang, J.-Y. et al., 2007. Corticofugal influences on thalamic neurons during nociceptive

transmission in awake rats. *Synapse* , 61(5), pp.335–342.

Wang, N. et al., 2016. Differential modulation of electrical stimulation of periaqueductal gray and thalamus on nociceptive behaviors of rats. *Sheng li xue bao: [Acta physiologica Sinica]*, 68(2), pp.115–125.

Wang, N., Wang, J.-Y. & Luo, F., 2009. Corticofugal outputs facilitate acute, but inhibit chronic pain in rats. *Pain*, 142(1-2), pp.108–115.

Wang, W. et al., 2018. Focal Gain Control of Thalamic Visual Receptive Fields by Layer 6 Corticothalamic Feedback. *Cerebral cortex* , 28(1), pp.267–280.

Wang, X. et al., 2013. Excitatory superficial dorsal horn interneurons are functionally heterogeneous and required for the full behavioral expression of pain and itch. *Neuron*, 78(2), pp.312–324.

Whilden, C.M. et al., 2021. The synaptic inputs and thalamic projections of two classes of layer 6 corticothalamic neurons in primary somatosensory cortex of the mouse. *The Journal of comparative neurology*. Available at: http://dx.doi.org/10.1002/cne.25163.

Whitmire, C.J. et al., 2016. Information Coding through Adaptive Gating of Synchronized Thalamic Bursting. *Cell reports*, 14(4), pp.795–807.

Whitt, J.L. et al., 2013. Pathological activity in mediodorsal thalamus of rats with spinal cord injury pain. *The Journal of neuroscience: the official journal of the Society for Neuroscience*, 33(9), pp.3915–3926.

Wiley, R.G., Kline, R.H. & Vierck, C.J., 2007. Anti-nociceptive effects of selectively destroying substance P receptor-expressing dorsal horn neurons using [Sar9,Met(O2)11]-substance P-saporin: behavioral and anatomical analyses. *Neuroscience*, 146(3). Available at: https://pubmed.ncbi.nlm.nih.gov/17418497/ [Accessed August 1, 2024].

Willis, W.D. et al., 1974. Responses of primate spinothalamic tract neurons to natural stimulation of hindlimb. *Journal of neurophysiology*, 37(2), pp.358–372.

Willis, W.D., Jr et al., 2001. Projections from the marginal zone and deep dorsal horn to the ventrobasal nuclei of the primate thalamus. *Pain*, 92(1-2), pp.267–276.

Willis, W.D., Jr, 2007. The somatosensory system, with emphasis on structures important for pain. *Brain research reviews*, 55(2), pp.297–313.

Willis, W.D., Kenshalo, D.R., Jr & Leonard, R.B., 1979. The cells of origin of the primate spinothalamic tract. *The Journal of comparative neurology*, 188(4), pp.543–573.

Willis, W.D. & Westlund, K.N., 1997. Neuroanatomy of the pain system and of the pathways that modulate pain. *Journal of clinical neurophysiology: official publication of the American Electroencephalographic Society*, 14(1), pp.2–31.

Wolfart, J. et al., 2005. Synaptic background activity controls spike transfer from thalamus to cortex. *Nature neuroscience*, 8(12), pp.1760–1767.

Wrigley, P.J. et al., 2009. Neuropathic pain and primary somatosensory cortex reorganization following spinal cord injury. *Pain*, 141(1-2), pp.52–59.

Yaksh, T.L., 1989. Behavioral and autonomic correlates of the tactile evoked allodynia produced by spinal glycine inhibition: effects of modulatory receptor systems and

excitatory amino acid antagonists. *Pain*, 37(1), pp.111–123.

Yen, C.T., Honda, C.N. & Jones, E.G., 1991. Electrophysiological study of spinothalamic inputs to ventrolateral and adjacent thalamic nuclei of the cat. *Journal of neurophysiology*, 66(3), pp.1033–1047.

Yokota, T. et al., 1988. Nociceptive body representation in nucleus ventralis posterolateralis of cat thalamus. *Journal of neurophysiology*, 60(5), pp.1714–1727.

Yokota, T., Koyama, N. & Matsumoto, N., 1985. Somatotopic distribution of trigeminal nociceptive neurons in ventrobasal complex of cat thalamus. *Journal of neurophysiology*, 53(6), pp.1387–1400.

Yu, J. et al., 2019. Recruitment of GABAergic Interneurons in the Barrel Cortex during Active Tactile Behavior. *Neuron*. Available at: http://dx.doi.org/10.1016/j.neuron.2019.07.027.

Zemlan, F.P. et al., 1978. Ascending tracts of the lateral columns of the rat spinal cord: A study using the silver impregnation and horseradish peroxidase techniques. *Experimental neurology*, 62(2), pp.298–334.

Zhang, C. et al., 2017. Reduced GABAergic transmission in the ventrobasal thalamus contributes to thermal hyperalgesia in chronic inflammatory pain. *Scientific reports*, 7, p.41439.

Zhang, J. et al., 2013. The modality-specific contribution of peptidergic and non-peptidergic nociceptors is manifest at the level of dorsal horn nociresponsive neurons: Modality-specific nociceptor contributions to dorsal horn physiology. *The journal of physiology*, 591(4), pp.1097–1110.

Zhang, Z.G. et al., 2012. Gamma-band oscillations in the primary somatosensory cortex--a direct and obligatory correlate of subjective pain intensity. *The Journal of neuroscience: the official journal of the Society for Neuroscience*, 32(22), pp.7429–7438.

Zhang, Z.W. & Deschênes, M., 1998. Projections to layer VI of the posteromedial barrel field in the rat: a reappraisal of the role of corticothalamic pathways. *Cerebral cortex* , 8(5), pp.428–436.

Zhan, X.J. et al., 1999. Current clamp and modeling studies of low-threshold calcium spikes in cells of the cat's lateral geniculate nucleus. *Journal of neurophysiology*, 81(5), pp.2360–2373.

Zhou, W. et al., 2022. Sound induces analgesia through corticothalamic circuits. *Science*, 377(6602), pp.198–204.

Ziegler, K. et al., 2023. Primary somatosensory cortex bidirectionally modulates sensory gain and nociceptive behavior in a layer-specific manner. *Nature communications*, 14(1), p.2999.

Zimmer, Z. et al., 2022. A global study of pain prevalence across 52 countries: examining the role of country-level contextual factors: examining the role of country-level contextual factors. *Pain*, 163(9), pp.1740–1750.

Zylka, M.J., Rice, F.L. & Anderson, D.J., 2005. Topographically distinct epidermal nociceptive circuits revealed by axonal tracers targeted to Mrgprd. *Neuron*, 45(1), pp.17–25.

# 8. Supplementary Materials

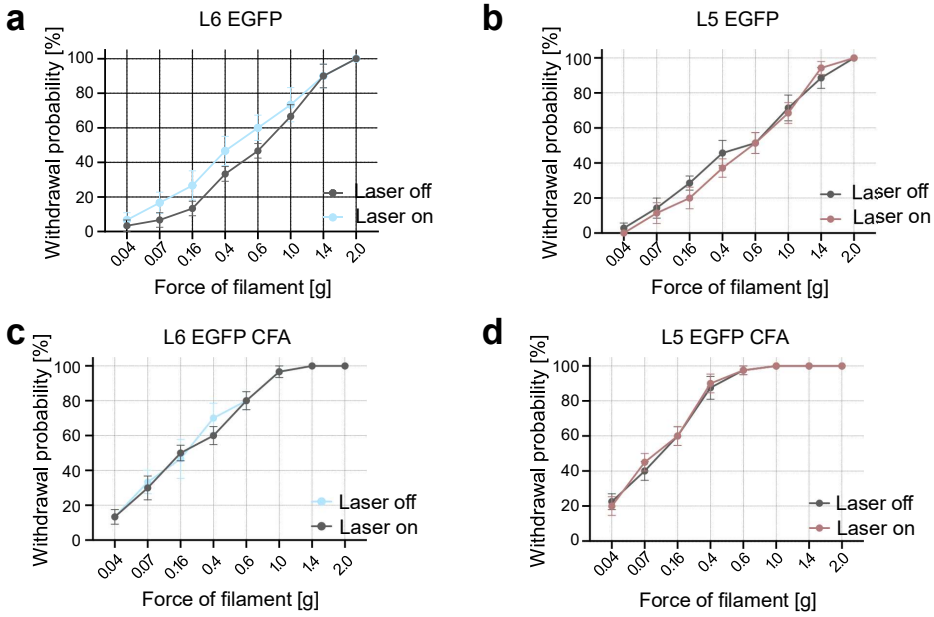


**Supplementary Figure 1: von Frey mechanical sensitivity test in EGFP control mice with and without optogenetic stimulation in S1 hindlimb cortex (S1-HL) with a fibre implant. Related to Figures 2, 5 and 6.**

Within-animal comparison of paw withdrawal probabilities in response to graded von Frey stimulation of the left hindpaw at baseline (black, Laser off) and during contralateral optogenetic stimulation (Laser on, 5 s continuous) of either Ntsr1-Cre (blue lines) or Rbp4-Cre (red lines) mice injected with AAV-DIO-EGFP in the contralateral S1-HL.
**(a)** L6-EGFP, *n* = 6 mice.
**(b)** L5-EGFP, *n* = 6 mice.
**(c)** L6-EGFP, CFA, *n* = 6 mice.
**(d)** L5-EGFP, Complete Freund's adjuvant (CFA), *n* = 8 mice.
Data from Katharina Ziegler and Antonio Gonzalez. Figure contains panels adapted from *Ziegler et al.* (Ziegler et al. 2023).
Two-way repeated measures ANOVA with post-hoc Bonferroni test. Exact *F* and *p* values in Supplementary Table 1. Data are shown as mean ± S.E.M.

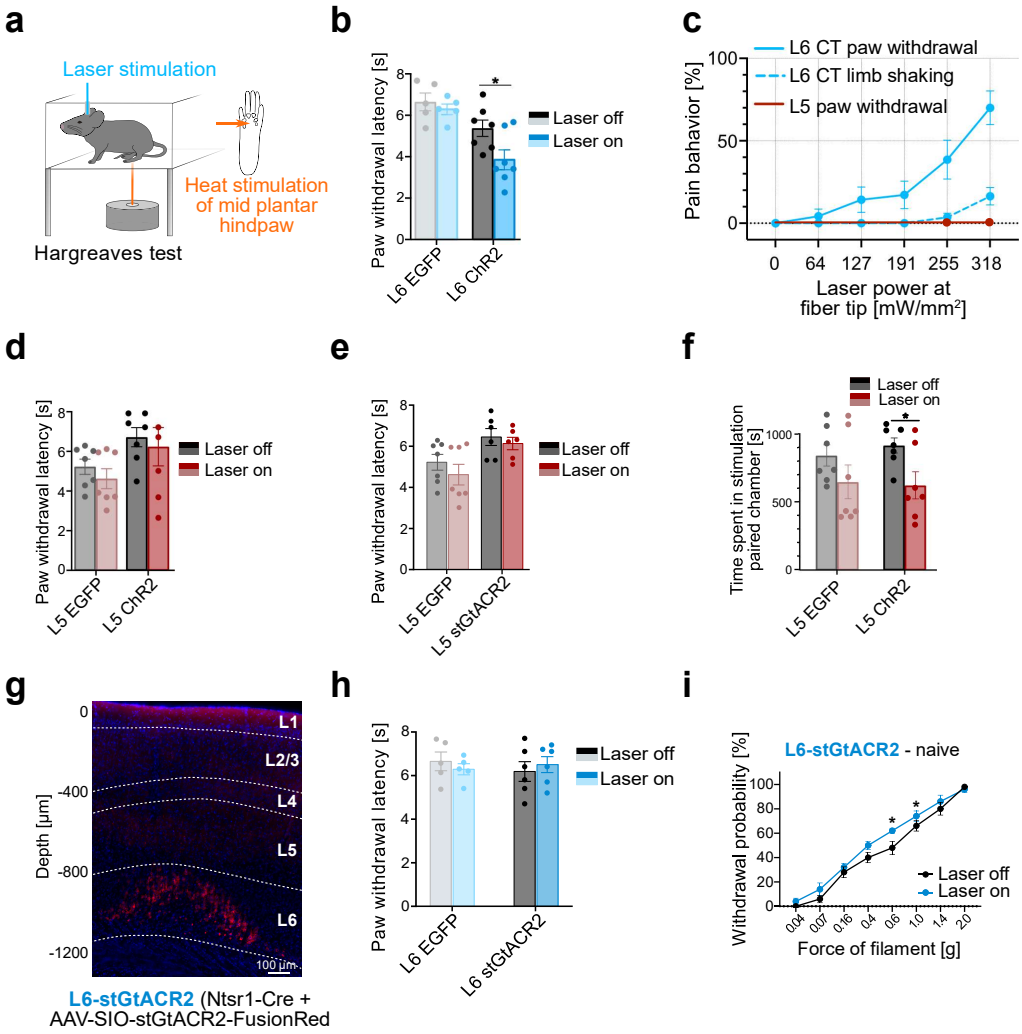


**Supplementary Figure 2: Further L6CT and L5 investigation reveals differences between layers in behavioural effects.**

**(a)** Schematic denoting the Hargreaves test (Cheah et al. 2017) to assess thermal sensitivity to noxious heat laser stimulation (orange) of the contralateral hindpaw in the presence and absence of optogenetic stimulation in S1-HL.
**(b)** Paw withdrawal latency responses to heat stimulation of the contralateral hindpaw without (black/grey, Laser off) and with (blue, Laser on, 5 s continuous pulse) optogenetic stimulation in S1-HL of L6-EGFP ($n$ = 5) and L6-ChR2 ($n$ = 7) mice.
**(c)** Optogenetically-evoked pain-like behaviours (i.e. paw shaking and withdrawal) were absent in response to L5 stimulation (red, $n$ = 6). L6CT (blue, $n$ = 11, replotted from Fig. 2b). Behavioural responses were considered in the 5 s optogenetic stimulation period, paw lifting (solid line) and limb shaking (dashed line).
**(d)** Paw withdrawal latency responses to heat stimulation of the contralateral hindpaw without (black/grey, Laser off) and with (red, Laser on, 5 s continuous pulse) optogenetic stimulation in S1-HL of L5-EGFP ($n$ = 7) and L5-ChR2 ($n$ = 7) mice.
**(e)** Optogenetic inhibition of S1-HL L5 activity. Paw withdrawal latency responses to heat stimulation of the contralateral hindpaw without (black/grey, Laser off) and with (red, Laser on, 5 s continuous pulse) optogenetic stimulation in S1-HL of L5-EGFP ($n$ = 7) and L5-stGtACR2 ($n$ = 6) mice.
**(f)** CPP. Population analysis of total time spent in the laser-paired chamber at baseline (Laser off, black/grey) and during optogenetic stimulation (Laser on, red 20 Hz laser stimulation in S1-HL cortex) of L5-EGFP ($n$ = 7) and L5-stGtACR2 ($n$ = 6) of mice with CFA-induced paw inflammation contralateral to optogenetic stimulation. Animals were injected with CFA (see Methods) one day before initiating the first baseline session.
**(g)** Expression of stGtACR2-FusionRed (red) in a Ntsr1-Cre mouse displaying fluorescence in L6CT neurons in S1-HL. Depth is registered relative to S1-HL layer borders (dashed lines, estimated based on soma sizes and densities using DAPI signals, blue). Representative example of $n$ = 16 independent experiments with similar results.
**(h)** Optogenetic inhibition of S1-HL L6CT activity. Paw withdrawal latency responses to heat stimulation of the contralateral hindpaw without (black/grey, Laser off) and with (blue, Laser on, 5 s continuous pulse) optogenetic stimulation in S1-HL of L6-EGFP ($n$ = 5) and L6-stGtACR2 ($n$ = 6) mice.
**(i)** Within-animal comparison of paw withdrawal response probabilities to graded von Frey stimulation of the contralateral hindpaw at baseline (black, laser off) and during optogenetic inhibition (blue, laser on, 5 s continuous pulse) L6CT in S1-HL of L6-stGtACR2 mice ($n$ = 10).

Data from Katharina Ziegler and Antonio Gonzalez. Figure contains panels adapted from *Ziegler et al.* (Ziegler et al. 2023).

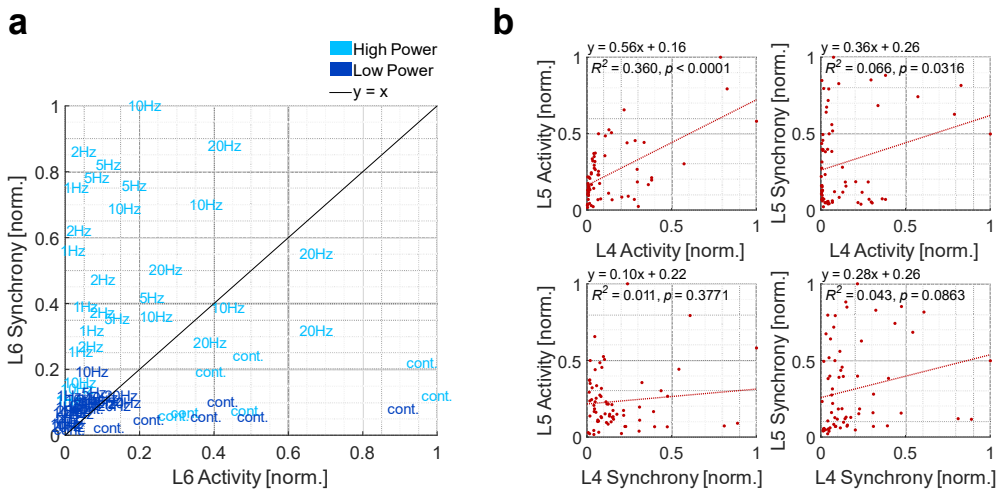


**Supplementary Figure 3: Effect of different optogenetic stimulation conditions on Synchrony-Activity Ratios, and effect of L4 on L5.**

**(a)** Activity vs synchrony plot for the different stimulation conditions and light intensities (High Power > 382mW/mm², Low Power <= 382mW/mm²) for tagged L6CT populations from *n* = 5 mice (Data points are identical as for **Fig. 11d**).
**(b)** Effect of L4 activity (top) and synchrony (bottom) on activity (left) and synchrony (right) in L5 (red). L4 activity predicts >35% of L5 activity variability. *n* = 5 mice.
Data from Ross Folkard

| Figure | Group | *F*, *p* values, 95% confidence interval (*CI*) | Statistical test |
|---|---|---|---|
| 2d | L6-ChR2 naive von Frey | $F = 72.25$; $p = 1.36 \times 10^{-5}$<br>0.04 g; $p = 0.357$<br>0.07 g; $p = 0.049$<br>0.16 g; $p = 0.035$<br>0.4 g; $p < 0.001$<br>0.6 g; $p = 0.001$<br>1.0 g; $p = 0.007$<br>1.4 g; $p = 0.567$<br>2.0 g; $p = 1$<br>CI Baseline = 45.5 to 62<br>CI Laser = 63.3 to 78.2 | Repeated measures ANOVA with post-hoc Bonferroni test |
| 2f | L6-ChR2 CPA preference indices | $F = 17.93$, $p = 0.002$<br>Between timepoints (within groups):<br>L6-EYFP (control) $p = 0.3946$, CI -0.24 to 0.77<br>L6-ChR2 (exper.) $p = 0.0012$, CI 0.37 to 1.2<br>Between groups (within timepoints):<br>Baseline $p = >0.999$, CI -0.45 to 0.53<br>Conditioning $p = 0.0227$, CI 0.07 to 1.06 | Two-way repeated measures ANOVA with post-hoc Bonferroni test |
| 3f | VPL modulation index | $p = 2.38 \times 10^{-49}$<br>L-M: $p = 1.73 \times 10^{-15}$<br>L-ML: $p = 3.63 \times 10^{-10}$<br>M-ML: $p = 1.15 \times 10^{-43}$ | Friedman test with post-hoc Wilcoxon signed-rank test |
| 3g | VPL response probability | $p < 0.001$<br>L-M: $p = 0.002$<br>L-ML: $p < 0.001$<br>M-ML: $p < 0.001$ | Friedman test with post-hoc Wilcoxon signed-rank test |
| 3h-i | Change in BP per unit | $p < 0.05$<br>See Source Data for p-values for individual units. | McNemar's test |
| | $BP_{ML}$ vs. $BP_{M}$ | $p < 0.001$ | Wilcoxon signed-rank test |
| 4c | Cortex modulation index (L2/3) | $p = 0.0019$<br>L-M; $p = 0.303$<br>L-ML; $p = 1.97 \times 10^{-5}$<br>M-ML; $p = 1$ | Friedman test with post-hoc Wilcoxon signed-rank test |
| | Cortex modulation index (L4) | $p = 5.97 \times 10^{-5}$<br>L-M: $p = 0.221$<br>L-ML: $p = 3.27 \times 10^{-9}$<br>M-ML: $p = 1$ | Friedman test with post-hoc Wilcoxon signed-rank test |
| | Cortex modulation index (L5) | $p = 6.48 \times 10^{-77}$<br>L-M: $p = 5.07 \times 10^{-49}$<br>L-ML: $p = 2.20 \times 10^{-12}$<br>M-ML: $p = 4.80 \times 10^{-47}$ | Friedman test with post-hoc Wilcoxon signed-rank test |

| | | | |
|---|---|---|---|
| | Cortex modulation index (L6) | $p = 2.10 \times 10^{-12}$<br>L-M: $p = 7.44 \times 10^{-6}$<br>L-ML: $p = 0.51$<br>M-ML: $p = 4.59 \times 10^{-5}$ | Friedman test with post-hoc Wilcoxon signed-rank test |
| | Change in spiking rate per unit | $p < 0.05$<br>See Source Data for p-values for individual units. | Wilcoxon signed-rank or ZETA test |
| 4c | MIs across layers | L condition *p* values<br>**L4 L5 L6**<br>**L2/3** 0.1129 0.00030 0.00043<br>**L4** na 0.01418 0.00180<br>**L5** na na 0.00355<br><br>M condition *p* values<br>**L4 L5 L6**<br>**L2/3** 0.4521 $2.1 \times 10^{-6}$ 0.00030<br>**L4** na $6.3 \times 10^{-10}$ $3.36 \times 10^{-9}$<br>**L5** na na $3.7 \times 10^{-58}$<br><br>ML condition *p* value<br>**L4 L5 L6**<br>**L2/3** 0.2828 $4.24 \times 10^{-11}$ 0.0232<br>**L4** na $1.97 \times 10^{-23}$ $4.05 \times 10^{-5}$<br>**L5** na na $1.88 \times 10^{-43}$ | Wilcoxon rank sum |
| 5d | Median and 1st/3rd quartiles $MI_L$ per layer | $p < 0.01$<br>L2/3: 14/29 (48%) units ($MI_L$ -0.26 **-0.09** 0.05); L4: 25/52 (48%) units ($MI_L$ 0.08 **0.22** 0.41); L5: 96/150 (65%) units ($MI_L$ -0.69 **-0.23** 0.03); L6: 27/52 (52%) units ($MI_L$ 0.07 **0.37** 0.52). L2/3 vs L5 and L4 vs L6. were not significant. | Wilcoxon signed-rank test |
| 5e | L5-stGtACR2 von Frey | $F = 13.787$; $p = 0.014$<br>0.04 g; $p = 0.203$<br>0.07 g; $p = 0.004$<br>0.16 g; $p = 0.013$<br>0.4 g; $p = 0.041$<br>0. 6 g; $p = 0.102$<br>1.0 g; $p = 0.175$<br>1.4 g; $p = 0.465$<br>2.0 g; $p = 1$<br>CI Baseline = 33.3 to 54.2<br>CI Laser = 46.6 to 65.1 | Two-way repeated measures ANOVA with post-hoc Bonferroni test |
| 5g | L5-stGtACR2 CPA preference indices | $F = 11.69$, $p = 0.006$<br>Between time points (within groups):<br>L5-EYFP (control) $p = 0.3306$, CI -0.25 to 0.91<br>L5-stGtACR2 (exper.) $p = 0.0146$, CI 0.17 to 1.42<br>Between groups (within time points):<br>Baseline $p = >0.999$, CI -0.81 to 0.59<br>Conditioning $p = 0.4805$, CI 0.35 to 1.05 | Two-way repeated measures ANOVA with post-hoc Bonferroni test |

| | | | |
|---|---|---|---|
| 6c | L5-ChR2 naive von Frey | $F$ = 273.49; $p$ = 1.48x10$^{-5}$<br>0.04 g; $p$ = 1<br>0.07 g; $p$ = 0.007<br>0.16 g; $p$ = 0.003<br>0.4 g; $p$ = 0.003<br>0.6 g; $p$ = 0.0003<br>1.0 g; $p$ = 0.003<br>1.4 g; $p$ = 0.003<br>2.0 g; $p$ = 0.012<br>CI Baseline = 44.7 to 64.9<br>CI Laser = 12.8 to 26.8 | Two-way repeated measures ANOVA with post-hoc Bonferroni test |
| 6d | L5-ChR2 CPP preference indices | $F$ = 5.334, $p$ = 0.046<br>Between timepoints (within groups):<br>L6-EYFP (control) $p$ = >0.999<br>L6-ChR2 (exper.) $p$ = 0.0298<br>Between groups (within timepoints):<br>Baseline $p$ = 0.6967, CI -0.46 to 0.20<br>Conditioning $p$ = 0.0019, CI -0.86 to -0.20 | Two-way repeated measures ANOVA with post-hoc Bonferroni test |
| 7a | L6-ChR2 CFA von Frey | $F$ = 17.07; $p$ = 0.002<br>0.04 g; $p$ = 0.005<br>0.07 g; $p$ = 0.02<br>0.16 g; $p$ = 0.41<br>0.4 g; $p$ = 1<br>0.6 g; $p$ = 0.96<br>1.0 g; $p$ = 1<br>1.4 g; $p$ = 1<br>2.0 g; $p$ = 1<br>CI Baseline = 71.7 to 84.3<br>CI Laser = 80.1 to 89.9 | Repeated measures ANOVA with post-hoc Bonferroni test |
| 7b | L5-ChR2 CFA von Frey | $F$ = 19.317; $p$ = 0.001<br>0.04 g; $p$ = 0.189<br>0.07 g; $p$ = 0.007<br>0.16 g; $p$ = 0.028<br>0.4 g; $p$ = 0.035<br>0.6 g; $p$ = 0.084<br>1.0 g; $p$ = 0.105<br>1.4 g; $p$ = 0.777<br>2.0 g; $p$ = 1<br>CI Baseline = 65.1 to 78.6<br>CI Laser = 46.7 to 62.5 | Two-way repeated measures ANOVA with post-hoc Bonferroni test |
| 7e | Saline vs CFA ISI probability distributions | $p$ = 5.32x10$^{-5}$ | Kolmogorov-Smirnov test |
| 7g | Left: Saline vs CFA burst event ratios | $p$ = 1.29x10$^{-13}$ | Wilcoxon rank sum |
| | Right: Saline vs CFA Firing Rate | $p$ = 0.48 | Wilcoxon rank sum |
| 7h | Saline v CFA Spikes per burst | Spikes per burst:<br><br>2; $p$ = 1.5x10$^{-5}$<br>3; $p$ = 1.01x10$^{-4}$<br>4; $p$ = 2.64x10$^{-5}$<br>5; $p$ = 2.83x10$^{-4}$ | Wilcoxon rank sum |

| | | | |
|---|---|---|---|
| | | 6; $p = 0.0024$<br>7; $p = 6.15 \times 10^{-4}$<br>8; $p = 0.0037$<br>9; $p = 0.0015$<br>10; $p = 0.0017$<br>11; $p = 0.0344$ | |
| 8d | Low L6CT Spontaneous vs Evoked | $p = 7.1 \times 10^{-38}$ | Wilcoxon signed-rank |
| | High L6CT Spontaneous vs Evoked | $p = 1.07 \times 10^{-38}$ | Wilcoxon signed-rank |
| | Low L6CT vs High L6CT Modulation Indices | $p = 2.13 \times 10^{-76}$ | Wilcoxon signed-rank |
| 9c | Low L6CT Spontaneous vs Evoked | L4; $p = 8.4 \times 10^{-5}$<br>L5; $p = 9.6 \times 10^{-35}$ | Wilcoxon signed-rank |
| | High L6CT Spontaneous vs Evoked | L4; $p = 1.2 \times 10^{-24}$<br>L5; $p = 1.8 \times 10^{-4}$ | Wilcoxon signed-rank |
| | Low L6CT vs High L6CT Modulation Indices | L4; $p = 2.0 \times 10^{-22}$<br>L5; $p = 1.5 \times 10^{-28}$ | Wilcoxon signed-rank |
| | L4 vs L5 Modulation indices | Low L6CT; $p = 5.2 \times 10^{-16}$<br>High L6CT; $p = 1.2 \times 10^{-29}$ | Wilcoxon rank sum |
| 10d | L4 Counts Facilitation | 1 Hz 1st vs 3rd pulse; $p = 5.16 \times 10^{-4}$<br>10 Hz 1st vs 3rd pulse; $p = 1.6 \times 10^{-19}$<br>1 Hz 3rd vs 10 Hz 1st pulse; $p = 0.75$<br>1st pulse 1 Hz vs 10 Hz; $p = 5.07 \times 10^{-4}$<br>3rd pulse 1 Hz vs 10 Hz; $p = 1.49 \times 10^{-18}$ | Wilcoxon signed-rank |
| | L5 Counts Facilitation | 1 Hz 1st vs 3rd pulse; $p = 0.0353$<br>10 Hz 1st vs 3rd pulse; $p = 2.98 \times 10^{-21}$<br>1 Hz 3rd vs 10 Hz 1st pulse; $p = 0.14$<br>1st pulse 1 Hz vs 10 Hz; $p = 0.59$<br>3rd pulse 1 Hz vs 10 Hz; $p = 9.09 \times 10^{-19}$ | Wilcoxon signed-rank |
| 10e | L4 Modulation Indices | 1 Hz vs 10 Hz; $p = 0.0466$<br>1 Hz vs continuous; $p = 9.5 \times 10^{-5}$<br>10 Hz vs continuous; $p = 2.7 \times 10^{-8}$ | Wilcoxon signed-rank |

| | | | |
|---|---|---|---|
| | L5 Modulation Indices | 1 Hz vs 10 Hz; $p = 0.0177$<br>1 Hz vs continuous; $p = 1.56 \times 10^{-7}$<br>10 Hz vs continuous; $p = 8.9 \times 10^{-11}$ | Wilcoxon signed-rank |
| 12d | VPL Counts Facilitation | 1 Hz 1st vs 3rd pulse; $p = 0.0757$<br>10 Hz 1st vs 3rd pulse; $p = 0.007$<br>1 Hz 3rd vs 10 Hz 1st pulse; $p = 0.50$<br>1st pulse 1 Hz vs 10 Hz; $p = 0.24$<br>3rd pulse 1 Hz vs 10 Hz; $p = 0.019$ | Wilcoxon signed-rank |
| 12f | VPL Burst Event Ratios | Baseline vs 1 Hz; $p = 5.2 \times 10^{-15}$<br>Baseline vs 10 Hz; $p = 4.7 \times 10^{-16}$<br>Baseline vs continuous; $p = 4.3 \times 10^{-17}$<br>1 Hz vs 10 Hz; $p = 0.00025$<br>1 Hz vs continuous; $p = 1.54 \times 10^{-34}$<br>10 Hz vs continuous; $p = 1.56 \times 10^{-49}$ | Wilcoxon signed-rank |
| 12g | VPL Total Bursts | Baseline vs 1 Hz; $p = 2.9 \times 10^{-39}$<br>Baseline vs 10 Hz; $p = 1.1 \times 10^{-40}$<br>Baseline vs continuous; $p = 5.4 \times 10^{-11}$<br>1 Hz vs 10 Hz; $p = 6.9 \times 10^{-15}$<br>1 Hz vs continuous; $p = 0.62$<br>10 Hz vs continuous; $p = 8.1 \times 10^{-13}$ | Wilcoxon signed-rank |
| 12h | VPL Median Firing Rates | Baseline vs 1 Hz; $p = 8.4 \times 10^{-17}$<br>Baseline vs 10 Hz; $p = 2.5 \times 10^{-38}$<br>Baseline vs continuous; $p = 1.5 \times 10^{-53}$<br>1 Hz vs 10 Hz; $p = 3.8 \times 10^{-31}$<br>1 Hz vs continuous; $p = 8.7 \times 10^{-18}$<br>10 Hz vs continuous; $p = 7.5 \times 10^{-41}$ | Wilcoxon signed-rank |
| S1a | L6-EGFP control von Frey | $F = 1.88$; $p = 0.229$<br>0.04 g; $p = 1$<br>0.07 g; $p = 1$<br>0.16 g; $p = 1$<br>0.4 g; $p = 1$<br>0.6 g; $p = 1$<br>1.0 g; $p = 1$<br>1.4 g; $p = 1$<br>2.0 g; $p = 1$<br>CI Baseline = 34.3 to 55.7<br>CI Laser = 42 to 63 | Two-way repeated measures ANOVA with post-hoc Bonferroni test |
| S1b | L5-EGFP control von Frey | $F = 0.625$; $p = 0.465$<br>0.04 g; $p = 1$<br>0.07 g; $p = 1$<br>0.16 g; $p = 0.651$<br>0.4 g; $p = 1$<br>0.6 g; $p = 1$<br>1.0 g; $p = 1$<br>1.4 g; $p = 1$<br>2.0 g; $p = 1$<br>CI Baseline = 38.6 to 58.9<br>CI Laser = 36.5 to 57.7 | Two-way repeated measures ANOVA with post-hoc Bonferroni test |
| S1c | L6-EGFP control von Frey | $F = 1.88$; $p = 0.229$<br>0.04 g; $p = 1$<br>0.07 g; $p = 1$<br>0.16 g; $p = 1$<br>0.4 g; $p = 1$<br>0.6 g; $p = 1$<br>1.0 g; $p = 1$<br>1.4 g; $p = 1$<br>2.0 g; $p = 1$ | Two-way repeated measures ANOVA with post-hoc Bonferroni test |

| | | | |
|---|---|---|---|
| | | CI Baseline = 34.3 to 55.7<br>CI Laser = 42 to 63 | |
| S1d | L5-EGFP control von Frey CFA | *F* = 0.04; *p* = 0.847<br>0.04 g; *p* = 1<br>0.07 g; *p* = 1<br>0.16 g; *p* = 1<br>0.4 g; *p* = 1<br>0.6 g; *p* = 1<br>1.0 g; *p* = 1<br>1.4 g; *p* = 1<br>2.0 g; *p* = 1<br>CI Baseline = 68.2 to 83.7<br>CI Laser = 68.8 to 84.3 | Two-way repeated measures ANOVA with post-hoc Bonferroni test |
| S2b | L6-ChR2 Hargreaves | *F* = 9.51; *p* = 0.012<br>L6-EGFP (control) *p* = 0.92, CI -0.87 to 1.59<br>L6-ChR2 (exper.) *p* = 0.006, CI 0.49 to 2.56 | Two-way repeated measures ANOVA with post-hoc Bonferroni test |
| S2d | L5-ChR2 Hargreaves | *F* = 2.15; *p* = 0.169<br>L6-EGFP (control) *p* = 0.55, CI -0.74 to 1.94<br>L6-ChR2 (exper.) *p* = 0.75, CI -0.86 to 1.82 | Two-way repeated measures ANOVA with post-hoc Bonferroni test |
| S2e | L5-stGtACR2 Hargreaves | *F* = 5.798, *p* = 0.0347<br>L5-EGFP (control) *p* = 0.0812, CI -0.07 to 1.27<br>L5-ChR2 (exper.) *p* = 0.5622, CI -0.41 to 1.04 | Two-way repeated measures ANOVA with post-hoc Bonferroni test |
| S2f | L5 ChR2 CPA | *F* = 17.56, *p* = 0.01<br>L6-EGFP (control) *p* = 0.218, CI -93.1 to 482.5<br>L6-ChR2 (exper.) *p* = 0.045, CI 6.0 to 581.6 | Two-way repeated measures ANOVA with post-hoc Bonferroni test |
| S2h | L6-stGtACR2 Hargreaves | *F* = 0.022, *p* = 0.88<br>L5-EGFP (control) *p* = 0.252, CI -0.21 to 0.93<br>L5-ChR2 (exper.) *p* = 0.277, CI -0.84 to 0.21 | Two-way repeated measures ANOVA with post-hoc Bonferroni test |
| S2i | L6-stGtACR2 von Frey | *F* =15.059; *p* = 0.004<br>0.04 g; *p* = 0.168<br>0.07 g; *p* =0.104<br>0.16 g; *p* = 0.343<br>0.4 g; *p* 0.096<br>0. 6 g; *p* =0.01<br>1.0 g; *p* = 0.037<br>1.4 g; *p* = 0.081<br>2.0 g; *p* = 0.343<br>CI Baseline = 38.1 to 53.4<br>CI Laser = 44.8 to 59.7 | Two-way repeated measures ANOVA with post-hoc Bonferroni test |

**Supplementary Table 1.** Description of statistical parameters and *p*- and *F*-values by figure.

# 9. Acknowledgements

Thank you very much to Alex and Rebecca for giving me the opportunity to work in the lab and complete my PhD here. Thank you for the time and mentoring you've given me over the years. I've been very grateful for the time you've given me. I feel like I'm a much better scientist after finishing my PhD than after the Masters, to the extent that I'm somewhat scared to go back and look at how bad my Masters thesis was! I've learnt so much in this lab, some invaluable lessons, and had some amazing experiences during my time here. I've got to meet some incredible people that I would likely have never met had I not been doing my PhD here, so I'm very grateful for that and the opportunities you've afforded me.

Thank you very much to Katharina Ziegler for help with proof-reading the thesis and making sure everything is at least reasonably comprehensible. Also with the formatting, aesthetics and all the other dressings and trimmings. We started in this lab together and I owe you a huge debt of gratitude and thanks for all the help and teaching you've given me over the years. In England we'd say you have the patience of a saint - it's really quite impressive to have seen over the years how you conduct yourself, I've learnt a lot from you!

Thank you very much Señor Emilio for first and foremost just being a bloody good chap! I can't say I've met a nicer person than you, and I wish you all the happiness in the future. As a colleague too, you treat everyone with honesty, respect, and dignity - it's noticed and very much appreciated! I've learnt that this is one of if not the most important things for me, and as a result I would not hesitate in following you into battle good sir! No one else seems to have the same indefatigable desire (well, tolerance) to discuss neuroscience with me, and some of our best ideas have come from intense discussions about tiny details and incongruences that might otherwise have been ignored. My progress as a scientific thinker has been most influenced by you (sorry pal, you gotta take some blame there), as I would not have had any of these many illuminating discussions with anyone else. I can't wait to celebrate your PhD graduation - hang in there, your thesis is coming!

Thank you to Martin Both, you've been an amazing mentor and friend to me. It's been invaluable to get an outside perspective on my projects and ideas, and considering we're not even in the same lab I'm so grateful for the amount of time you've had for me. The last couple of years have been a little intense but I'm really looking forward to you, Ivo, and me being back in the Boulderhaus again on Mondays. Damn those were good times!

Thanks also to Filippo, you're just another beautiful person, who I've got so much love and admiration for. Big congratulations on the paper submission…I think we can all agree that you earnt that and then some! It's been wild to see you join the lab and just acquire skill after skill and gradually become the most competent lab member, I'm just glad there are superstar people out there like you to drag the rest of us towards enlightenment; you're an inspiration to me, and others I'm sure - plus you're just the nicest, most aggressively humble guy. You're a great friend, I'll never forget our California road trip!

Thank you to the rest of the lab: Antonio, Jesus, Nadin, Jan, Lennox, Tim, Phine, Helena, James, and honorary member Berin for providing a very cohesive, jovial atmosphere and thoughtful insights into my projects.

Thanks very much to Charlotte, Damayanti, and Tara for being my students. You were all great, and I learnt a lot from supervising you.

Thank you also to Georg and Thomas for your advice throughout the years in our meetings. It's really cool that you seem so interested in what I have been researching, and your feedback over the years has been very helpful - many of the discussion points are still firmly etched into my memory. I feel like you've been very supportive of me and it's been very encouraging.

Lastly, thank you so much to Tabea for all your support and encouragement! You've been amazing and I hope I can return the favour. Thank you for enduring that gargantuan task of proof-reading my thesis:  you have a very keen eye for detail! You spotted many mistakes that no one else did. My thesis is so much better as a result of you having read it. I'm very pleased that your IZN 2021 poster on differences in PVT-CeA plasticity after chronic pain between males and females was just so damn interesting! Words cannot do justice to how grateful I am for your support throughout the last few years.

p.s. Thanks also to Leo and Tigger for editing the thesis at just the most inconvenient moments by deciding the laptop keyboard was the perfect place to take a nap. I kinda want to blame the typos on you but I suppose I should at some point take at least a modicum of responsibilty for this thesis.